



Michigan Technological University
Create the Future Digital Commons @ Michigan Tech

Dissertations, Master's Theses and Master's
Reports - Open

Dissertations, Master's Theses and Master's
Reports

2011

Quantum transport in a single molecular junction

Partha Pratim Pal
Michigan Technological University

Follow this and additional works at: <https://digitalcommons.mtu.edu/etds>


 Part of the [Physics Commons](#)

Copyright 2011 Partha Pratim Pal

Recommended Citation

Pal, Partha Pratim, "Quantum transport in a single molecular junction", Dissertation, Michigan Technological University, 2011.
<https://doi.org/10.37099/mtu.dc.etds/114>

Follow this and additional works at: <https://digitalcommons.mtu.edu/etds>

 Part of the [Physics Commons](#)

QUANTUM TRANSPORT IN A SINGLE MOLECULAR JUNCTION

By

Partha Pratim Pal

A DISSERTATION

Submitted in partial fulfillment of the requirements for the degree of

DOCTOR OF PHILOSOPHY

(Physics)

MICHIGAN TECHNOLOGICAL UNIVERSITY

2011

© 2011 Partha Pratim Pal

This dissertation, "Quantum Transport in a Single Molecular Junction," is hereby approved in partial fulfillment of the requirements for the degree of DOCTOR OF PHILOSOPHY IN Physics.

Department of Physics

Signatures:

Dissertation Advisor

Dr. Ranjit Pati

Committee

Dr. Ravindra Pandey

Dr. Maximilian Seel

Dr. Gregory Odegard

Department Chair

Dr. Ravindra Pandey

Date

To Prabhuji ...

Contents

Contents	vii
List of Figures	xviii
List of Tables	xix
Acknowledgments	xxi
Abstract	xxiii
1 The Beginning of Molecular Electronics	1
2 Modern Density Functional Theory	7
2.1 Quantum Many-body Theory	7
2.2 The Born-Oppenheimer Approximation	9
2.3 Hartree Theory	10
2.4 Hartree-Fock Theory	12
2.5 Density Functional Theory (DFT)	14
2.6 Kohn-Sham formulation	18
2.7 Modern Density Functional Theory	21

3	Quantum Transport	23
3.1	Introduction	23
3.2	Green's Function Approach	26
3.2.1	Coherent Transport	30
3.2.2	Incoherent Transport	33
4	Revisiting the Au/BDT/Au junction.	37
4.1	Introduction	37
4.2	Computational Details	42
4.3	Results	44
4.3.1	Structural effects	44
4.3.2	Field dependent Potential Profile	46
4.3.3	Current and Conductance Features	48
4.4	Modification to a parameter free approach	54
4.5	Summary	62
5	Coherent Elastic Transport	65
5.1	Introduction	65
5.2	Computational Procedure	69
5.3	Results and Discussions	72
5.3.1	Potential Profile	72
5.3.2	I-V characteristics	76
5.3.3	Transmission Function	79

5.4	Summary	81
6	Incoherent Elastic Transport	83
6.1	Introduction	83
6.2	Computational Details	88
6.3	Results and Discussions	91
6.3.1	Geometry	91
6.3.2	Potential Profile	93
6.3.3	Current(I_{sd})-Voltage(V_{sd}) characteristics	96
6.3.3.1	Coherent Tunneling	96
6.3.3.2	Phase-breaking tunneling	99
6.3.4	Electron Phonon Coupling	103
6.4	Summary	110
7	Conclusion and Future work	113
7.1	Conclusions	113
7.2	Future Directions	116
	Bibliography	117
A	Hartree Approximation	133
B	Hartree-Fock Theory	135
C	Estimation of Electron-phonon coupling using the Holstein Model.	137

D	Copyrights	140
E	Copyrights	143
F	Copyrights	145

List of Figures

1.1	Size of a transistor since the last 3 decades. accessed on May 1, 2011; Copyright - refer Appendix D for permission.	2
1.2	Schematic of a field effect transistor (FET). Figure is adapted from the "News and views" article in Nature ²	3
1.3	Schematic of first single molecular junction. Figure is adapted from the research article by Reed <i>et al.</i> ⁵ in Science.	4
1.4	I-V characteristics obtained by Reed <i>et al.</i> ⁵	5
2.1	Mapping of a system of interacting particles to a system of non-interacting particles. The figure is adapted from a power point presentation "Efficient implementation of time-dependent density functional theory for the dynam- ical description of biomolecules and nanostructure" by A. Rubio ³⁸	14
3.1	A prototype molecular scale device. Adapted from the book "Electron Transport in Nanoscale Systems" by M. Di Ventra ¹²²	24
3.2	The active region of a molecular scale device.	26
3.3	Büttiker's multiprobe approach to incoherent but elastic transport. Adapted from the book "Electron Transport in Mesoscopic Systems" by S. Datta ⁵⁶	34

4.1	Schematic of a Benzene-1,4-dithiolate prototype junction ⁹³	45
4.2	Potential profile along the axis of the molecule (Basis set: 6-311G*) ⁹³	47
4.3	Calculated Current-Voltage and Conductance-Voltage characteristics ($\omega =$ 1; Basis set: 6-311G*) ⁹³	49
4.4	Calculated Current-Voltage and Conductance-Voltage characteristics ($\omega =$ 0.0015; Basis set: 6-311G*) ⁹³	50
4.5	Calculated Current-Voltage and Conductance-Voltage characteristics ($\omega =$ 0.003; Basis set: 6-311G*) ⁹³	51
4.6	DOS of bulk Gold.	54
4.7	I-V characteristics of Au/BDT/Au junction with bulk Au Green's function and 3 Au atoms on each side of the molecule.	55
4.8	DOS of a simulated Gold surface.	56
4.9	I-V and conductance characteristics of Au/BDT/Au junction with Au sur- face DOS.	57
4.10	A supercell of the Gold nanowire to calculate the 1-D DOS.	58
4.11	1-D DOS of Gold nanowire whose supercell is given in Fig. 4.10.	59
4.12	I-V characteristics of Au/BDT/Au junction with nanowire Au Green's func- tion and 3 Au atoms on each side of the molecule.	60
4.13	I-V characteristics of Au/BDT/Au junction with bulk Au Green's function and 13 Au atoms on each side of the molecule.	61

4.14	I-V characteristics of Au/BDT/Au junction with surface Au Green's function and 13 Au atoms on each side of the molecule.	62
4.15	I-V characteristics of Au/BDT/Au junction with nanowire Au Green's function and 13 Au atoms on each side of the molecule.	63
5.1	Schematic of a two-terminal device built out of a molecular wire containing two BCP cages ¹⁷³ . Reprinted figure with permission from Partha P. Pal and Ranjit Pati, Phys. Rev. B 82 , 045424 (2010),©(2011)The American Physical Society.	69
5.2	Variation of the Hartree-Fock energy with distance between the S and the first plane containing the Au atoms.	72
5.3	Potential profile of the two-cage molecular wire for different electric fields, $\epsilon_1, \epsilon_2, \epsilon_3$. The notation 'S' refers to the position of the terminal S atoms in the device ¹⁷³ . Reprinted figure with permission from Partha P. Pal and Ranjit Pati, Phys. Rev. B 82 , 045424 (2010),©(2011)The American Physical Society.	73
5.4	Potential profile of the three different wires at V=0.24 Volts. The notation 'S' refers to the position of the terminal S atoms in the device. The arrows indicate the height of the effective potential barriers ¹⁷³ . Reprinted figure with permission from Partha P. Pal and Ranjit Pati, Phys. Rev. B 82 , 045424 (2010),©(2011)The American Physical Society.	75

5.5	Charge profile depicting bias induced polarization effect on the terminal ‘S’ atoms in the molecular wire containing one BCP cage unit ¹⁷³ . Reprinted figure with permission from Partha P. Pal and Ranjit Pati, Phys. Rev. B 82 , 045424 (2010),©(2011)The Americal Physical Society.	76
5.6	I-V characteristics of the three different wires under the influence of applied external bias. Inset shows the plot of $\ln(G_c)$ vs. length of the molecule (L). A straight line is fitted into the data points in order to calculate β ¹⁷³ . Reprinted figure with permission from Partha P. Pal and Ranjit Pati, Phys. Rev. B 82 , 045424 (2010),©(2011)The Americal Physical Society.	77
5.7	Transmission function as a function of injection energy in the three molecular wires under the same applied external voltage(= 0.41 V). The chemical potential window is shown by the dotted line ¹⁷³ . Reprinted figure with permission from Partha P. Pal and Ranjit Pati, Phys. Rev. B 82 , 045424 (2010),©(2011)The Americal Physical Society.	80
6.1	Schematic of a two-terminal device built out of a Cubane oligomer with N=2 i.e with two cubane cages ¹⁶⁹ . Reprinted figure with permission from Partha P. Pal and Ranjit Pati, J. Phys. Chem. C 2011,©(2011)The Americal Chemical Society. Copyright permission in Appendix F.	90
6.2	Hartree-Fock energy as a function of the distance between the S atom and the plane of the first layer of Au atoms.	93

6.3	Relative Electrostatics Potential (REP) profile of the <i>active region</i> in the three different molecular wires at an external voltage of $V_{sd} = 0.27$ V ¹⁶⁹ . Reprinted figure with permission from Partha P. Pal and Ranjit Pati, J. Phys. Chem. C 2011, ©(2011)The Americal Chemical Society. Copyright permission in Appendix F.	94
6.4	Current (I_{sd}) as a function of source-drain bias (V_{sd}). Inset shows the plot of $\ln(G_c)$ vs. length of the molecular wire (L). A straight line is fitted into the data points to calculate β ¹⁶⁹ . Reprinted figure with permission from Partha P. Pal and Ranjit Pati, J. Phys. Chem. C 2011, ©(2011)The Americal Chemical Society. Copyright permission in Appendix F.	95
6.5	Variation of transmission function [$T(E, V_{sd})$] with injection energy (E) in the 3 molecular wires for a fixed external voltage of $V_{sd} = 0.06$ V. N = 1, 2, 3 denotes the number of cubane cages in the oligomer. The dotted line denotes the chemical potential window. The scale for y-axis is same for all the panels ¹⁶⁹ . Reprinted figure with permission from Partha P. Pal and Ranjit Pati, J. Phys. Chem. C 2011, ©(2011)The Americal Chemical Society. Copyright permission in Appendix F.	97

6.6 (a) Transmission function $[T(E, V_{sd})]$ vs. injection energy (E) in the three molecular devices. The plots are for a fixed external voltage of $V_{sd} = 1.87, 1.88, 1.84$ Volts for $N = 1, 2$, and 3 respectively. The chemical potential window is shown by the dotted line. The Fermi level is scaled to zero in the x-axis. (b) Current (I_{sd}) as a function of source-drain bias (V_{sd}) in the three molecular wires. ‘In-phase’ denotes the current in the absence of vibronic probe. ‘Total’ denotes the current in the presence of the vibronic probe. Note that the scale of y-axis of the 3 cubane wire is different. $N = 1, 2, 3$ denotes the number of cubane cages in the oligomer¹⁶⁹. Reprinted figure with permission from Partha P. Pal and Ranjit Pati, J. Phys. Chem. C 2011, ©(2011)The Americal Chemical Society. Copyright permission in Appendix F. 100

6.7 Electron-phonon coupling energies ($I_{i,n}$) for various vibrational modes in the molecular wire with a single cage-unit. i and n denote electronic energy eigen states and normal modes of vibration respectively. The lower panel and the upper panel correspond to $V_{sd} = 0$ V and $V_{sd} = 0.97$ V respectively¹⁶⁹. Reprinted figure with permission from Partha P. Pal and Ranjit Pati, J. Phys. Chem. C 2011, ©(2011)The Americal Chemical Society. Copyright permission in Appendix F. 105

6.8	Electron-phonon coupling energies ($I_{i,n}$) for various vibrational modes in the molecular wire with 2 cage-units. i and n denote electronic energy eigen states and normal modes of vibration respectively. The lower panel and the upper panel correspond to $V_{sd}=0$ V and $V_{sd}=0.98$ V respectively ¹⁶⁹ . Reprinted figure with permission from Partha P. Pal and Ranjit Pati, J. Phys. Chem. C 2011,©(2011)The Americal Chemical Society. Copyright permission in Appendix F.	106
6.9	One of the many vibrational modes of the $N = 2$ oligomer which interact strongly with frontier orbitals at zero bias ¹⁶⁹ . Reprinted figure with permission from Partha P. Pal and Ranjit Pati, J. Phys. Chem. C 2011,©(2011)The Americal Chemical Society. Copyright permission in Appendix F.	107
6.10	One of the newer modes of the $N = 2$ oligomer which starts to interact strongly with frontier molecular orbitals at $V_{sd} = 0.98$ V ¹⁶⁹ . Reprinted figure with permission from Partha P. Pal and Ranjit Pati, J. Phys. Chem. C 2011,©(2011)The Americal Chemical Society. Copyright permission in Appendix F.	108
E.1	Copyright permission from American Physical Society (APS) for using all or a portion of the text from the article Phys. Rev. B 82 , 045424 (2010), by Partha P. Pal and Ranjit Pati.	144

F.1	Copyright permission from American Chemical Society (ACS) for using all or a portion of the text from the article in J. Phys. Chem. C 2011, by Partha P. Pal and Ranjit Pati.	146
-----	---	-----

List of Tables

4.1	Synopsis of experimental and theoretical results ⁹³	52
6.1	Frequency of vibrational modes in three different oligomers, N=1,2,3. ¹⁶⁹ . .	103

Acknowledgments

I would like to acknowledge the Department of Physics at Michigan Technological University, Houghton, for giving me the opportunity to conduct the exotic research and compile the dissertation towards a Doctoral degree. In this regards, I would like to mention the people who have backed me for the last five years or so.

First and foremost, I would like to thank my advisor, Dr. Ranjit Pati, for his tremendous support and tireless guidance through out. I would like to express my deepest gratitude to Dr. Ravindra Pandey for his constant support as the Chair of the Department of Physics and also for his inputs being one of the committee members.

I would also like to thank Dr. Maximilian Seel and Dr. Gregory Odegard for critically reviewing my work and giving me some helpful suggestions during the defense of the original proposal of the project.

I am also thankful to my current and ex group members Puspamitra, Pavan, Brandon, Mike, Subhasish and Kamal for many fruitful discussions. It has been a pleasure to discuss science with them. I would also to acknowledge the CEC for providing me with such good computational facilities. Also I will take this opportunity to thank all the teaching and the non-teaching staff members of the Department of Physics for all their help. I would like to

acknowledge the National Science Foundation (NSF) of the United States of America for their monetary support towards the projects I worked on. Also, I would like to thank Saikat and Wil Slough for their contribution towards my scientific understanding and Gowtham, Siladitya for their help with Latex.

Finally, I seek the blessings of my “Prabhuji”. It is because of Him, I am, where I am right now. I would also like to express my deepest gratitude towards my parents and parent-in-laws for their love and care. I wish to thank my entire extended family for their strong support. My wife, Colina has been my biggest support throughout. Her patience, unselfish support and encouragement has helped me pull this through.

Abstract

The craze for faster and smaller electronic devices has never gone down and this has always kept researchers on their toes. Following Moore's law, which states that the number of transistors in a single chip will double in every 18 months, today "30 million transistors can fit into the head of a 1.5 mm diameter pin". But this miniaturization cannot continue indefinitely due to the 'quantum leakage' limit in the thickness of the insulating layer between the gate electrode and the current carrying channel. To bypass this limitation, scientists came up with the idea of using vastly available organic molecules as components in an electronic device. One of the primary challenges in this field was the ability to perform conductance measurements across single molecular junctions. Once that was achieved the focus shifted to a deeper understanding of the underlying physics behind the electron transport across these molecular scale devices. Our initial theoretical approach is based on the conventional Non-Equilibrium Green Function(NEGF) formulation, but the self-energy of the leads is modified to include a weighting factor that ensures negligible current in the absence of a molecular pathway as observed in a Mechanically Controlled Break Junction (MCBJ) experiment. The formulation is then made parameter free by a more careful estimation of the self-energy of the leads. The calculated conductance turns out to be atleast an order more than the experimental values which is probably due to a strong chemical bond at the metal-molecule junction unlike in the experiments. The focus is then shifted

to a comparative study of charge transport in molecular wires of different lengths within the same formalism. The molecular wires, composed of a series of organic molecules, are sandwiched between two gold electrodes to make a two terminal device. The length of the wire is increased by sequentially increasing the number of molecules in the wire from 1 to 3. In the low bias regime all the molecular devices are found to exhibit Ohmic behavior. However, the magnitude of conductance decreases exponentially with increase in length of the wire. In the next study, the relative contribution of the ‘in-phase’ and the ‘out-of-phase’ components of the total electronic current under the influence of an external bias is estimated for the wires of three different lengths. In the low bias regime, the ‘out-of-phase’ contribution to the total current is minimal and the ‘in-phase’ elastic tunneling of the electrons is responsible for the net electronic current. This is true irrespective of the length of the molecular spacer. In this regime, the current-voltage characteristics follow Ohm’s law and the conductance of the wires is found to decrease exponentially with increase in length which is in agreement with experimental results. However, after a certain ‘off-set’ voltage, the current increases non-linearly with bias and the ‘out-of-phase’ tunneling of electrons reduces the net current substantially. Subsequently, the interaction of conduction electrons with the vibrational modes as a function of external bias in the three different oligomers is studied since they are one of the main sources of phase-breaking scattering. The number of vibrational modes that couple strongly with the frontier molecular orbitals are found to increase with length of the spacer and the external field. This is consistent with the existence of lowest ‘off-set’ voltage for the longest wire under study.

Chapter 1

The Beginning of Molecular Electronics

In this section, I will give a brief introduction to the field of study of transport of electrons across molecular scale junctions. Such is the thirst for faster and smaller electronic devices in the modern world that scientists are working day in and day out to meet the demands. Electronic devices are made up “working units” which function in unision just as “cells” do for living things. The first step to make an electronic device work faster is to pack in more and more “working units” into it. Then there would be the issue of making them work “in concert”. Does packing more and more “working units” means an increase in the size of the electronic device ? The logical answer would be “Yes” unless the size of each “working unit” is reduced. Sacrificing size for speed is not what a modern day world would demand. A portable or handy device would always be preferred over a bulky one. So, the answer would be to reduce the size of each “working unit” and pack more of these into the device.

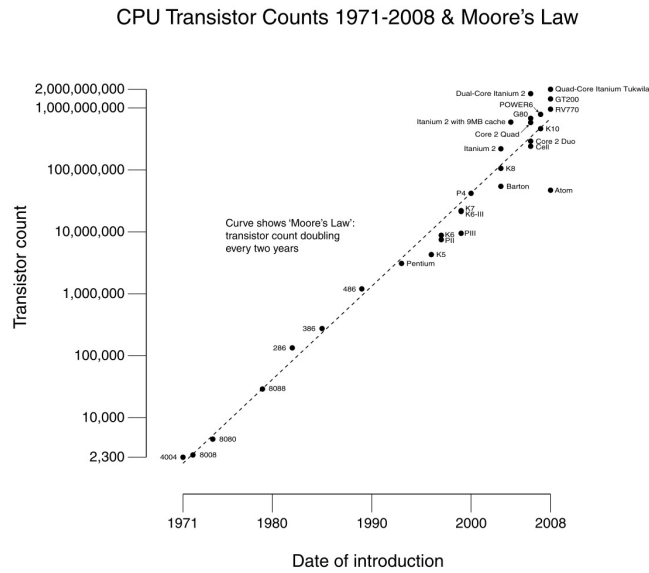


Figure 1.1: Size of a transistor since the last 3 decades. accessed on May 1, 2011; Copyright - refer Appendix D for permission.

The “working units” of electronic devices are transistors. Several transistors make up a chip and these chips work “in tandem” inside an electronic device. The size of a single transistor in a commercial chip has been decreasing since the two to three decades following the empirical law stated by Moore and is given in Fig. 1.1. Moore’s law¹ states that the number of transistors in a single chip will be doubled in 18 months. The next question would :- "how long is this miniaturization possible ?" For that, we need to take a look at the structure of a typical field effect transistor in Fig. 1.2. Reducing the size of the transistor includes a reduction in the thickness of the insulating layer which prevents the electrons in the gate electrode to interact directly with the electrons in the main channel. Research says that the insulating

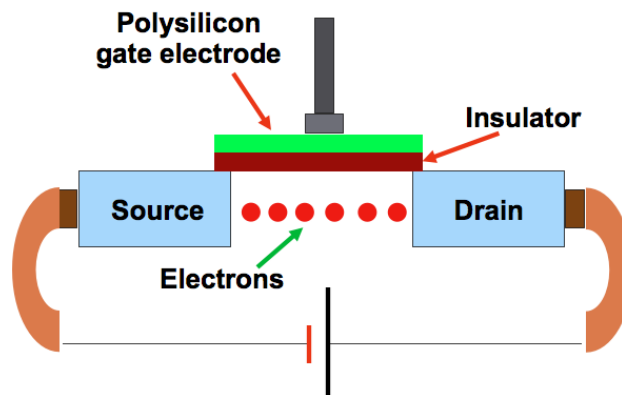


Figure 1.2: Schematic of a field effect transistor (FET). Figure is adapted from the "News and views" article in Nature².

layer has to be at least 5 atomic layer thick in order to prevent the electronic wavefunctions in the gate electrode to spill over into the current carrying channel³. If Moore's law holds true, then by the year 2020 the insulating layer will be 5 atomic layers thick and reducing the size of the transistor further would be impossible. So, the question would be: "how can one further progress towards more efficient electronic devices ?" One of the smarter solutions is to build molecular scale devices i.e build devices out of organic molecules. This idea was first proposed by Aviram and Ratner in the year 1973⁴. Through their theoretical calculation they predicted that an organic molecule which has an acceptor part and a donor part can act a rectifier. Organic molecules are available in plenty and can be easily syn-

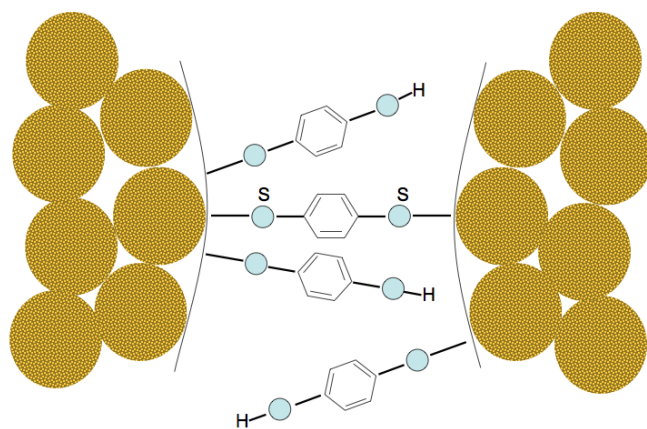


Figure 1.3: Schematic of first single molecular junction. Figure is adapted from the research article by Reed *et al.*⁵ in Science.

thesized in the laboratory. They are versatile, for e.g they can be metallic, semiconducting or insulating depending upon their conformation or surroundings. They can form reasonably strong bonds with the source/drain for electrons with the help of anchoring atoms. In other words, it is reasonably easy to form mono-layers of organic molecules using the anchoring atoms. But the real challenge was to perform current/conductance measurements across a single or few molecules. This challenge was overcome for the first time in the year 1997 by an experimental group at Yale University headed by Mark Reed⁵. They were able to carry out current measurements across a single or at best few benzene[1,4]dithiolate molecules attached between two Gold electrodes. A schematic of the junction created in

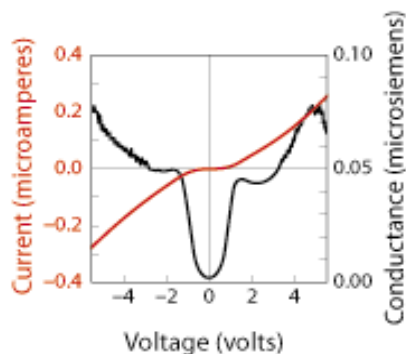


Figure 1.4: I-V characteristics obtained by Reed *et al.*⁵.

this experiment is given in Fig. 1.3 and Fig. 1.4 shows the measured current and the conductance characteristics. From the conductance characteristics it is quite evident that transport characteristics clearly has two regimes. One is the “off-resonant” regime in which current increases slowly and linearly. This is mostly in the low bias regime. After ~ 1.0 V the current rises sharply and around that same bias a peak is observed in the conductance curve. This peak signals the occurrence of “resonant” tunneling which means that a molecular energy level is providing a pathway for the electrons to move from the source to the drain. As one moves away from the “resonant” tunneling regime, the conductance again starts to increase gradually before its another “resonant” tunneling ~ 5.0 V. Here another peak in the conductance curve is observed. After this ground breaking experiment lots of other experimental groups from different parts of the world have successfully measured current across single molecular junctions^{6–12}. The transport characteristics have been successfully tuned across these molecule sized junctions. Electronic current tuning has been done through application of gate field^{13–23}, change in molecular conformation²⁴, adding

functional groups to the molecular spacer^{25–29}, or through doping/codoping³⁰. In spite of a number of successful experiments there are lots of unanswered questions in this field. With regards to experiments - a controlled fabrication of the molecule-lead contact is yet to be achieved. During the fabrication of these type of nano-scale junctions multiple contact structures are formed and they have different conductance characteristics^{8,10,11}. And then there is always the issue of impurity atoms getting into the junctions which will definitely have drastic effects on the transport characteristics. Theoretically modeling these junctions is an extremely challenging task since these are open systems. An unknown contact geometry adds to the problem of modeling the junction. A promising scheme for miniaturizing electronic devices together with a lot of unanswered questions makes it an exotic area of research.

Chapter 2

Modern Density Functional Theory

2.1 Quantum Many-body Theory

All realistic systems, are many-body systems in which either the number of nucleus, electrons or both are present in multiple numbers. Performing quantum mechanical calculations of many-body systems is very challenging and often requires drastic approximations most of which are physically sound. The starting point of any quantum calculation is the time independent Schrödinger equation^{32,33} which is given by^{34,35}:

$$\hat{H}_{ne}\psi_{ne}(r_1, r_2, \dots, r_N, R_1, R_2, \dots, R_Q) = E_{ne}\psi_{ne}(r_1, r_2, \dots, r_N, R_1, R_2, \dots, R_Q) \quad (2.1)$$

where the \hat{H}_{ne} is the time independent Hamiltonian of the multi-particle system containing N electrons and Q nuclei. $\psi_{ne}(r_1, r_2, \dots, r_N, R_1, R_2, \dots, R_Q)$ is the many-body wavefunction which is a function of the coordinates of both the electrons and the nuclei. Our aim is to concoct a many-body wavefunction which will satisfy equation 2.1, i.e an eigen function for the many-body Hamiltonian and thus the quantized energy eigen-values(E_{ne}) can be determined. The Hamiltonian consists of the kinetic energy operator of the nucleus, the electrons and the operator corresponding to the interaction of electrons with other electrons and with the nuclei. Thus the Hamiltonian containing all these terms can be written as:

$$\hat{H}_{ne} = -\frac{\hbar^2}{2m_e} \sum_i^N \nabla_i^2 - \frac{\hbar^2}{2} \sum_A^Q \frac{1}{M_A} \nabla_A^2 - \sum_i^N \sum_A^Q \frac{Z_A e^2}{|\vec{r}_i - \vec{R}_A|} + \sum_{i>j}^N \sum_{j>i}^N \frac{e^2}{|\vec{r}_i - \vec{r}_j|} + \frac{1}{2} \sum_{A \neq B}^Q \frac{Z_A Z_B e^2}{|\vec{R}_A - \vec{R}_B|} \quad (2.2)$$

where the electrons are numbered by i,j and nuclei are marked as A,B. The first two terms denote the kinetic energies of the electron and the nuclei respectively. The third term is the interaction of electrons with the nuclei. The fourth term denotes the electron-electron interactions. The last term marks the nucleus-nucleus interactions with a factor 1/2 to negate the double counting.

2.2 The Born-Oppenheimer Approximation

The ratio of rest mass of a proton to that of an electron(m_e) is ~ 1836 ³⁶. The nucleus consists of protons and neutrons and is obviously much heavier than the electrons. So, the kinetic energy of the nucleus is much less than that of the electrons. The other way to interpret is: the nucleus can be assumed to be stationary when the electrons are moving around³⁶. Thus the second term in eqn. 2.2 can be neglected with respect to the other terms in the equation. Since the nuclei can be assumed to be stationary, the last term in the Hamiltonian will be a constant number which can always be added later on. Thus, this approximation that allows us to treat the electronic and the nuclear degrees of freedom independently is known as the Born-Oppenheimer Approximation(BOA). The many-body wavefunction can hence be re-written as a product of electronic and nuclear wavefunctions³⁷:

$$\psi_{ne}(r_1, r_2, \dots, r_N, R_1, R_2, \dots, R_Q) = \psi_n(R_1 R_2, \dots, R_Q) \psi_e(r_1 r_2, \dots, r_N) \quad (2.3)$$

BOA holds true unless there are severe inelastic effects within the system. Recent research suggests that a one-dimensional system which is longer than 30 \AA and has two electronic energy levels that are coupled strongly to a particular ionic vibrational mode might violate the BOA³¹. By separating the electronic and nuclear degrees of freedom we are now ready

to solve the Schrödinger equation for the many-electron Hamiltonian which now looks like:

$$\hat{H}_e = -\frac{1}{2} \sum_i^N \nabla_i^2 - \sum_i^N \sum_A^Q \frac{Z_A}{|\vec{r}_i - \vec{R}_A|} + \sum_{i>j}^N \sum_{i>j}^N \frac{1}{|\vec{r}_i - \vec{r}_j|} \quad (2.4)$$

In the above equation we have used atomic units in which \hbar , m_e , and e are all considered to be 1. The Schrödinger equation for the multi-electron system in presence of multiple nuclei is:

$$\hat{H}_e \psi_e(r_1, r_2, \dots, r_N) = E_e \psi_e(r_1, r_2, \dots, r_N) \quad (2.5)$$

From now on we will drop the ‘ e ’ subscript from the Hamiltonian and the energy eigenvalues. Solving eqn 2.5 requires several approximations. The first step towards solving the equation was proposed by Hartree and is described in the next section.

2.3 Hartree Theory

In the Hartree theory³³ each electron faces a central potential due to the nuclei and also due to the other electrons. Hartree assumed that the many-electron wavefunction is a simple product of all the single electron wavefunctions. This is a consequence of the probability theory which states that the probability of two independent events occurring simultaneously is the product of the probability of the two events occurring separately. Thus the many-

electron wavefunction in the Hartree theory is given by³³:

$$\psi(r_1, r_2, \dots, r_N) = \phi_1(r_1)\phi_2(r_2)\dots\phi_N(r_N) \quad (2.6)$$

ϕ 's are the single electron orthogonal wavefunctions. Using the variational principle, the expectation of H (i.e. $\langle \psi | H | \psi \rangle$) hits a minimum when the following condition is satisfied (ref. Appendix A):

$$\left[-\frac{1}{2} \nabla_i^2 - \sum_A \frac{Z_A}{|\vec{r}_i - \vec{R}_A|} + \sum_{j \neq i} \int |\phi_j^* \phi_j| \frac{1}{|\vec{r}_i - \vec{r}_j|} d^3 r_j \right] \phi_i(r_i) = \epsilon_i \phi_i(r_i) \quad (2.7)$$

Thus, in this approximation the interaction between the electrons is restricted to a mean field type which means that each and every electron interacts with a cloud of charge due to all the other electrons³³. The energy associated with this type of a wavefunction is:

$$E = \langle \psi | H | \psi \rangle = \sum_i^N \epsilon_i - \sum_{i>j} \sum \int \int |\phi_j^* \phi_j| |\phi_i^* \phi_i| \frac{1}{|\vec{r}_i - \vec{r}_j|} d^3 r_j d^3 r_i \quad (2.8)$$

The last term is added to nullify the double counting of the electron-electron interactions. From equation 2.8 it is seen that the total energy of the multi-electron system is not just the summation of all the single particle energies. Thus for the removal/addition of i^{th} electron from the system the Coulomb potential is altered and due to self-consistency is reflected within the values of ϵ_i . A change in the last term is negligible in the case of an inner electron (x-ray level) and thus Hartree approximation works well in this case³³.

However, since electrons are fermions ψ should be antisymmetric with respect to particle interchange. This aspect of the wavefunction is not accounted for in the Hartree theory.

The next improvement of guess wavefunction comes under the Hartree-Fock theory.

2.4 Hartree-Fock Theory

Hartree-Fock theory³³ assumes that the many-electron wavefunction is the Slater determinant of all the single electron wavefunctions. This takes care of the antisymmetric property of the electronic wavefunctions when the position of two electrons are interchanged. The trial wavefunction in the Hartree-Fock approximation is given by:

$$\psi = \frac{1}{\sqrt{N!}} \begin{vmatrix} \phi_1(r_1) & \phi_2(r_1) & \cdots & \cdots & \phi_N(r_1) \\ \phi_1(r_2) & \phi_2(r_2) & \cdots & \cdots & \phi_N(r_2) \\ \cdots & \cdots & \cdots & \cdots & \cdots \\ \cdots & \cdots & \cdots & \cdots & \cdots \\ \phi_1(r_N) & \phi_2(r_N) & \cdots & \cdots & \phi_N(r_N) \end{vmatrix} \quad (2.9)$$

When the total energy is minimized with respect to this wavefunction, we arrive at the following equation³³:

$$\begin{aligned} \left(-\frac{1}{2} \nabla_i^2 - \sum_A \frac{Z_A}{|\vec{r}_i - \vec{R}_A|}\right) \phi_i(r_i) + \sum_j \int \phi_j^*(r_j) \frac{1}{|\vec{r}_i - \vec{r}_j|} \phi_j(r_j) d^3 r_j \phi_i(r_i) \\ - \sum_j \int \phi_j^*(r_j) \phi_i(r_j) \frac{1}{|\vec{r}_i - \vec{r}_j|} \phi_i(r_i) d^3 r_j = \epsilon_i \phi_i(r_i) \end{aligned} \quad (2.10)$$

The first three terms in the left hand side of equation 2.10 are the same as those obtained from the Hartree theory in equation 2.7. The last term, which is the exchange term, arises from the antisymmetric property of the multi-electron wavefunction. However, there are still deficiencies in this approximation as the electron-electron correlation is not described beyond the Pauli's exclusion principle. The correlation energy can be expressed as:

$$E_c = E_0 - E_{HF} \quad (2.11)$$

where E_c , E_0 and E_{HF} are the correlation, exact ground state and the Hartree-Fock ground state energies respectively. The correlation energy becomes considerably important for inhomogeneous distribution of interacting electrons which is generally the case for mostly studied systems of practical importance. Configuration interaction(CI), many-body perturbation theory(MBPT) and density functional theory(DFT) are some of the many formalisms which possess the capability to include the correlation energy upto various degrees of accuracy. Out of them, DFT is computationally the least expensive method. But as is the usual case, accuracy is sacrificed at the expense of computational time.

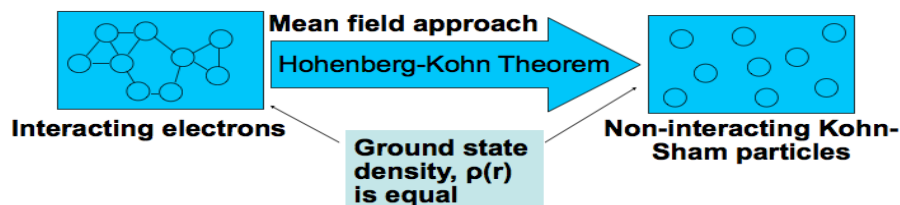


Figure 2.1: Mapping of a system of interacting particles to a system of non-interacting particles. The figure is adapted from a power point presentation "Efficient implementation of time-dependent density functional theory for the dynamical description of biomolecules and nanostructure" by A. Rubio³⁸.

2.5 Density Functional Theory (DFT)

As the name suggests, DFT^{49,50} is a formulation based on functionals, i.e function of a function namely a function of spatial electron density. Since this approach is based on the density of the system and not the many-body wavefunctions it is computationally the most favoured method. DFT is mainly based on the two Hohenberg-Kohn theorems. They are:

Theorem 1: *The external potential V_{ext} is uniquely determined by the electronic charge density $n(\mathbf{r})$ within a trivial additive constant.*⁵⁰

Proof: Let us consider $n(\mathbf{r})$ to be the electron density for a N-electron system. They are related by: $\int n(\mathbf{r})d\mathbf{r} = N$. The Hamiltonian of a N-electron system is given by equation 2.4. The nucleus-electron interaction term (second term) can be rewritten as $\sum_i^N V_{ext}(\vec{r}_i)$ where the external potential, $V_{ext}(\vec{r}_i) = \sum_A^Q \frac{Z_A}{|\vec{r}_i - \vec{R}_A|}$. Suppose there are two external potentials V_{ext} and V'_{ext} which differ by more than a trivial constant but correspond to the same ground state density $n(\mathbf{r})$. In that case we will have two Hamiltonians \hat{H} and \hat{H}' with ground state wavefunctions as Ψ and Ψ' but with same ground state density $n(\mathbf{r})$ ⁵⁰. If Ψ' is taken as the trial wavefunction for \hat{H} then

$$\begin{aligned} E_0 &< \langle \Psi' | \hat{H} | \Psi' \rangle = \langle \Psi' | \hat{H}' | \Psi' \rangle + \langle \Psi' | (\hat{H} - \hat{H}') | \Psi' \rangle \\ &= E'_0 + \int n(\mathbf{r})[V_{ext}(\mathbf{r}) - V'_{ext}(\mathbf{r})]d\mathbf{r} \end{aligned} \quad (2.12)$$

where E_0 and E'_0 are the exact ground state energies for \hat{H} and \hat{H}' respectively. It is to be noted that the above equation holds true because all the terms in \hat{H} and \hat{H}' are identical (since both are N electron systems) except the term with the external potential. In a similar manner, if we consider Ψ as a trial wavefunction for \hat{H}' then we have⁵⁰:

$$\begin{aligned} E'_0 &< \langle \Psi | \hat{H}' | \Psi \rangle = \langle \Psi | \hat{H} | \Psi \rangle + \langle \Psi | (\hat{H}' - \hat{H}) | \Psi \rangle \\ &= E_0 - \int n(\mathbf{r})[V_{ext}(\mathbf{r}) - V'_{ext}(\mathbf{r})]d\mathbf{r} \end{aligned} \quad (2.13)$$

Adding equations 2.12 and 2.13 we arrive at the relation $E_0 + E'_0 > E'_0 + E_0$, which is a contradictory equation. Hence it can be concluded that two different external potentials $V_{ext}(\mathbf{r})$ and $V'_{ext}(\mathbf{r})$ cannot exist for the same ground state electron density $n(\mathbf{r})$ ⁵⁰. Thus for

every ground state electron density distribution there exists an unique external potential.

Theorem 2⁵⁰: *The density which minimizes the expectation value of the energy is the ground state density and the corresponding energy being the ground state energy.*

This is an analogy of the variational principle where the fundamental quantity is the density of the system rather than the many-body wavefunctions.

Proof: From the previous theorem we learn that the $n(\mathbf{r})$ determines N and V_{ext} and the rest of the ground state properties. So we can write the total energy as⁵⁰:

$$\begin{aligned} E_{V_{ext}} &= T[n(\mathbf{r})] + V_{ne}[n(\mathbf{r})] + V_{ee}[n(\mathbf{r})] \\ &= \int n(\mathbf{r})V_{ext}(\mathbf{r})d\mathbf{r} + F_{HK}[n(\mathbf{r})] \end{aligned} \quad (2.14)$$

where $F_{HK}[n(\mathbf{r})] = T[n(\mathbf{r})] + V_{ee}[n(\mathbf{r})]$. The second term can also be written as⁵⁰:

$$V_{ee}[n(\mathbf{r})] = J[n(\mathbf{r})] + \text{exchange term} \quad (2.15)$$

The *exchange term* contains the information of the exchange and correlation energies. Now, for a trial density $n'(\mathbf{r})$ satisfying the conditions $n'(\mathbf{r}) \geq 0$ and $\int n'(\mathbf{r})d\mathbf{r} = N$ there exists an unique external potential V'_{ext} . If we take a trial wave function Ψ' for a Hamiltonian H then:

$$\langle \Psi' | \hat{H} | \Psi' \rangle = \int n'(\mathbf{r})V_{ext}(\mathbf{r})d\mathbf{r} + F_{HK}[n'(\mathbf{r})] = E_{V'_{ext}}[n'(\mathbf{r})] \geq E_{V_{ext}}[n(\mathbf{r})] \quad (2.16)$$

which is basically the analogous argument for the variational principle but not with the wave functions. Assuming that $E_{V_{ext}}[n(\mathbf{r})]$ is differentiable, the ground state density has to satisfy the stationary principle which is required by the variational principle⁵⁰.

$$\delta \{ E_{V_{ext}}[n(\mathbf{r})] - \mu \left(\int n(\mathbf{r}) d\mathbf{r} - N \right) \} = 0 \quad (2.17)$$

giving way to the Euler-Lagrange equation:

$$\mu = \frac{\delta E_{V_{ext}}[n(\mathbf{r})]}{\delta [n(\mathbf{r})]} = V_{ext}(\mathbf{r}) + \frac{\delta F_{HK}[n(\mathbf{r})]}{\delta n(\mathbf{r})} \quad (2.18)$$

where μ is defined to be the chemical potential. Note that the term $F_{HK}[n(\mathbf{r})]$ is independent of the external potential i.e it will be an universal functional of $n(\mathbf{r})$. If we can estimate the exact form of $F_{HK}[n(\mathbf{r})]$ we can apply to it any system and calculate the ground state properties. Equation 2.18 is the basic working equation of DFT⁵⁰.

However, equation 2.18 is very difficult to be implemented for practical calculations since the exact analytical form of $F_{HK}[n(\mathbf{r})]$ is still unknown. An analytical expression for $F_{HK}[n(\mathbf{r})]$ is the real challenge. In the year 1965, Kohn and Sham devised a clever method for a reasonably accurate and computationally feasible scheme to estimate $F_{HK}[n(\mathbf{r})]$.

2.6 Kohn-Sham formulation

For an interacting system N-electron system, the ground state kinetic energy can be written as^{50,51}:

$$T = \sum_i^N \lambda_i \langle \psi_i | -\frac{1}{2} \nabla_i^2 | \psi_i \rangle \quad (2.19)$$

where ψ_i is the i_{th} orbital and λ_i is the corresponding occupation number. According to Pauli's exclusion principle: $0 \leq \lambda_i \leq 1$. The total electron density of the N electron is:

$$n(\mathbf{r}) = \sum_i^N \lambda_i |\psi_i(\mathbf{r})|^2 \quad (2.20)$$

From Hohenberg-Kohn theorems it is guaranteed that T is a functional of $n(\mathbf{r})$. But for an interacting system there can be infinite number of terms in equations 2.19 and 2.20. However, for a non-interacting N electron system the kinetic energy functional can be written as⁵⁰:

$$T = \sum_i^N \langle \psi_i | -\frac{1}{2} \nabla_i^2 | \psi_i \rangle \quad (2.21)$$

and the ground state density can be written as:

$$n(\mathbf{r}) = \sum_i^N |\psi_i(\mathbf{r})|^2 \quad (2.22)$$

It can be seen that equations 2.21 and 2.22 are special cases of equations 2.19 and 2.20 with $\lambda_i = 1$ for N orbitals and $\lambda_i = 0$ for the rest. The Hamiltonian for the reference non-interacting system of N -electrons can then be written as⁵⁰:

$$\hat{H}_{ks} = \sum_i^N \left(-\frac{1}{2} \nabla_i^2 \right) + \sum_i^N V_{ks}(\mathbf{r}) \quad (2.23)$$

with no electron-electron interaction terms in the Hamiltonian. The ground state density can be constructed out of a Slater determinant of the single particle wave functions as:

$$\Psi_{ks} = \frac{1}{\sqrt{N!}} \det [\psi_1, \psi_2 \dots \psi_N] \quad (2.24)$$

where the each single particle ψ 's satisfy the equation:

$$\hat{h}_{ks} = \left[-\frac{1}{2} \nabla^2 + V_{ks} \right] \psi_i = \epsilon_i \psi_i \quad (2.25)$$

The total kinetic energy is then given by⁵⁰:

$$\begin{aligned} T_{ks} &= \langle \Psi_{ks} | \sum_i^N \left(-\frac{1}{2} \nabla_i^2 \right) | \Psi_{ks} \rangle \\ &= \sum_i^N \langle \psi_i | -\frac{1}{2} \nabla^2 | \psi_i \rangle \end{aligned} \quad (2.26)$$

It should be noted here that T_{ks} is not same as T which was defined earlier in equation 2.14. Equation 2.26 is true if there exists a non-interacting density $n(\mathbf{r})$, which always exists for antisymmetric wave functions. To separate out T_{ks} from T one needs to rewrite the

quantity F_{HK} as:

$$F_{HK} = T_{ks}[n(\mathbf{r})] + J[n(\mathbf{r})] + E_{xc}[n(\mathbf{r})] \quad (2.27)$$

where E_{xc} can be written as⁵⁰:

$$E_{xc}[n(\mathbf{r})] = T[n(\mathbf{r})] - T_{ks}[n(\mathbf{r})] + V_{ee}[n(\mathbf{r})] - J[n(\mathbf{r})] \quad (2.28)$$

$E_{xc}[n(\mathbf{r})]$ is known as the exchange-correlation energy. The Euler-Lagrange in equation 2.18 then becomes⁵⁰:

$$\begin{aligned} \mu = V_{ext}(\mathbf{r}) + \frac{\delta F_{HK}[n(\mathbf{r})]}{\delta n(\mathbf{r})} &= V_{ext}(\mathbf{r}) + \frac{\delta T_{KS}[n(\mathbf{r})]}{\delta n(\mathbf{r})} + \frac{\delta J[n(\mathbf{r})]}{\delta n(\mathbf{r})} + \frac{\delta E_{xc}[n(\mathbf{r})]}{\delta n(\mathbf{r})} \\ &= V_{eff}[n(\mathbf{r})] + \frac{\delta T_{KS}[n(\mathbf{r})]}{\delta n(\mathbf{r})} \end{aligned} \quad (2.29)$$

where the effective Kohn-Sham potential is⁵⁰:

$$\begin{aligned} V_{eff}[n(\mathbf{r})] &= V_{ext}(\mathbf{r}) + \frac{\delta J[n(\mathbf{r})]}{\delta n(\mathbf{r})} + \frac{\delta E_{xc}[n(\mathbf{r})]}{\delta n(\mathbf{r})} \\ &= V_{ext}(\mathbf{r}) + \int \frac{n(\mathbf{r}')}{|\mathbf{r} - \mathbf{r}'|} d\mathbf{r}' + V_{xc}(\mathbf{r}) \end{aligned} \quad (2.30)$$

where $V_{xc}(\mathbf{r})$ is the exchange-correlation potential and is given by:

$$V_{xc}(\mathbf{r}) = \frac{\delta E_{xc}[n(\mathbf{r})]}{\delta n(\mathbf{r})} \quad (2.31)$$

For a system of non-interacting particles $V_{ks}(\mathbf{r}) = V_{eff}(\mathbf{r})$. Hence for a given $V_{eff}(\mathbf{r})$ one can obtain a $n(\mathbf{r})$ that satisfies equation 2.29 by solving the N one-electron equations:

$$[-\frac{1}{2}\nabla^2 + V_{eff}(\mathbf{r})]\psi_i = \psi_i\epsilon_i \quad (2.32)$$

and setting

$$n(\mathbf{r}) = \sum_i^N |\psi_i(\mathbf{r})|^2 \quad (2.33)$$

Also, here $V_{eff}(\mathbf{r})$ depends on $n(\mathbf{r})$ through equation 2.31. The Kohn-Sham method is employed by solving equations 2.30, 2.32, and 2.33 self-consistently starting from a guess $n(\mathbf{r})$. The choice of $E_{xc}[n(\mathbf{r})]$ is determined by the user.

2.7 Modern Density Functional Theory

In this section we introduce the B3LYP functional^{50,118} and its application within DFT. Exchange and correlation are the two terms which are not accounted for in the Hartree and the Hartree-Fock formalisms. DFT⁵⁰ includes both of these, but in form of functionals. So, the challenge is to find a good functional which accounts for these two terms. Efforts resulted in many hybrid functionals out of which B3LYP is the most popular one. This functional includes a part of the exact Hartree-Fock exchange and the some local and non-local correlational terms are included through the Lee-Yang-Parr(LYP) part of the

functional. Mathematically it looks like^{50,118}:

$$E_{exc}^{B3LYP} = E_{exc}^{LDA} + a_0(E_{ex}^{HF} - E_{ex}^{LDA}) + a_{ex}(E_{ex}^{GGA} - E_{ex}^{LDA}) + a_c(E_c^{GGA} - E_c^{LDA}) \quad (2.34)$$

where $a_0(= 0.20)$, $a_{ex}(= 0.72)$, and $a_c(= 0.81)$ are semi-empirical coefficients calculated from appropriate fitting of experimental data of atomization energies, ionization potentials, proton affinities, and total atomic energies. E_{exc}^{LDA} , E_{ex}^{LDA} , and E_c^{LDA} are respectively the exchange-correlation, exchange, and correlation energies obtained from the LDA^{50,118} approximation of DFT. E_{ex}^{HF} is the exact exchange estimated from the Hartree-Fock formulation. E_{ex}^{GGA} and E_c^{GGA} are the exchange and correlation energies respectively calculated within the GGA approximation^{50,118}. The combination of DFT+B3LYP has been a big success in predicting band gaps for a variety of materials³⁹. Particularly in wide-gap semiconductors, the direct and indirect band gaps estimated within this formulation^{40,41} has been in good qualitative agreement with the experimentally measured values.

Chapter 3

Quantum Transport

3.1 Introduction

Field driven electronic current in the macroscopical classical frame depends on the number of collisions per unit time each electron suffers while travelling from a lower potential to a higher potential region^{42,43}. The distance which the electron travels between successive collisions is known as the mean free path (Λ_L). Typical values of Λ_L would be few hundreds of Å in bulk systems^{122–124}. What happens if the length of an conductor/insulator is less than the value of the mean free path ? From the classical theory the electron should be travelling “collision-free” within the insulator/conductor. Transport in this regime is considered to be *Ballistic*. The classical theory of transport fails in this regime but the *Quantum*

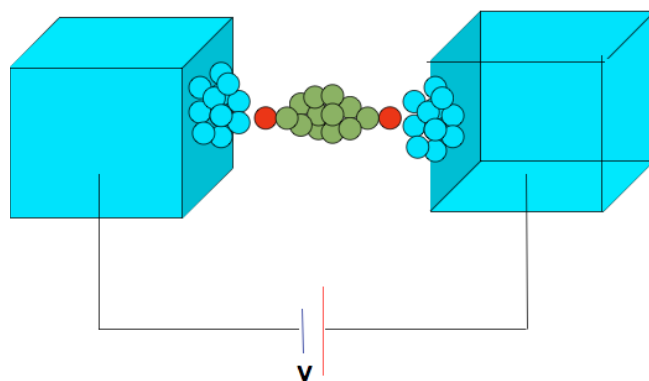


Figure 3.1: A prototype molecular scale device. Adapted from the book "Electron Transport in Nanoscale Systems" by M. Di Ventra¹²².

theory does not^{42,43}. Thus the nomenclature of the chapter is “Quantum Transport”. Parallel school of theories have been developed to study electron transport in this regime. In this chapter, I will elaborate on our approach I used to study this subject.

An archetypal molecular device consists of a finite-sized molecule slotted in between two semi-infinite metallic electrodes as shown in Fig. 3.1. To simulate a directional motion of electrons within the device one needs to concoct a non-equilibrium situation at the two metal-molecule junctions. Theoretically the non-equilibrium situation can be created either by applying an electric field as a result of which current would flow or by piling up a dif-

ferent number of charge carriers at the two junctions thus generating an electrostatic field between the two junctions. In the first approach, field is the cause and electronic current is the outcome whereas in the second approach, field is the consequence of flow of charge¹²². We use the former approach within the BOA, which allows us to calculate current in a frozen geometry. Recent findings show that the BOA breaks down³¹ for longer molecular wires ($\sim > 30 \text{ \AA}$) but in our studies the longest molecular wire considered is $\sim 15 \text{ \AA}$. Within the BOA the electronic energy levels can be computed independently, considering all the nuclei to be stationary. The two semi-infinite electrodes which act as the electron reservoirs are held at different chemical potentials. The presence of the electrodes render the device to be an *open* system. To model such a heterogeneous system, we divide it into two parts as shown in Fig. 3.2. One is the *active* region (marked in Fig. 3.2), which consists of a molecule sandwiched inbetween two clusters comprising of a finite number of electrode atoms that are perturbed when the molecule adsorbs onto the electrode surface. The rationale behind the choice of a finite number of electrode atoms in the *active* region of the device is due to the fact that the adsorption of the molecule on the electrode results in a local-charge screening within the metallic electrode at the interface^{45,46}. The second part of the device consists of the rest of the electrode on each side and is considered to retain its bulk properties. Thus, this part is considered to be the unlimited “source” for electrons on one side and the “sink” on the other side in the non-equilibrium condition. There are numerous theoretical methods to calculate the steady state electronic current under this ‘non-equilibrium’ condition. Throughout, I have used the single particle Green’s function

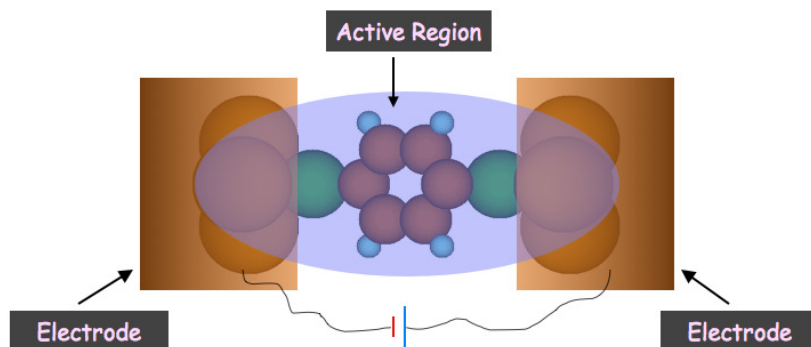


Figure 3.2: The active region of a molecular scale device.

approach to transport in conjunction with DFT which follows in the next section.

3.2 Green's Function Approach

The *active* region consists of a single or a chain of molecules and a part of the electrode (lead) on both sides. The molecular moiety interacts with the left and the right leads through coupling potentials. However, the right and the left leads are decoupled from each other.

In the absence of any electric field, the Hamiltonian can be written as¹²²:

$$H = H_C + H_L + H_R + V_{LC} + V_{CR} + \text{complex conjugates} \quad (3.1)$$

where H_L and H_R are the Hamiltonians for the isolated semi-infinite leads. The molecular Hamiltonian in the absence of electrodes is describes by H_C . The molecule couple to the left and the right leads through the coupling potential V_{LC} and V_{RC} . Going by the earlier assumption that the leads do not interact with each other, the terms V_{LR} and V_{RL} are considered to be zero. Using matrix formalism the Schrödinger equation can be written as¹²²:

$$\begin{bmatrix} H_L & V_{LC} & 0 \\ V_{LC}^\dagger & H_C & V_{CR}^\dagger \\ 0 & V_{CR} & H_R \end{bmatrix} \begin{bmatrix} |\phi_L\rangle \\ |\phi_C\rangle \\ |\phi_R\rangle \end{bmatrix} = E \begin{bmatrix} |\phi_L\rangle \\ |\phi_C\rangle \\ |\phi_R\rangle \end{bmatrix} \quad (3.2)$$

where the elements of the vector in the right hand side of the above equation are the single-particle wave functions associated with the Hamiltonians in the three different regions, i.e $|\phi_L\rangle$ is an eigen function of the Hamiltonian H_L . The three equation thus obtained from the matrix multiplication are:

$$H_L |\phi_L\rangle + V_{LC} |\phi_C\rangle = E |\phi_L\rangle \quad (3.3)$$

$$V_{LC}^\dagger |\phi_L\rangle + H_C |\phi_C\rangle + V_{CR} |\phi_R\rangle = E |\phi_C\rangle \quad (3.4)$$

$$V_{CR} |\phi_C\rangle + H_R |\phi_R\rangle = E |\phi_R\rangle \quad (3.5)$$

One can rearrange the last equation to write it as:

$$(E - H_R) | \phi_R \rangle = V_{CR} | \phi_C \rangle \quad (3.6)$$

To reflect the semi-infiniteness in the right lead we replace $E \longrightarrow E \pm i\varepsilon$ and then the equation reduces to¹²²:

$$| \phi_R \rangle = G_R(z) V_{CR} | \phi_C \rangle \quad (3.7)$$

where the Green's function of the right lead is defined as:

$$G_R(z) = \frac{\hat{1}}{z - H_R} \quad (3.8)$$

Similarly we obtain:

$$| \phi_L \rangle = G_L(z) V_{LC} | \phi_C \rangle \quad (3.9)$$

Substituting the above equation into the middle equation of the three equations we have¹²²:

$$[E - H_C - V_{LC}^\dagger G_L(z) V_{LC} - V_{CR}^\dagger G_R(z) V_{CR}] | \phi_C \rangle = 0 \quad (3.10)$$

where $\Sigma_L(z) = V_{LC}^\dagger G_L(z) V_{LC}$ and $\Sigma_R(z) = V_{CR}^\dagger G_R(z) V_{CR}$ are the self-energy operators. Writing the above equation in terms of the self energies:

$$[E - H_C - \Sigma_L(z) - \Sigma_R(z)] | \phi_C \rangle = 0 \quad (3.11)$$

So, the Green's function associated with the above equation is¹²²:

$$G(z) = \frac{1}{E - H_C - \Sigma_L(z) - \Sigma_R(z)} \quad (3.12)$$

The Green's function in equation 3.12 is the main entity in the single particle Green's function approach to electron transport in molecular scale devices. There are several other methods to derive this equation, for example from the Dyson's equation⁴⁷ but this is the simplest one. Now, I will focus on the determination of the various quantities in the right hand side of equation 3.12 in a realistic calculation.

The first task is solving the Schrödinger equation or in other words calculating the energy levels for the *active region* of the device. In the presence of an electric field the modified Hamiltonian for the region can be written as³²:

$$H(\epsilon) = H(0) + \vec{\epsilon} \cdot \sum_i \vec{r}(i), \quad (3.13)$$

where $H(0)$ is the unperturbed ground-state mean field DFT Hamiltonian; $\vec{\epsilon}$ is the applied electric field to replicate the bias effect where only the dominant dipolar term is taken into account; and $\vec{r}(i)$ is the coordinate of the i^{th} electron. The real space approach allows us to partition $H(\epsilon)$ into the Hamiltonian corresponding to the central part, which consists of of an organic molecule ($H_C \equiv H_{mol}$) in our studies and the molecule-lead (only few perturbed atoms of the electrode) coupling matrices ($V_{LR,CR} \equiv C_{l,r}$). It is worth mentioning here that

including the bias effect in formulations beyond the ground state mean-field DFT¹⁷⁴ is a very difficult task. In covalently bonded junctions, which is the case in all my studies, the modification of the molecule-lead coupling with change in external bias is an important quantity that should be captured in the formulation. In this context the ground state based DFT is a reasonably good approach and is being successfully used^{55,57,121,175}. $H(\epsilon)$, if solved using first order perturbation theory will give only linear shifts to the zeroth order energy eigenvalues. However, a fully self-consistent evaluation of $H(\epsilon)$ reveals a non-linear increase in the energy eigenvalues with the application of $\vec{\epsilon}$. Thus this approach not only includes the first order effect of the field on the dipole moment of the molecule, but also on its polarizability and higher order terms. In the next two sections I will describe the phase-coherent and phase-incoherent elastic transport.

3.2.1 Coherent Transport

In this section, phase relaxation scattering of electrons is not considered. Also, this formalism is only valid for elastic scattering of electrons. One can rewrite the Green's function in a matrix formulation using the notation mentioned towards the end of last section 3.2 as:

$$G(E, \epsilon) = [E \times S - H_{mol}(\epsilon) - \Sigma_l(\epsilon) - \Sigma_r(\epsilon)]^{-1} \quad (3.14)$$

E is the injection energy of the tunneling electron, $H_{mol}(\epsilon)$ is the molecular part of the orthogonalized Hamiltonian matrix obtained from $H(\epsilon)$ in equation 3.13, and S is an identity matrix. $\Sigma_{l,r}(\epsilon)$ (previously called as $\Sigma_{L,R}$) are the bias-dependent self-energy functions^{56,57}, which depict the molecule-contact interactions. The expressions for $\Sigma_{l,r}(\epsilon)$ are:

$$\Sigma_{l,r}(\epsilon) = C_{l,r}^\dagger G_p(E) C_{l,r} \quad (3.15)$$

where $C_{l,r}$ (previously denoted as $V_{LR,CR}$ in equation 3.12) are the orthogonalized bias-dependent molecule-lead coupling matrices. Thus, in our calculations, the non-equilibrium nature of the electronic coupling between the molecule and the electrode is accounted for at each bias value; structural reorganization under bias is not considered. It is important to note that under non-equilibrium situation (i.e. in the presence of applied bias), structural arrangements at the molecule-lead interface cannot be expected to be the same as those under the equilibrium condition. However, for a strongly coupled molecular junction that is considered here, a mass-scale rearrangement of atoms at the interfacial geometry is not expected to occur. G_p , the Green's function of the lead (Au), was previously defined as G_L and G_R for the left and the right electrodes respectively. But here the left and the right electrodes are made of the similar atoms (Au) and thus $G_L = G_R \equiv G_p$. Being an implicit function of injection energy E it is defined as:

$$G_p(E) = -i\pi\eta(E) \times I \quad (3.16)$$

I is an identity matrix of dimension $m \times m$; m is the total number of Gaussian basis functions used to represent the Au atoms in the active region of the device. $\eta(E)$ is obtained from the density of states (DOS) of the bulk Au, which is calculated using the periodic DFT implemented within the VASP code⁵⁸. The probability of electrons pumped into the system from the source reaching the drain is determined by the bias dependent transmission function, which is a summation of the transmission probabilities over all conducting channels, and is calculated as^{56,57}:

$$T_{lr} = \text{Tr}[\Gamma_l G \Gamma_r G^\dagger] \quad (3.17)$$

where $\Gamma_{l,r}$ are the broadening functions, which determine the escape rate of electrons; they are given by:

$$\Gamma_{l,r} = i[\Sigma_{l,r}(\epsilon) - \Sigma_{l,r}^\dagger(\epsilon)]. \quad (3.18)$$

Finally, within the coherent scattering approximation, the current through the molecular junction is calculated using the multi-channel Landauer-Büttiker formalism^{56,57,59,60}. In this approach, the expression for the current is:

$$I = \frac{2e}{h} \int_{\mu_1}^{\mu_2} T_{lr} [f(E, \mu_2) - f(E, \mu_1)] dE, \quad (3.19)$$

where f is the Fermi distribution function. $\mu_{1,2}$ is calculated as:

$$\mu_{1,2} = E_f \mp V_{low,high}, \quad (3.20)$$

The $V_{low,high}$ is calculated self-consistently for each applied ε using the difference between the electrostatic potentials¹⁰³ at finite and zero bias at the two metal-molecule junctions; E_f is the equilibrium Fermi energy. The potential difference, V , is obtained from the difference of V_{low} and V_{high} for each applied ε . It should be noted that at equilibrium (zero bias) $V_{low}=V_{high}$. An additional thermal smearing term, $k_B T$ ($=0.026$ eV) is subtracted from μ_1 and added to μ_2 to take into account the electronic temperature at the contact in the non-equilibrium condition; it essentially increases the integration window width by an additional constant of 0.052 eV for each applied bias.

3.2.2 Incoherent Transport

Now the scheme is modified to include the phase-breaking scattering of electrons but within the same elastic transport formalism. Büttiker's multi-probe approach^{56,65,126}, is used to include the phase randomization. In this approach an imaginary third electrode is assumed to be present; electrons injected from the source reach the sink via this fictitious probe as shown in Fig. 3.3. Entering the pseudo-probe on its way to the sink forces the electron to lose its phase information. Thus, the contribution of the electronic current due to these electrons is the 'out of phase' current. It is important to note that the current in the third probe is zero, i.e the number of electrons going into the probe is same as the number coming out of it, thus rendering the name 'pseudo' probe. The effect of the third probe is included

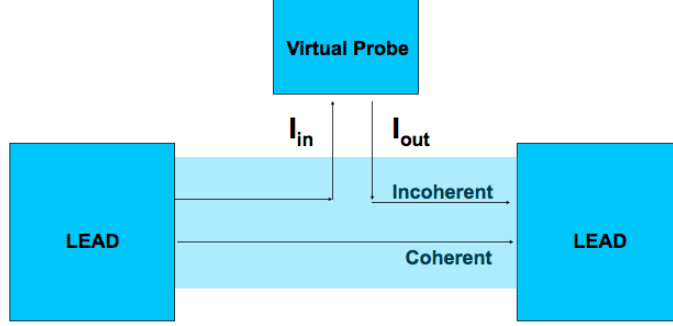


Figure 3.3: Büttiker's multiprobe approach to incoherent but elastic transport. Adapted from the book “Electron Transport in Mesoscopic Systems” by S. Datta⁵⁶.

into the formalism with the help of an additional self-energy term to $G(E, \epsilon)$. The modified Green's function can now be written as⁶⁵:

$$G(E, \epsilon) = [E \times S - H_{mol}(\epsilon) - \Sigma_l(E, \epsilon) - \Sigma_r(E, \epsilon) - \Sigma_{e-ph}(E, \epsilon)]^{-1} \quad (3.21)$$

where the new term Σ_{e-ph} is the additional self-energy function which accounts for the phase-breaking scattering. Since electron-phonon interactions are one of the main sources of dephasing or phase-breaking, the additional self-energy can be thought to arise from the interaction of conduction electrons with the molecular vibrations. Thus, the brute force

method of computing Σ_{e-ph} would require the determination of the density of states of the phonon modes for each energy(E). An alternative method of determining Σ_{e-ph} would be to recourse to the Datta's model,^{65,131} where $\Sigma_{e-ph} = D_{e-ph}G$; D_{e-ph} is a scalar dephasing parameter with the unit of (energy²). It is estimated from the average coupling energies between the vibrational modes and the electronic energy levels. Since Σ_{e-ph} depends upon G and vice-versa, they are determined self-consistently at each injection energy within each bias point. Thus even though D_{e-ph} is kept constant for the current calculations, the bias effect is incorporated self-consistently in Σ_{e-ph} through G . More over, even if we use a constant for D_{e-ph} , as the dimension of the matrix increases with the increase in length of the oligomer, the strength of dephasing increases. The expressions for $\Sigma_{l,r}(\epsilon)$ and G_p can be determined as before from equation 3.15 and equation 3.16 respectively. The escape-rate of the electrons from one electrode to the other is determined by the broadening function defined as:

$$\Gamma_{l,r,e-ph} = i[\Sigma_{l,r,e-ph}(\epsilon) - \Sigma_{l,r,e-ph}^\dagger(\epsilon)]. \quad (3.22)$$

In a two probe system, the ‘in-phase’ current can be described by the bias dependent transmission function given by equation 3.17. However, for modeling the “out of phase” electronic current using Büttiker's multi-probe approach^{56,65,126}, equation 3.17 is not enough. The transmission function now has to include both the “in-phase” and the “out of phase” current and is given by:^{56,57,59,60}

$$T_{12} = T_{lr} + \frac{T_{(e-ph)r}T_{(e-ph)l}}{T_{(e-ph)r} + T_{(e-ph)l}} \quad (3.23)$$

T_{lr} is the transmission contribution due to “in-phase” transport of electrons from the source to the sink. The second term in equation 3.23 is due to the ‘phase-breaking’ transport. It is derived by exploiting the boundary condition that there is no net current flowing into or out from the fictitious probe. T_{lr} , $T_{(e-ph)l}$, and $T_{(e-ph)r}$ are calculated using equation 3.17. The total current is then obtain by integrating the transmission function over all injection energies, within the Landauer-Büttiker regime:

$$I = \frac{2e}{h} \int_{\mu_1}^{\mu_2} T_{12} [f_2(E, \mu_2) - f_1(E, \mu_1)] dE, \quad (3.24)$$

where $f_{1,2}$ are the Fermi distribution functions at the two electrodes; $\mu_{1,2}$ are the chemical potentials at the electrodes. The integration in equation 5.1 should ideally include all possible injection energies, which is not feasible. Moreover, the functions f_1 and f_2 become almost identical when one goes far away from the tail of the Fermi distribution function i.e outside $\mu_1 < E < \mu_2$. So, the integration is restricted to the states between μ_1 and μ_2 which have the highest probability of contributing to the net electronic current across the device. This summarizes the complete picture of the formalism which will be used in the next few chapters to study some molecular scale devices.

Chapter 4

Revisiting the Au/BDT/Au junction.

4.1 Introduction

Since the ground-breaking measurement of current across a single molecular junction⁵, researchers have taken a lot more interest delving into the subject with the promise of building nano-devices with molecules. One of the primary concerns of researchers is the reproducibility of the experimental observations which ensure its reliability and sustainability when used as an electronic device or at least as a component of an electronic device. Already, several single-molecule conductance measurements⁶⁻¹² have been reported with a fair amount of success. These premier experiments created the thirst for understanding the underlying physics behind the electron transport characteristics across molecular nano-

junctions. Being “nano-systems” *ab-initio* method would arguably be the best approach to study these type of systems. Various research groups across the world have used diverse “first-principles” schemes to study these systems with varying degrees of success.

A prototype system of this category consists of an organic molecule sandwiched between two semi-infinite metallic electrodes. Bulk Au or Pt are the most commonly used electrode materials. It has been observed that the presence of an anchoring group facilitates the formation of a metal-molecule bond. Studies on the effect of various anchoring groups on the binding strength of metal-molecule junctions reveal that thiol (-S-) end groups along with Au electrodes form the most stable junction^{12,61,62}. Such is the strength of the S-Au bond that the stretching of the metal-molecule junction actually results in stretching of Au-Au bonds. This creates a Au nanowire before finally snapping off the Au-Au bond. This was first predicted by Molecular Dynamics(MD) calculations⁶³ and later observed experimentally⁶⁴. So, now the question is - how the atoms of the anchoring group and its neighboring electrode atoms are arranged? Statistical analysis of all single-molecule conductance measurements clearly indicates peaks^{10,11} corresponding to different values of conductance, which are attributed to different contact structures. Thus, the control over the fabrication of a certain type of contact becomes very challenging. But the ability to create single molecule junctions brought in a lot of excitement to this field and thus theoreticians started to investigate the underlying physics behind the flow of charge through these nano-scale junctions. It is a big challenge to model these open systems as they consist of both finite (molecule + anchoring group) and semi-infinite (electrode) pieces. Various theoret-

ical schemes have been applied to model both the finite and the semi-infinite parts. One of the earliest approaches in modelling current flow through these devices centered around the simple assumption that the electrostatic potential of the finite piece is constant and that its value is half-way in between the chemical potential of the leads on both sides⁵². The molecule-electrode distance and the equilibrium Fermi energy is adjusted so that the theoretical and the experimental value of the current through the junction is of the same order⁶⁵. Using this scheme within the Non-Equilibrium Green's Function (NEGF) formalism Damle *et al.*⁶⁶ calculated current and conductance through Au/Benzene-1,4-Dithiolate(BDT)/Au system. But they could not reproduce the two “resonant tunneling peaks” in the conductance curve as observed experimentally. The binding site of the anchoring group(-S-) to the electrode(Au) was shown to have a big influence in the transport characteristics of the same system⁶⁷. Thereafter, Density Functional Theory(DFT) in combination with time-dependent perturbation theory and Mulliken population procedure was used to study the electrical conductance of the same system⁶⁸. The calculated current was of the same order as that of the experimental results⁵ only for external voltages in between 0-3 V but there was little qualitative agreement. Reasonably accurate modelling of the electrodes which are semi-infinite systems is a pretty complicated task. Instead of using standard bulk Au properties, the electrodes were treated by the tight binding approach⁶⁹ within the Newns-Anderson model⁷⁰. The Lippmann-Schwinger scattering approach with the electrodes being modelled by the jellium model^{71,72} was also used in several attempts to model these nano-systems. This model was tested by studying the *I-V* characteristics of BDT placed in

between two Au electrodes. The current-voltage curve⁷¹ agreed well qualitatively with the experimental curve⁵ but the current values were three orders of magnitude more than that measured experimentally. It was also argued⁷¹ that the insertion of Au atoms in between the BDT and the electrodes will decrease the current by two orders of magnitude. But later on, it was reported that adding more gold atoms in between the electrode and the BDT actually increases the current through the junction⁷³. So the quandary remained unsolved. Hybrid DFT has also been used in modelling these kind of molecular devices^{74,75}. The periodic supercell approach involving open boundary conditions for matching the Kohn-Sham potential at the interface has also been used to model nano-junctions⁵³. The difficulty with this approach, however, is that the interaction of the supercell atoms with their periodic image causes the system to fail to represent the nature of a true single-molecular device. So, the contact structure still kept the theoreticians interested. In another attempt the contact was modelled by the electrode atom being connected to the molecule at one end and the other end being connected to the bulk electrode⁷⁶. Since these are multi-electron systems, a more realistic approach would be the many-body approach. With this approach, for low external bias, the magnitude of the calculated current values⁷⁷ were pretty close to those obtained experimentally⁵, but the two did not match for higher biases. Several groups tried to improve upon the scheme of calculating the molecular eigen-states so far done using Local Density Approximation (LDA) or Generalized Gradient Approximation (GGA) methods within DFT. Self-interaction corrections^{78,79}, calculated self-consistently, were introduced. Improved exchange-correlation functionals were incorporated^{80,81}, which re-

sulted in agreement of low-bias current with the measured values. Dynamical correlation corrections were introduced within the LDA-DFT⁸² and proved to be a major contribution to the quantum resistance when a molecule is attached to the electrode. The *GW* approach has shown significant promise when applied to studying these nano-contacts^{54,83}. A piece-wise thermal equilibrium approach based on first-principles calculation produced values of current and conductance, same order as the experimental ones, but only for a bias range of 0-1.5 V⁸⁴. Varga *et al.*⁸⁵ used NEGF but added an imaginary Dirac-Delta potential to the Kohn-Sham Hamiltonian to replicate the electrodes. So far the contact structure still remains illusive. Very recently, with the help of MD simulations, it was shown that the contact (molecule-electrode) structure is stochastic and that the conductance value changes by orders even when there is a slight ($\sim 0.2\text{\AA}$) change in distance at the atomic level⁸⁶. Recently a new approach has been reported in which the current through the molecular junction was calculated in the presence of a few excited states⁸⁷ of the molecule. Some recent review articles⁸⁸⁻⁹² which summarize the field of “Quantum Transport” in a molecular junction have also been published.

Bottomline, nobody has a concrete, robust scheme to determine the experimental contact geometry required for the quantitative prediction of transport characteristics in a molecular scale junction. This proved to be one of the major hurdles in replicating the experimental current-voltage features through the theoretical calculations. In this project⁹³, the quandary of the unknown contact structure is addressed by viewing it from a different angle. The term in the transport equation affected by the contact structure is singled out, and a scheme is

devised to make a better quantitative estimate of that term by exploiting a certain result in a typical Mechanical Controlled Break Junction (MCBJ) experiment. The term singled out is the self-energy of the leads. The well-known result in a MCBJ experiment is that the current through the junction suddenly increases by at least an order when a molecular pathway is created in-between the two electrodes, is exploited. To incorporate this into the self-energy, a multiplicative weighting factor ω is added, which is determined using the fact that the current through the device in the absence of the molecule is negligible when compared to the current in the presence of a molecular pathway. This value of ω is used to estimate the self-energy of the leads at different biases. Using this self-energy, current through the metal-molecule junction is calculated within the single particle Green's function approach. In the next few sections details of the computational approach and the results obtained are described.

4.2 Computational Details

The *active region* consists of a BDT molecule sandwiched in between two clusters of 3 Au atoms. A real space approach is used in which the many-body wavefunction of the electron is expanded in terms of a finite set of Gaussian atomic orbitals⁴⁸. DFT poses a well-known built-in problem of demanding the exact exchange; this plays a significant role in determining accurate energy levels in the *active region* and hence the current through

the molecule/electrode junctions. Dynamical correlation corrections to the exchange functionals have already been proposed,⁸² but it often ends up estimating a wrong band-gap especially for semi-conductor insulators. In our approach we have used the hybrid Becke's three parameter functional(B3LYP)^{48,50} approach within DFT, which uses a part of the exact Hartree-Fock exchange. Hence this approach treats to a huge extent, the drawback of self-interaction errors within conventional DFT. The Los Alamos double zeta effective core potential(LANL2DZ)⁴⁸ basis set, which includes the scalar relativistic effects. We have used tight convergence criterion throughout our calculations which sets 10^{-6} , 10^{-6} , and 10^{-8} a.u. as the convergence criterion for energy, maximum, and root mean square electron density respectively. The Green's function is calculated using the Kohn-Sham Hamiltonian matrix which has an implicit dependence on the applied electric field as described in equation 3.13. The Green's function which was initially defined in equation 3.14 is now modified to include the weighting factor ω and is defined as:

$$G(\epsilon) = [E \times S - H_{mol}(\epsilon) - \omega \times \Sigma_l(\epsilon) - \omega \times \Sigma_r(\epsilon)]^{-1} \quad (4.1)$$

E is the injection energy of the tunneling electron, $H_{mol}(\epsilon)$ is the orthogonalized Kohn-Sham hamiltonian matrix obtained from $H(\epsilon)$, and S is the identity matrix. $\Sigma_{l,r}(\epsilon)$ are the self-energy functions^{56,60} (defined in equation 3.15) calculated from the bias-dependent coupling matrices and the Green's function for the Au leads. The Green's function for the Au leads, which is kept fixed for all bias points, is approximated from the Density of States(DOS) at the Fermi level of the 6s band in bulk Au⁹⁵. ω is the additional weighting

factor introduced in this approach. This factor is calculated while employing the boundary condition that negligible current (\sim nA) flows between the electrodes in the absence of the molecular pathway. Hence, this factor takes us closer to an accurate estimation of the realistic self energy in the experimental situation. The transmission function and the current is calculated using equations 3.17 and 3.19 respectively.

4.3 Results

The first section will deal with the junction-structure that we have studied. In the second part, we will show the importance of estimating an accurate self-energy of the leads while calculating current and conductance across the molecular junction.

4.3.1 Structural effects

Inspite of the number of available sophisticated instruments for imaging nano-structures, it is practically impossible to obtain the atomic level structural details of the metal-molecule junction. Things become more complicated when an external field is applied because it destroys the equilibrium of the contact configuration. The organization of the electrode

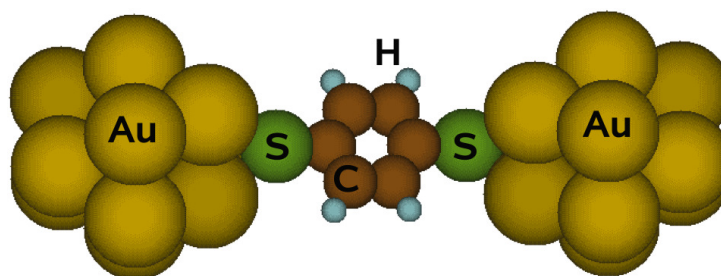


Figure 4.1: Schematic of a Benzene-1,4-dithiolate prototype junction⁹³.

and molecule atoms at the contact in a non-equilibrium situation can not be expected to be the same as that under equilibrium conditions. On the other hand, mass-scale rearrangement of the contact atoms supposedly does not occur. This assumption does not seem to be far off as different theoretical groups have used various equilibrium contact structures and had considerable success in explaining some of the experimental findings^{65,71,76,85}. Amongst them, some have concluded that the molecule is not coupled strongly to both of the junctions⁶⁵. It is also argued that the anchoring thiol (-S-) group at the end of the molecule is bonded to a single Au atom⁷⁶. Calculations that assume interaction of S with more than one Au atom of the electrode do not seem to agree with the experimental results. Surprisingly, a

substantial amount of qualitative agreement is achieved even when the atomic level structural details of the contact are ignored by representing the electrodes with uniform-electron gas⁷¹ or with a Dirac-Delta potential⁸⁵. Lately, it has been proposed that the contact structure is probably stochastic⁸⁶ which practically rules out any particular time-independent contact geometry. Theoretically it is not feasible to deal with stochastic contact structures under non-equilibrium conditions, but one can always manage the non-equilibrium nature of the contact coupling at the electronic level. This is exactly what we have done in our work. We do not consider the structural changes at the metal-molecule junction when the external field is applied, but the electronic energy level rearrangement under external field has been taken into account within the DFT framework. The equilibrium structure is obtained by applying optimization techniques while keeping the Au atoms fixed and allowing the molecule along with the anchoring thiol group to relax. It is found that the structure in which the S is in the three-fold hollow site but is closer to one of the three Au atoms to be energetically favourable. The current and the conductance calculations are done using this structure. The schematic structure is given in Fig. 4.1.

4.3.2 Field dependent Potential Profile

To simulate the effect of external voltage on the molecule, an external electric dipole field is applied along the axis of the molecule as discussed in Section II. The field dependent

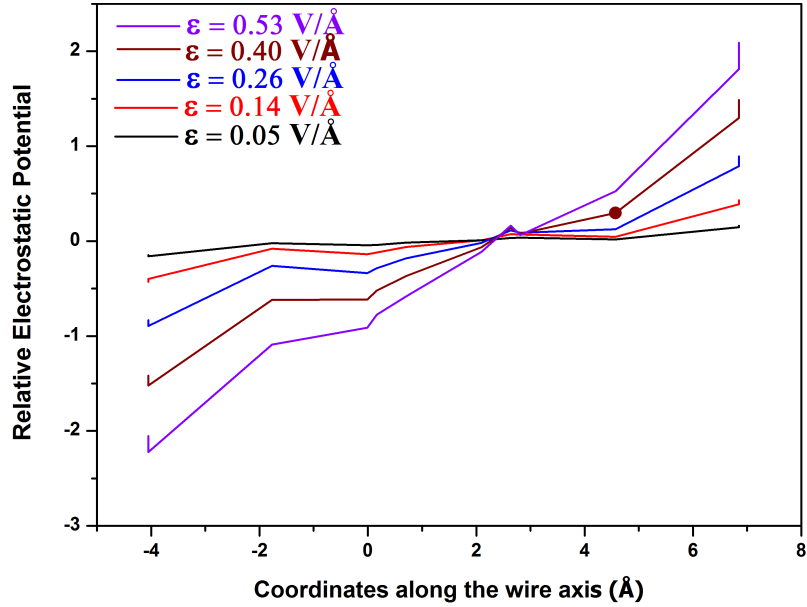


Figure 4.2: Potential profile along the axis of the molecule (Basis set: 6-311G*)⁹³.

potential profile across the active region of the device is plotted in Fig. 4.2. It is interesting to note that there is a substantial amount of change in the electrostatic potential profile within the molecule as the external bias increases. Earlier assumptions have incorporated the potential change at the metal-molecule junctions only and have neglected the potential gradient across the molecule⁵². Infact, the majority of current calculations have been carried out using the zero bias Hamiltonian with the argument that the coupling between the molecule and the electrode is very weak and hence the external field will have negligible effect on the eigen-spectrum^{65,87} of the device's active part. However, our plot shows that the potential gradient across the molecule is not negligible. Thus, it is essential to include

the external field explicitly within the Hamiltonian of the active region of the device for every bias point. The other aspect to note is that the potential profile is slightly asymmetric even though the geometric profile is identical at the two junctions. For e.g, at a field strength of $\varepsilon = 0.05 \text{ V/\AA}$ the lead-molecule junction on the left in Fig. 4.2 is at 2.11 V whereas the right junction is at 1.90 V. It is also noted that the asymmetry increases with an increase in the strength of the electric field. This is due to the presence of the electric dipole term in the Hamiltonian which breaks the symmetry of the wave function; consequently an asymmetric potential drop is noted with increasing the strength of the dipole field. What follows is that the chemical potential at the metal-molecule junctions is now computed self-consistently for each and every bias point. As a result, the changes in the chemical potential with an increase or decrease in external voltage is accounted for more accurately.

4.3.3 Current and Conductance Features

To determine the current-voltage feature of the BDT junction, we need to determine the weighting factor ω mentioned in Section 4.1 and Section 4.2 . How important is ω ? We performed a current and conductance calculation without incorporating ω in eqn. 4.1 i.e for $\omega = 1$. The results (in Fig 4.3) predict a single broadened peak in the conductance curve unlike the experimental findings⁵. The following calculations will reveal the importance of

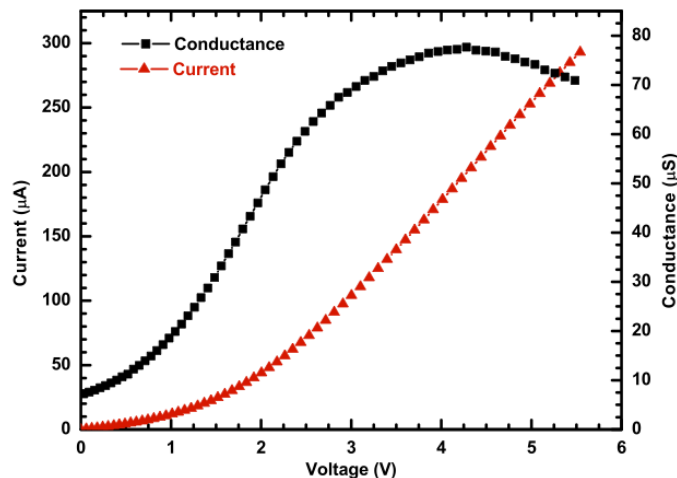


Figure 4.3: Calculated Current-Voltage and Conductance-Voltage characteristics ($\omega = 1$; Basis set: 6-311G*)⁹³.

ω . The weighting factor ω in eqn. 4.1 is obtained using the fact that the current through the junction at a finite external bias should be negligible or atleast an order less when the BDT molecule is absent. The value of ω is found to be 0.0015. With this value of ω and for an external voltage of 0.182 V, the current in the absence of BDT is 17.5 nA whereas in the presence of BDT the current is ~ 400 nA. The current in the absence of BDT is modelled by calculating the current for a pseudo-molecule junction consisting of only the two Sulphur atoms of the BDT placed in their respective positions. By doing this we expect to make a better estimate of a realistic S-Au coupling. This is required to reduce the screening error caused from the finite size of the Au cluster used in the active part of the device region

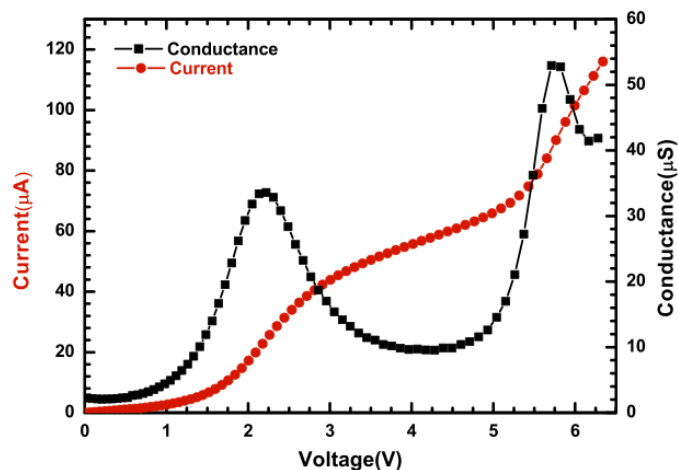


Figure 4.4: Calculated Current-Voltage and Conductance-Voltage characteristics ($\omega = 0.0015$; Basis set: 6-311G*)⁹³.

when estimating the molecule-lead coupling. Subsequently, we have calculated the current and conductance of the BDT junction as a function of applied bias; these are plotted in Fig. 4.4. To facilitate the comparison of various theoretical approaches, we have tabulated the results of the original experiment and some earlier theoretical results in Table 4.1. The abbreviations for LBC, V-1, V-2, C-1, C-2, are ‘Low bias conductance’, ‘Voltage corresponding to the first peak’, ‘Voltage corresponding to the second peak’, ‘peak value at the first peak’, ‘peak value at the second peak’ respectively in Table 4.1. It is evident that the LBC value of $2.28\mu\text{S}$ obtained in our calculation is relatively close to the experimental value⁵ and most of the reported theoretical LBC values. The first “resonant tunneling

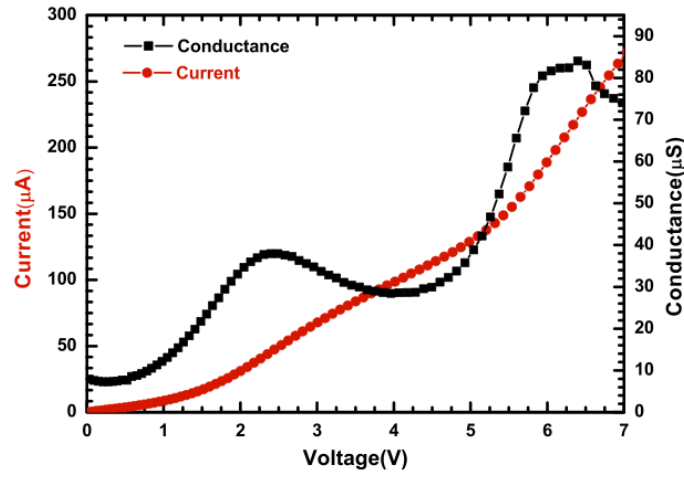


Figure 4.5: Calculated Current-Voltage and Conductance-Voltage characteristics ($\omega = 0.003$; Basis set: 6-311G*)⁹³.

peak” which occurs in the conductance curve of the original experiment⁵, has been reproduced in a number of theoretical approaches. However, that is not the case for the second “resonant tunneling peak”. Only three (including ours) of the schemes listed in Table 4.1 have reported the second peak. All of them predict the peak conductance values atleast a couple of orders higher than the experimental values. Similarly, our calculations resulted in an over-estimation of both the voltages at which the peak occurs and also the magnitude of conductance at those voltages. The first conductance peak of our calculation and that of ref.[29] are relatively closer to the experimental value, but the second conductance peak in our calculation is at a higher voltage than what is observed experimentally. The peak

Table 4.1
Synopsis of experimental and theoretical results⁹³

Method	LBC(μ S)	V-1(V)	V-2(V)	C-1(μ S)	C-2(μ S)
Experiment ⁵	0.003	1.6	4.7	0.045	0.079
DFT + Jellium ⁷¹	3	2.9	4.8	18	33
DFT + Dirac-Delta ⁸⁵	1.25	2	4	9	22.5
DFT + Bulk States ⁷³	5	1.5		15	
TransSIESTA ⁹⁶	35				
Bias-dependent DFT ⁹⁷	5	1.6		30	
thermal equilibrium ⁸⁴	0.0062	0.8		0.05	
Many-body ⁷⁷		2.5		3.0	
**symmetric(this work)	1.73	2.23	5.51	25.71	59.37

heights we obtained are of the same order as the results obtained from previous theoretical calculations. The disagreement in the voltage (experimental and theoretical) at which the resonant tunneling occurs is probably due to the failure of replicating of the realistic unoccupied energy levels of the device's active region at higher biases; this can be corrected by using the computationally intense GW^{54,83}, Coupled Cluster(CC)⁹⁸ or Configuration Interaction(CI)⁹⁹ or MP2¹⁰⁰ approach. The difference of 2 or more orders in the magnitude of the conductance values is again due to the *indeterminable* contact structure in the experiments. In other words, this suggests that the contact structure we have considered may not be the true representative of the contact structure in the experimental case. Moreover, even if the choice of the magnitude of the negligible current through the junction in the absence of the BDT can be made arbitrarily small in our calculation ensuring negligible direct transmission in the nano-gap, we may not obtain the exact self-energy. Now the question arises: How does ω influence the transport characteristics ? We do see changes in the transport

characteristics when we use a different ω . For e.g for $\omega = 0.003$ (Fig. 4.5), there is a slight shift in the conductance peaks. They are now at 2.4 V and 6.4 V with conductance values of $0.49 G_0$ and $1.08 G_0$ respectively. With a smaller ω of 0.0001, the conductance curve shows two peaks that are sharper than the ones previously obtained. The two peaks occur at 2.13 V and 5.71 V which are almost the same as those obtained with the $\omega = 0.0015$. The sharp peaks essentially reflect the molecular features. To understand whether or not the two conductance peaks are intrinsic to the molecule, we used an arbitrary self-energy in eqn. 4.1 (an imaginary diagonal matrix with 0.025 as the diagonal elements) to recalculate the I vs. V and dI/dV vs. V characteristics. This ensures the absence of the realistic non-equilibrium molecule-electrode coupling at the electronic level. Our results indeed show two peaks in the conductance curve at 2.3 V and 5.15 V with peak values of $1.22 G_0$ and $1.87 G_0$ respectively. It can be concluded that the two peaks seem to be predominantly a feature of two broadened energy-levels of the BDT molecule in resonance with the Fermi energy of the lead. This also further explains why various groups were successful in obtaining a qualitative agreement despite ignoring the atomic level structural details of the contact.

In the approach described so far, the current and conductance values are dependent on the parameter ω . Also, the method for the determination of ω is not well defined. A parameter free formalism to calculate transport properties is desired. In the next section, a modification of the current calculating scheme is described which is parameter independent.

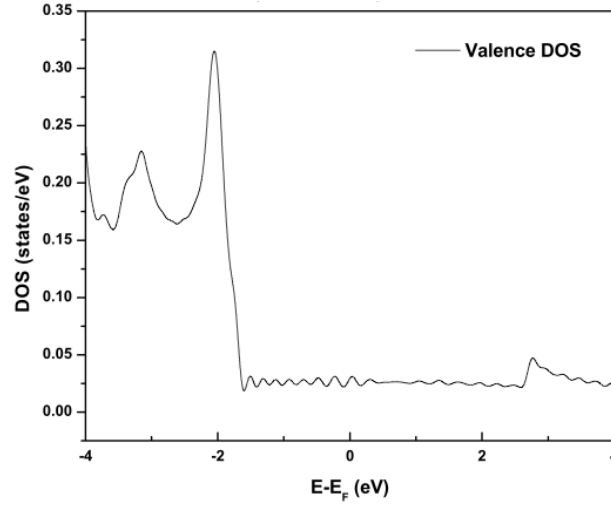


Figure 4.6: DOS of bulk Gold.

4.4 Modification to a parameter free approach

In this section we used a modified expression for the Green's function of the lead. The rationale behind this being that the atomic level structural details of the lead being undeterminable. Whether the lead has a electronic property of a bulk, surface, or 1-D system is not unknown. So, we recalculate the I-V characteristics for the same nano-junction using three different electronic structural properties of the lead, namely bulk, surface, and wire. Previously, the Green's function of the lead was calculated using the bulk DOS at the Fermi

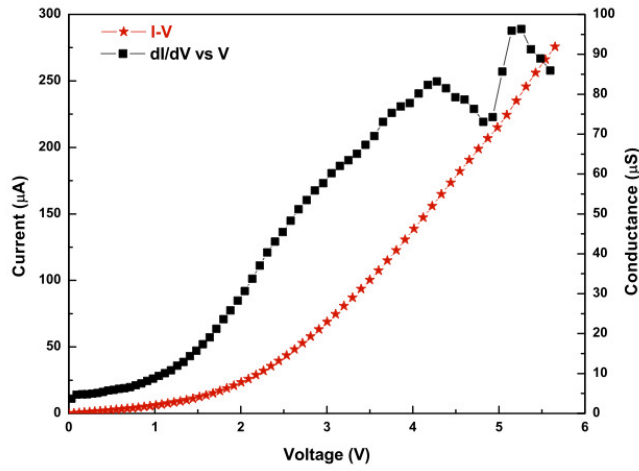


Figure 4.7: I-V characteristics of Au/BDT/Au junction with bulk Au Green's function and 3 Au atoms on each side of the molecule.

level which is a constant number($=0.035$ states/eV). Now, the Green's function of the lead is a function of energy i.e the variation of DOS with respect to energy is taken into account in equation 3.16. First let us look at the DOS as a function of energy in bulk Au, which is calculated using a periodic supercell approach within VASP⁵⁸. We have used a plane wave basis function and density functional theory within generalized gradient approximation for the exchange-correlation. The core electrons are represented by the ultra-soft pseudo potential. The 11 valence electrons for each gold atom undergoes the all electron calculations. The valence-core interaction is described by the projector-augmented wave (PAW) approach. Thus the DOS obtained from this calculation is basically the valence

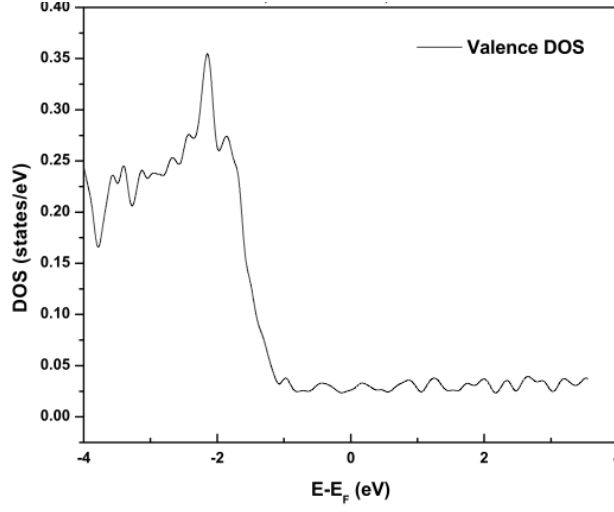


Figure 4.8: DOS of a simulated Gold surface.

DOS. The optimized lattice parameter for the fcc gold is found to be 4.175 \AA . To calculate the DOS, we have used $61 \times 61 \times 61$ k-point sampling within the Monkhorst-Pack scheme to sample the Brillouin zone. The robustness of the k-point sampling is tested by comparing the energy of the system for different k-points (the energy convergence criterion with respect to the choice of k-points was less than 0.001 eV). The value for $\eta(E)$ is calculated as DOS(E) per electron in the unit cell. The energy grid (0.002 eV) is taken as the same grid used for the integration in eqn. 3.19. Fermi energy of the bulk gold is aligned with the Fermi level of the active region of the device at equilibrium ($V = 0$). The bulk DOS is plotted in Fig. 4.6. The contribution to DOS around the Fermi level comes mostly from

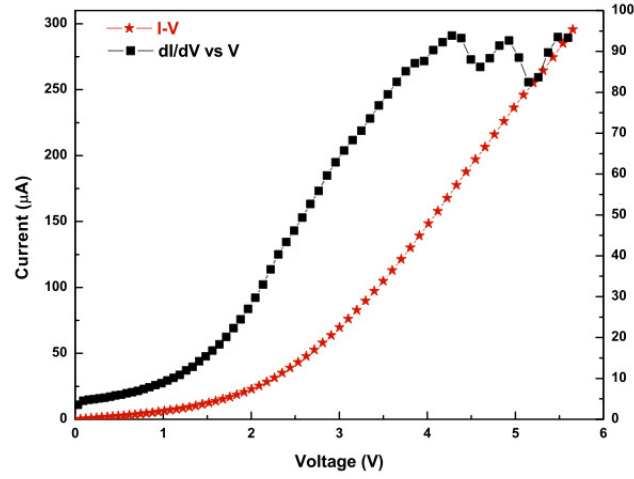


Figure 4.9: I-V and conductance characteristics of Au/BDT/Au junction with Au surface DOS.

the s-orbitals. This is reason behind the initial choice of s-density of states at the Fermi level in equation 3.16. But, away from the Fermi level d-orbitals start to contribute to the DOS. With this new method, the Green's function of the lead (G_p) is now a function of energy and takes into the change in the DOS with energy. The calculated current (Fig. 4.7) with the new lead Green's function is of the same order of that obtained in calculations in the previous section. However, the conductance plot reveals two peaks at ~ 4.0 V and 6.0 V. Also, the conductance curve is now more ragged than before due to the fluctuations in the DOS of the lead. Thereafter, the same calculations were done using surface DOS of the lead. The surface DOS for Au is also calculated by creating a supercell in VASP.

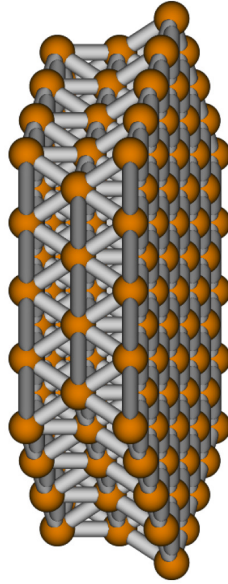


Figure 4.10: A supercell of the Gold nanowire to calculate the 1-D DOS.

The kpoints used for this calculation is $61 \times 61 \times 1$ with a Monkhorst-pack scheme. The surface DOS which is very similar to the bulk DOS qualitatively is shown in Fig. 4.8. The only difference is in the peak height of DOS which is around 2 eV from the Fermi level. The value is 0.35 states/eV for the surface where same value is ~ 0.325 states/eV for bulk Au. The I-V and the conductance characteristics, shown in Fig. 4.9 has now become more rugged as expected. The height and the position of the conductance peaks do not change. Since both the surface and the bulk lead DOS did not have much effect on the I-V and the conductance characteristics we recalculated the same quantities using a 1-D DOS for the lead. The 1-D DOS for Au is calculated by simulating an infinite Au nanowire consisting

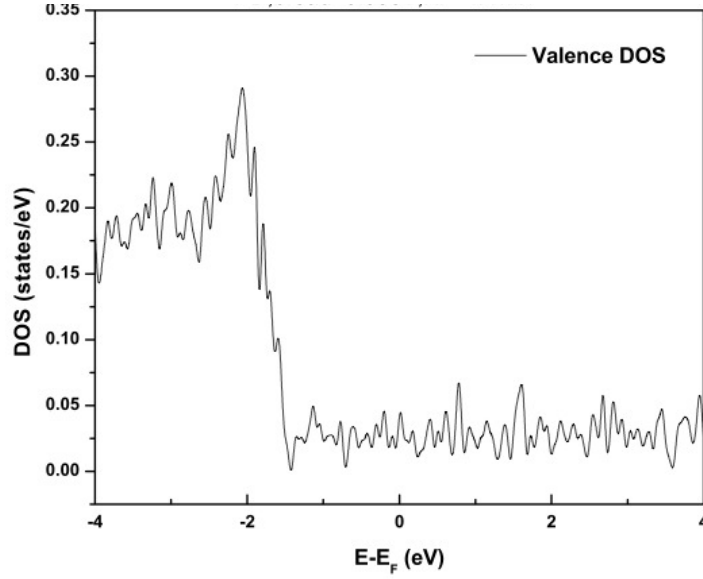


Figure 4.11: 1-D DOS of Gold nanowire whose supercell is given in Fig. 4.10.

of 157 Au atoms. The supercell to build the Au nanowire is shown in Fig. 4.10. The wire is infinitely long in the z-axis. The wire is prevented from interacting with its images by keeping the supercell 50Å long in the x and y directions. The DOS for the Au nanowire is plotted in Fig. 4.11. It is similar to the bulk and the surface DOS but has more fluctuations due to the quantum confinement effects. The I-V and the conductance characteristics also is similar to the ones with the bulk and the surface DOS. This is expected since there is similarity between the bulk, surface and 1-D wire DOS.

A more realistic approach to model an electrode would be to include the more number of lead atoms in the *active* region of the device. So, in this section we study the I-V and the

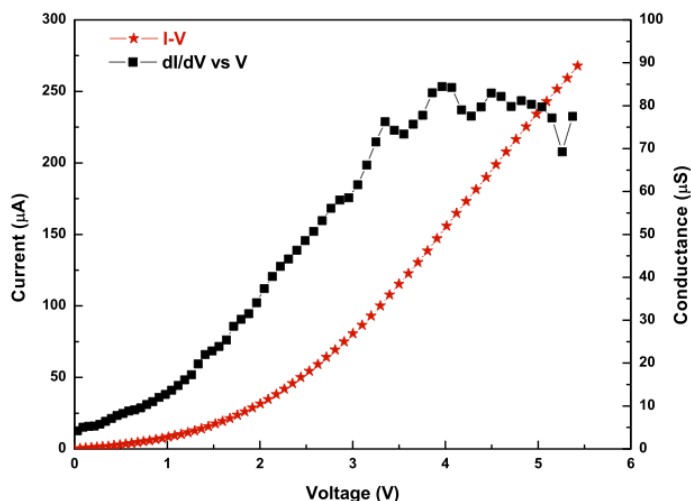


Figure 4.12: I-V characteristics of Au/BDT/Au junction with nanowire Au Green's function and 3 Au atoms on each side of the molecule.

conductance characteristics of the same molecular device but with 13 Au atoms on each side of the molecule. In this calculation, the molecule along with the 13 Au atom cluster on each side is first optimized using Gaussian G03. It is observed that the 13 Au atom cluster retains its bulk structure but the S-Au distance decreases. As before, the S atom is seen to get closer to one of the nearest Au atom. This structure has also been obtained in previous theoretical calculations¹⁶⁴. The inclusion of the 13 Au atom cluster on either side of the molecule increases current and conductance of the device by almost an order as seen in Fig. 4.13. The purely molecular orbitals are now renormalized due to the presence of the 26 Au atoms. More over there is considerable spill-over of the atomic orbitals of Au

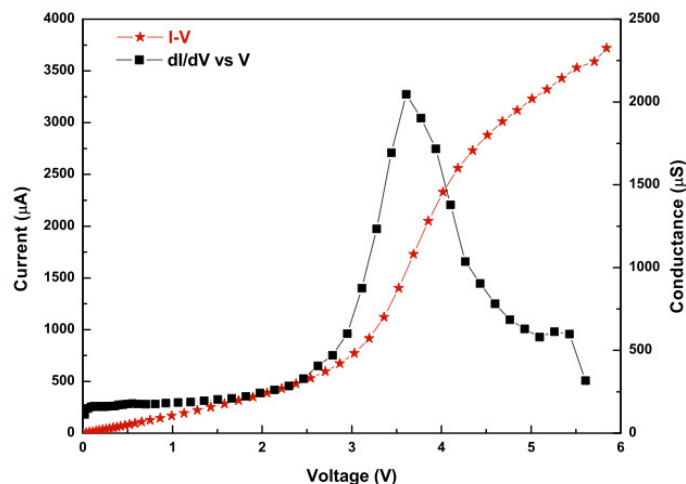


Figure 4.13: I-V characteristics of Au/BDT/Au junction with bulk Au Green's function and 13 Au atoms on each side of the molecule.

into the molecule which is responsible for the increase in the transmission and the hence current and conductance. Also now, there is prominent sharp peak in the conductance curve around 3.5 V which was around 4.5 V with 3 Au atoms. When the current and conductance is calculated using the surface DOS I-V characteristics remains similar as has been the case before. The magnitude of current and conductance is of the same order, as shown in Fig. 4.14 but the curves become more rugged. This ruggedness increase when 1-D DOS is used for the same calculations as seen in Fig. 4.15.

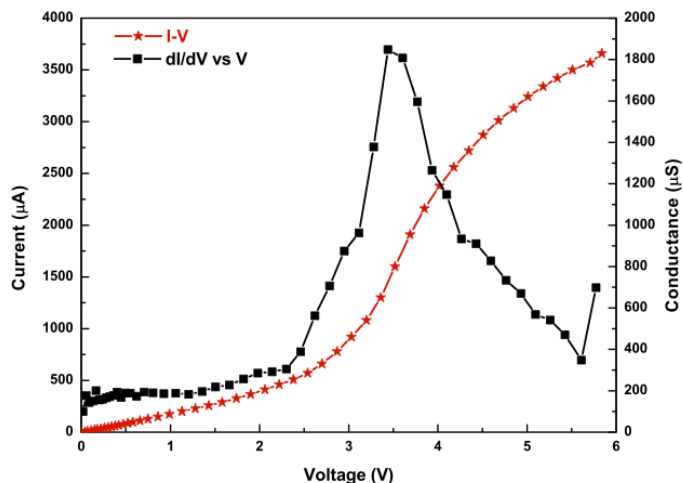


Figure 4.14: I-V characteristics of Au/BDT/Au junction with surface Au Green's function and 13 Au atoms on each side of the molecule.

4.5 Summary

To summarize, we found that the estimation of accurate self-energy of the lead portion of the electrode that replicates the experimental junction, is the most challenging task in theoretically modeling these devices. This problem can be remedied by multiplying a weighting factor to the self-energy term and thus exploiting the fact that there is negligible current in the absence of a molecular pathway between the electrodes as observed in MCBJ. We also stress that it is not possible to reproduce the experimental result quantitatively since it is

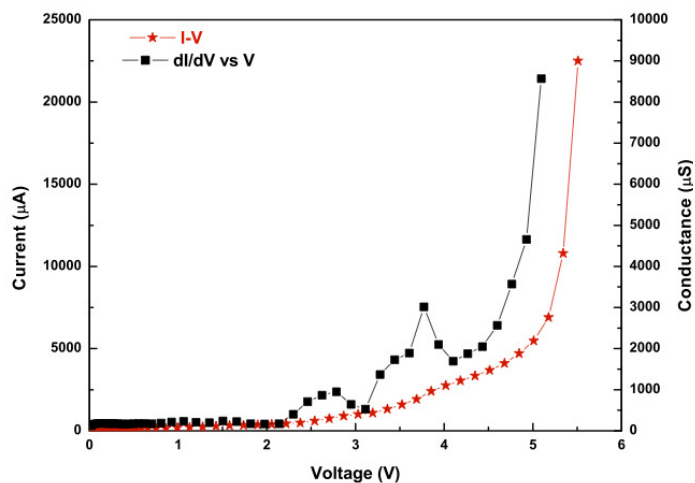


Figure 4.15: I-V characteristics of Au/BDT/Au junction with nanowire Au Green's function and 13 Au atoms on each side of the molecule.

difficult to identify the exact contact structure in the non-equilibrium condition. However, one can improve the theoretical schemes for modelling these devices by self-consistent evaluation of the non-equilibrium nature of the contact at the electronic level. This would include the self-consistent evaluation of the chemical potential and the inclusion the Stark-effect explicitly within the “extended molecular” Hamiltonian. The inclusion of DOS as a function of energy does not have a severe effect on the current and the conductance characteristics. With inclusion of more number of Au atoms in the active region of the device the magnitude of current and conductance increases by an order. This is due to a stronger spill over of the Au orbitals into the molecule which increases the transmission function quite

significantly. The 1-D, 2-D or 3-D DOS of the lead does not have any significant effect on the transport characteristics of the device. So, the issue of overestimating the current and conductance values for these type of molecular devices persists. A strongly coupled junction is the most probably the reason behind this disagreement. Lack of atomic level details of the contact structure does not help the cause either. To conclude, it would be very difficult to match the experimental values without including any external parameters such as the ω . To avoid this, we shifted our focus to studying the change in transport characteristics with increase in the length of the molecular spacer which is present in between the two electrodes. Since the calculations are done within the same model, it is expected to show similar trends as seen in experiments or theory using some other formulation.

Chapter 5

Coherent Elastic Transport

Portions of this chapter is copied from the Physical Review B vol. 82, page - 045424, year - 2010 article¹⁷³ by Partha P. Pal and Ranjit Pati. Copyright - Appendix E.

5.1 Introduction

Inter/intra-molecular electron/hole transfer has been a fascinating topic of research since the last few decades¹⁰⁴. The obvious reason behind this upsurge in research interest being the continuous desire to better understand the natural biological processes. In nature, each and every chemical/biological phenomenon is dictated by the interaction of several

molecules. How do these molecules interact between themselves? ‘Electron’ is the agent, and the transfer of electrons from one molecule to another is one of the dominant modes of ‘signal’ the molecules use to communicate¹⁰⁵. In this perspective, ‘controlled’ electron transfer would be an important subject to unearth. Another driving force behind the study of electron transfer in molecules is the craze for miniaturizing electronic devices where the “toy idea” of building electronic devices with molecules would be a phenomenal solution⁴. In fact, electron transport measurements in single molecular junctions have been reported successfully by several research groups^{5–12,23,106,107} ; for a comprehensive review see Ref.^{88,89,108,109}. These premier experiments have generated significant interest towards understanding the underlying physics behind the current-voltage characteristics across molecular nano-junctions.

The next question would be: “What kind of molecules would one choose to study electron transfer?” A certain category of organic molecules known as ‘rigid molecular rods’¹¹⁰ can be considered to be good candidates for studying electron transport owing to their stability in adverse conditions. The name ‘rod’ is actually deceptive as they are very flexible¹¹⁰ and are not easily distorted. One should not mistake them to be ‘tough iron rods’ used in our daily life. In fact, they can be thought of as ‘soft elastic rods’ which can withstand distortions whether externally or internally and still retain their electronic properties. It is due to this property that they can act as mediators or interconnects in between two ‘active centers/units’ without getting their own electronic structure reorganized. One also finds them to be useful in the construction of big molecules and supramolecular assemblies¹¹⁰.

Bicyclo[1.1.1]pentane(BCP) is one of the smallest synthesized ‘rigid molecular rods’. Producing¹¹¹ and storing this molecule is quite simple. They are stable in temperatures up to 280-300°C and are transparent in the UV spectrum up to 200nm¹¹⁰. Several groups have already reported electron transfer coupling matrix (V_{AB}) calculations for this system^{112–114} using Koopman’s theorem approximation and Marcus-Hush two state model^{115–117} within Hartree-Fock (HF) theory. However, to understand the current-voltage characteristics of this molecular wire, one needs to consider a device geometry where the finite molecule is attached in between two semi-infinite electrodes used as a source and a drain. In such an *open* and heterogeneous system, applied bias drives the electron from source to drain; it is a non-equilibrium process. Modeling such a process in a heterogeneous system is a challenging task as it depends not only on the intrinsic properties such as geometry, conformation, length, electronic, and magnetic structure of the molecular system but also on the electronic structure at the molecule-lead interface. To the best of our knowledge, no such theoretical modeling has been performed on such a system in device configuration thus far. A two-terminal prototype device made out of this molecule would contain a BCP molecule sandwiched between two semi-infinite metallic electrodes. Bulk Au or Pt are the most commonly used electrode materials. It has been observed that the presence of an anchoring group facilitates the formation of a metal-molecule bond. Studies on the effect of various anchoring groups on the binding strength of metal-molecule junctions reveal that thiol (-SH) end groups along with Au electrodes form the most stable junction^{12,61,62}. Such is the strength of the S-Au bond that the stretching of the metal-molecule junction

actually results in stretching of Au-Au bonds. This creates a Au nanowire before breaking the Au-Au bond. This was first predicted by Molecular Dynamics(MD) calculations⁶³ and was later observed experimentally⁶⁴. With these strong evidences, we choose thiolate(-S) to be the anchoring group and Au as the electrode.

We then proceed to study the current-voltage characteristics of this model-device using a parameter-free, non-equilibrium Green's function (NEGF) formalism. A first-principles density functional method with Becke's three parameter hybrid functional¹¹⁸ is used to construct the non-equilibrium Green's function; the bias effect is explicitly included in our approach within a *many-body* framework. The calculated current-voltage characteristic in the device shows an Ohmic behavior in a low-bias regime. An increase in the length of the BCP 'molecular wire' results in an exponential decay in the magnitude of conductance, which is in excellent agreement with the the exponential decay feature^{112,114} of the electron transfer rate predicted from the length dependent trend of electron transfer coupling matrix value, V_{AB} . The decay constant(β) is calculated to be 0.59 \AA^{-1} . It is found that by increasing the number of BCP cage units from 1 to 3 in the wire, one can completely suppress the current in the molecular device for a bias up to 0.4 V.

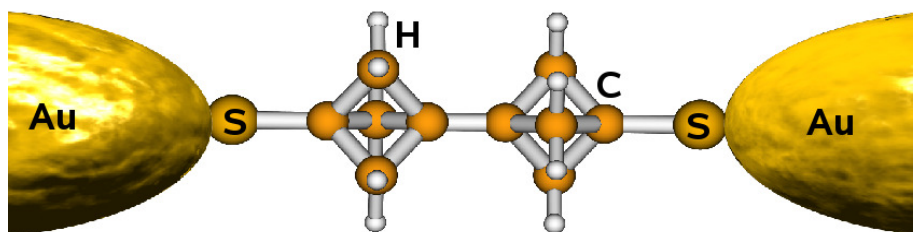


Figure 5.1: Schematic of a two-terminal device built out of a molecular wire containing two BCP cages¹⁷³. Reprinted figure with permission from Partha P. Pal and Ranjit Pati, Phys. Rev. B **82**, 045424 (2010), ©(2011)The American Physical Society.

5.2 Computational Procedure

As mentioned earlier, we have constructed a BCP two-terminal molecular device by sandwiching a molecular moiety between two Au electrodes with thiolate as the anchoring group. Initially, the isolated molecular wires containing 1, 2, 3 cages and terminated by thiol groups (-SH) at both ends are fully relaxed with Gaussian electronic structure code. B3LYP is the functional used and the basis set 6-311G(d,p) is used for all C, H, S atoms.

The neighboring cages in the optimized structures are found to be rotated by 180° along the wire axis. The distance between the S to the plane of the 3-Au atom cluster is estimated from single point calculations by varying the distance between the S and the plane. A real space approach in which the *many-body* wavefunction of the electron is expanded in terms of a finite set of Gaussian atomic orbitals⁴⁸ is adopted to calculate $H(\epsilon)$. In our calculation we have used a *posteriori* Becke's three parameter hybrid functional (B3LYP)¹¹⁸ that includes a part of the exact Hartree-Fock (HF) exchange and the Lee-Yang-Parr (LYP) functional, which ensures the inclusion of local and non-local correlation terms^{48,50}. The inclusion of a part of the exact HF exchange, calculated using the Slater determinant of the Kohn-Sham orbitals¹¹⁸, allows us to avoid the self-interaction errors that occur in conventional DFT. The Los Alamos double zeta effective core potential(LANL2DZ) basis set⁴⁸ that includes the scalar relativistic effects is used for the electrode(Au) atoms. A triple valence zeta Gaussian basis function with an additional polarization function on heavy atoms (6-311G*) is used for the atoms of the molecule. To ensure tight convergence during self-consistent calculations, the convergence criterion for energy, maximum, and root mean square electron density are set at 10^{-6} , 10^{-6} , and 10^{-8} a.u. respectively.

We have calculated the bias driven current for the three different wires containing 1, 2, and 3 BCP cages. A prototype two-terminal device built out of a molecular wire containing two BCP cages is shown in Fig. 5.1. Though the structure of the free BCP molecule is known^{110,114}, the atomic level structural details of the contact geometry at the molecule-gold interface is unknown. Hence, we first optimize each of the molecular wires with thiol

(-SH) as the anchoring group using DFT within B3LYP formalism; Gaussian electronic structure code is used⁴⁸ for the optimization. The distance between the terminal C atom and the S atom in the thiol group to which it is bonded is found to be 1.8 Å. The distance between the two terminal C atoms is 1.86 Å, which is in good agreement with the previously reported value of 1.87 Å^{110,114}. Subsequently, the optimized molecular structure with thiolate (-S) as the anchoring group is embedded between two clusters of 3-Au atoms on each side to model the *active* region. The S atom is incorporated into the three-fold hollow site of the Au atoms on the Au(111) surface¹¹⁹. It should be noted that for practical purposes, we have considered only three gold atoms on each side which are directly involved in bonding with the S atoms. The distance between the Au and S is varied to determine the minimum energy configuration(Fig 5.2). The optimized S-Au distance is found to be 2.80 Å; to discern the role of the molecular spacer on conductance, the interfacial contact geometry is kept the same for all the three molecular devices.

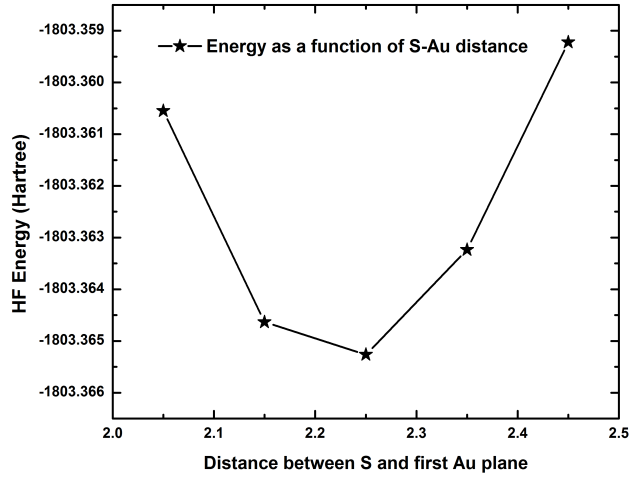


Figure 5.2: Variation of the Hartree-Fock energy with distance between the S and the first plane containing the Au atoms.

5.3 Results and Discussions

5.3.1 Potential Profile

To understand the response of the molecule to external bias, we applied a dipole electric field along the molecular wire axis as discussed in Section II. The electrostatic potential is then calculated self-consistently¹⁰³ at each atomic center in the *active region* for each

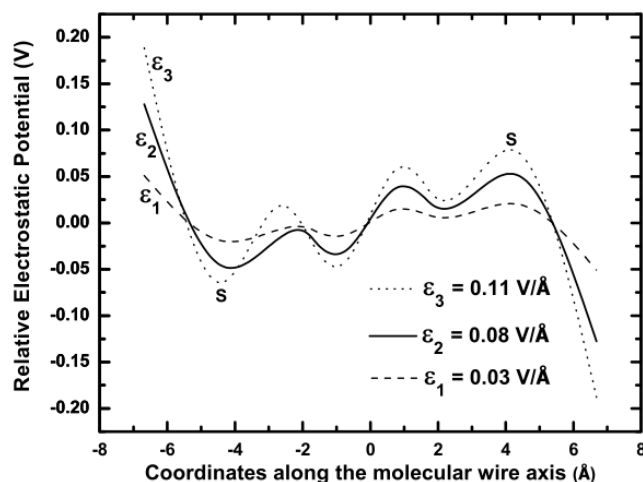


Figure 5.3: Potential profile of the two-cage molecular wire for different electric fields, ϵ_1 , ϵ_2 , ϵ_3 . The notation ‘S’ refers to the position of the terminal S atoms in the device¹⁷³. Reprinted figure with permission from Partha P. Pal and Ranjit Pati, Phys. Rev. B **82**, 045424 (2010), ©(2011)The American Physical Society.

applied field as well as for the zero bias. The difference between the electrostatic potentials at $\epsilon = 0$ ($V = 0$) and $\epsilon \neq 0$ is then obtained at each atomic center, which is subsequently averaged over the degrees of freedom perpendicular to the wire axis to obtain the relative electrostatic potential (REP) profile along the wire axis. The REP values are then plotted along the molecular wire axis for three different externally applied fields (Fig. 5.3). For brevity, we have only presented the results for a molecular wire containing two BCP cages in Fig. 2.

The magnitude of REP at the molecule-lead interface increases with the increase of applied field as expected (Fig. 5.3). For example, at an external applied field of 0.11 V/\AA , the REP at the left and right junction is 0.19 V and -0.19 V respectively. For an applied field of 0.03 V/\AA , the respective REPs are 0.05 V and -0.05 V . However, an intriguing feature is revealed by examining the potential profile between the two terminal S-atoms; one can clearly notice two effective potential barriers. Furthermore, the barrier height changes with the increase of applied field. This clearly suggests that for quantitative evaluation of bias induced response in a molecular device, the explicit inclusion of field effect is essential. Next, we focus on the potential profile of the molecular wires containing one, two, and three BCP cages. The potential profiles at $V = 0.24 \text{ V}$ for the three molecular wires are encapsulated in Fig. 5.4. For the molecular wire containing one BCP cage, there is only one effective potential barrier between the two terminal S-atoms. For the wire with two and three BCP cages, two and three effective potential barriers are noticeable. This suggests that by increasing the number of BCP cage units in the wire, we are essentially increasing the number of effective potential barriers in the conducting molecular channels. Another interesting, noticeable feature from Fig. 5.4 is that the barrier height for the wire with a single BCP cage is relatively smaller than that of the wires containing two and three BCP cages. The height and the number of effective barriers have important implication on the quantum transport properties of these wires, which will be revisited in the next section. To account for the origin of valley and hill at the terminal S-atom position in the potential profiles (Fig. 2 and Fig. 3), we analyzed the variation of Mulliken charge associated with

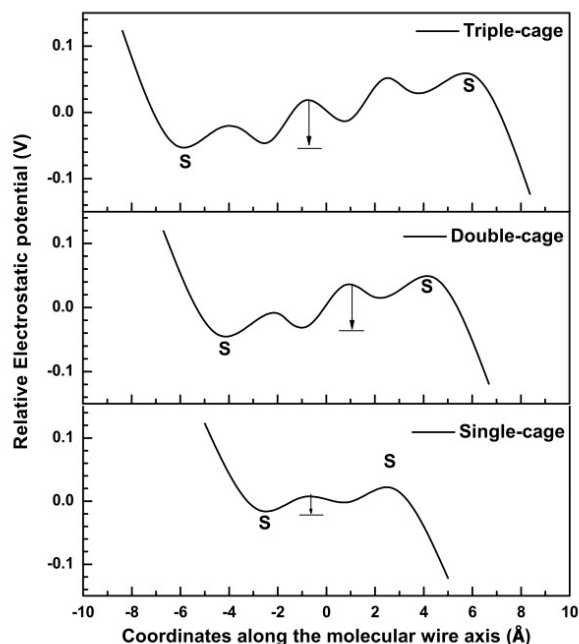


Figure 5.4: Potential profile of the three different wires at $V=0.24$ Volts. The notation ‘S’ refers to the position of the terminal S atoms in the device. The arrows indicate the height of the effective potential barriers¹⁷³. Reprinted figure with permission from Partha P. Pal and Ranjit Pati, Phys. Rev. B **82**, 045424 (2010), ©(2011)The American Physical Society.

S-atoms as a function of bias. For a wire containing a single BCP cage, the charge profile is presented in Fig. 5.5. At equilibrium (zero applied bias), both of the terminal S atoms have equal amounts of charge (scaled to zero in the charge scale in Fig. 5.5). As the bias increases, the negative charge on the left S increases steadily; at the same time positive charge accumulation increases for the right S atom. This bias induced polarization effect is responsible for the hill and valley observed in the potential profile. Similar bias induced polarization effects were noted for wires containing two, and three BCP units.

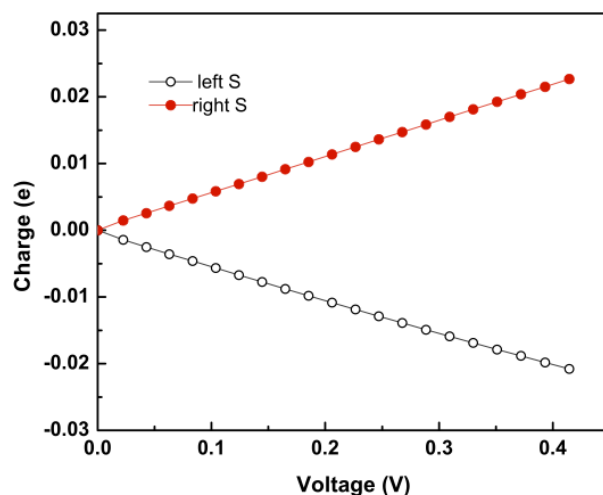


Figure 5.5: Charge profile depicting bias induced polarization effect on the terminal ‘S’ atoms in the molecular wire containing one BCP cage unit¹⁷³. Reprinted figure with permission from Partha P. Pal and Ranjit Pati, Phys. Rev. B **82**, 045424 (2010), ©(2011)The American Physical Society.

5.3.2 I-V characteristics

The calculated currents through the molecular wires as a function of external bias, V , are summarized in Fig. 5.6. For the low bias regime considered in our calculation, the I-V curves follow Ohm’s Law i.e the current increases linearly with the bias, V . As expected, the wire containing the three BCP cage units has the largest resistance of the three and hence the least current for a particular bias. For example at 0.41 V, the current in the

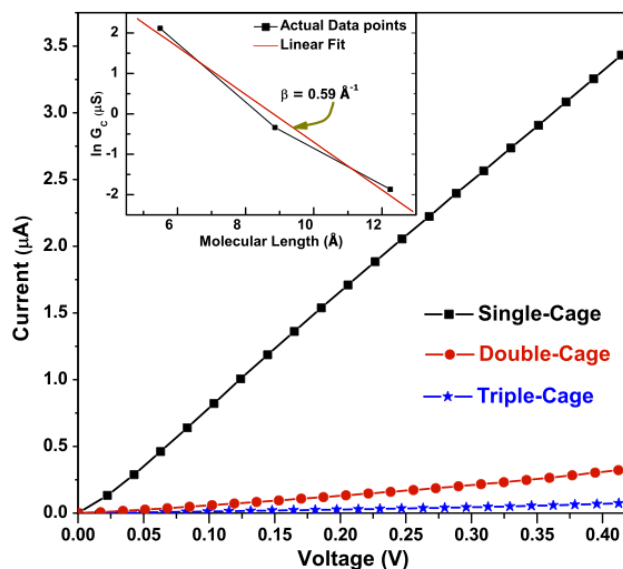


Figure 5.6: I-V characteristics of the three different wires under the influence of applied external bias. Inset shows the plot of $\ln(G_c)$ vs. length of the molecule (L). A straight line is fitted into the data points in order to calculate β ¹⁷³. Reprinted figure with permission from Partha P. Pal and Ranjit Pati, Phys. Rev. B **82**, 045424 (2010), ©(2011) The American Physical Society.

single-cage wire is $3.4 \mu\text{A}$; the current in the double-cage wire is $0.32 \mu\text{A}$; and the current in the triple cage wire is $0.07 \mu\text{A}$. The resistance of the three wires calculated from the slopes of the I-V curves are $0.12 M\Omega$, $1.4 M\Omega$, $6.5 M\Omega$ for the one-cage, two-cage, and three-cage wire respectively. The substantial increase in resistance or the decay in current with the increase in the number of cage units in the wire can also be understood from Fig. 5.4. The increase in the number of barriers with the increase in the number of cage units in the wire is responsible for the decrease in the current. From one-cage unit to two-cage unit in the wire, the number of effective potential barriers in between the terminal

S-atoms increases to two. In addition, the effective barrier heights also increase leading to a significant drop in current. Going from two-cage to three-cage unit in the wire, the number of effective potential barriers between the terminal S-atoms increases from two to three. However, the barrier height does not show a significant change. This explains why only a small drop in current is observed when increasing the number of cage-units from two to three. The conductance values, obtained from the inverse of resistances, are found to decrease exponentially with the increase of the number of cage-units in the wire. It follows a simple relation:

$$G_c[L] = G_c(L=0)e^{-\beta L} \quad (5.1)$$

where β is a decay constant associated with the decrease in the conductance value as the length of the molecular wire (L) is increased; $G_c(L=0)$ is the extrapolated conductance at the interface ($L=0$). This exponential decay feature of the conductance is in excellent agreement with the length dependent decay feature in the electron transfer rate predicted from the electron transfer coupling matrix values, which re-affirm the accuracy of our theoretical approach. It should be noted that the conductance value is proportional to the electron transfer rate, and hence V_{AB} . In the latter case the V_{AB} was calculated using the two-state Marcus-Hush model and the Koopman's theorem approximation; no bias effect was considered. The β value reported from the Koopman's theorem approximation¹¹² was 0.66 \AA^{-1} ; the two-state Marcus-Hush model yielded¹¹⁴ the β -value to be 0.97 \AA^{-1} . To determine the β -value, we plotted the variation in $\ln G_c$ with the length of the wire (L) as shown in the inset of Fig. 5.6. The distance between the terminal S-atoms is considered to

be the length of the wire. The data points are fitted to a straight line to calculate the β as 0.59 \AA^{-1} . The discrepancy between the current β value and the β value obtained from V_{AB} result could be ascribed to the fact that in the former case the bias effect was not explicitly considered. In addition, the electrode induced polarization effect on the molecular orbital was not taken into account during the calculation of V_{AB} .

5.3.3 Transmission Function

To gain a deeper insight into the I-V characteristics of this particular metal-molecular wire-metal system, we look into the entities that determine the electrical current through the junction, precisely the bias dependent transmission function, T_{lr} (Refer equation 3.17 and equation 3.19). T_{lr} as a function of injection energy E , is outlined in Fig. 5.7; a bias value of 0.41 V is considered. The chemical potential window [$\mu_1 = -0.2$, $\mu_2 = 0.21$] is shown by the dotted line; Fermi energy is set to zero in the energy scale. The transmission function looks fairly flat within the low-bias regime (0 - 0.41 Volts) considered in our calculation. T_{lr} is devoid of spikes as seen in some other molecular species⁵⁷. A rugged T_{lr} can give rise to non-linear I-V characteristics or even Negative Differential Resistance (NDR)⁵⁷. A relatively smooth T_{lr} within the integration window is the possible reason behind the Ohmic behavior in this type of molecular wires. A comparative study of the T_{lr} for the three devices within the same chemical potential window reveals a significantly higher

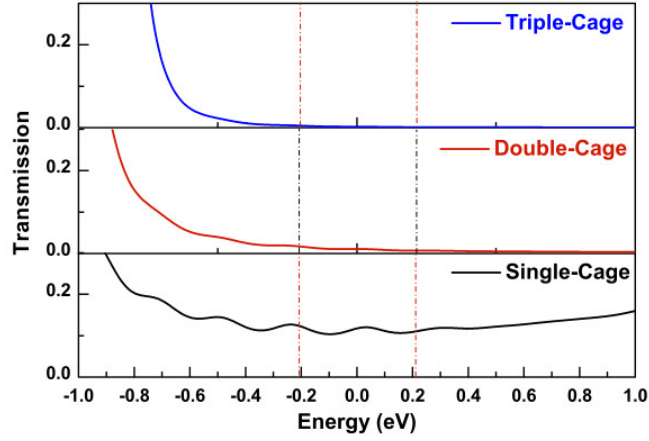


Figure 5.7: Transmission function as a function of injection energy in the three molecular wires under the same applied external voltage(= 0.41 V). The chemical potential window is shown by the dotted line¹⁷³. Reprinted figure with permission from Partha P. Pal and Ranjit Pati, Phys. Rev. B **82**, 045424 (2010), ©(2011)The American Physical Society.

transmission value for a single-cage wire when compared to the wire containing two cages. For instance at 0.1 eV injection energy, the value of the transmission function for the single cage wire is 0.11 as compared to 0.008 for the two cage wire. In the triple cage system, T_{lr} is 0.002 for the same injection energy. This clearly explains the length dependent I-V features observed in Fig. 5.6.

5.4 Summary

In summary, we have used first principles density functional method with a *posteriori* B3LYP approach to study the quantum transport properties of BCP molecular devices. A parameter free, non-equilibrium Green's function approach, where the bias effect is explicitly included within a *many-body* formalism, is used to compute the current-voltage characteristics of the device. In the low bias regime considered in our study, we found the I-V feature to follow Ohm's law. We estimated the resistance from the slope of the I-V curve. By increasing the number of BCP units in the molecular wire, the conductance value is found to decrease exponentially with a decay constant, β , of 0.59 \AA^{-1} . This is in excellent agreement with the exponential decay feature observed for the length dependent electron transfer rate in the same system predicted from the two-state Marcus-Hush approach. By including three BCP units in the wire, we found that the current can be completely suppressed for a bias upto 0.41 V. This suggests that the wire containing three BCP cage units could potentially be used as a gate throttle to avoid leakage gate current in a three terminal molecular transistor.

Chapter 6

Incoherent Elastic Transport

*Portions of this chapter is copied from the Journal of Physical Chemistry C, 2011 article¹⁶⁹
by Partha P. Pal and Ranjit Pati. Copyright - Appendix F.*

6.1 Introduction

Phase randomization or relaxation⁵⁶, which is defined as the loss of phase information of the particles after they undergo scattering, is an interesting aspect to study in a molecular scale device^{120,121}. A simple estimation of the mean free path associated with the inelastic scattering(which results in phase-loss) of electrons at very low temperatures gives the value

to few hundreds of Å,¹²² which is much longer than the length of the current carrying channel in molecular junctions^{122–124}. But owing to the small size of the junctions one expects a large number of scattering events to occur per unit time/volume^{122,124} that can even have an effect on the stability of local bonds. Thus the inclusion of phase incoherence^{123,125}, associated with inelastic scattering gives a more complete picture of the non-equilibrium charge transport at finite temperature. A scheme to include dephasing in a two-terminal device was first proposed by Büttiker in his multi-probe formulation¹²⁶. It can be incorporated within the Landauer-Büttiker formalism^{56,122,127,128} for the *elastic* transport. In this formulation the phase relaxation is allowed through a fictitious probe. Despite this being a phenomenological approach it has turned out to be appealing to a lot of theoretical groups modeling mesoscopic transport for its simplicity and the physical insights it provides^{65,121,129–131}.

Interactions of electrons with the quantized normal vibrational modes of atoms (phonons) is a dominant cause of phase randomization¹²¹. So, in order to study dephasing one needs to investigate the electron-phonon(e-ph) interactions^{132,133} both qualitatively and quantitatively. Experimentally, vibrational modes and its interaction with the conduction electrons can be studied with Inelastic Tunneling Spectroscopy(IETS)^{134,135}. IETS, which is generally restricted to the low-bias non-resonant tunneling regime, is a powerful tool that can provide structural informations at the molecular level by exploiting the active vibrational modes (ω) within the bias range $0 < V_{bias} < \frac{\hbar\omega}{e}$ ^{136–138}. Vibrational modes in molecular-scale junctions,¹³⁹ such as metal-insulator-metal,¹³⁵ or metal-molecule-metal

systems^{140–145} have been successfully studied with IETS. It is also found to be useful in studying nanoscale junctions which are highly conducting i.e the magnitude of conductance is quite close to the quantum of conductance unit(G_0), such as for a Pt-H₂-Pt system¹⁴⁶ or for a chain of few Gold atoms sandwiched between Gold electrodes^{147,148}. Theoretical investigation of the effect of e-ph coupling on charge transport is an overwhelming task since it demands a dynamic framework consisting of the lattice vibrations, their interaction with the traversing electrons, and further renormalization of the scattering states due to this e-ph coupling. Further, since this is a non-equilibrium charge transport process, the effect of bias needs to be included in the formulation which might require structural reorganization. However, in the low-bias regime, for weak e-ph coupling one can make lower order approximations for e-ph interaction and apply perturbation theory to see its effect on the non-equilibrium transport characteristics^{149–151}. Therefore most of the efforts have been restricted to tight-binding formulations^{152–155} or first principles calculations within the Born approximation or its self-consistent extensive counterpart^{101,156–162}. There are always some system specific debatable issues such as which atoms interact with the travelling electrons¹⁶³. Do they originate only from the molecular moiety or the electrode atoms which are perturbed when the molecule is attached ? Also, which are the modes of vibration that interact the most with the scattering states ? Some first-principles analysis suggested that the low-lying vibrational modes are the ones which mostly couple with the scattering states at the metal-molecule junction¹⁰¹. It has been pointed out that the e-ph coupling strength undergoes change with increase in external bias, but the vibrational spectrum of the

molecule essentially does not change much^{101,164}. In the non-equilibrium charge transport, e-ph coupling can give rise to multiple emission and absorption of phonons which can have an influence in the mechanical stability of the metal-molecule junction¹⁶⁵. Earlier, it was pointed out that in some systems the strength of the e-ph coupling is a function of the metal-molecule bonding at the junctions¹⁶⁶. Recently, the breakdown of Born-Oppenheimer(BO) approximation³¹ in a certain regime when two electronic energy levels of the molecule are coupled by a molecular vibration is suggested. This opens up the possibility of controlling electron transport in a molecular junction mechanically through the molecular vibrations. Whereas there has been a lot of research on the effect of molecular vibrations on non-equilibrium transport,^{167,168} comparative studies on the contribution of dephasing, but within the *elastic* tunneling, as a function of external bias in molecular wires of different lengths is still lacking.

In this chapter¹⁶⁹, we report a first principles study on the effect of “phase-breaking” scattering to the net charge transport across strongly coupled molecular junctions. In particular, we study the evolution of the “out of phase” current with external bias in three molecular wires of increasing length. The molecular wires are constructed out of cubane¹⁷⁰ molecules which have a rigid cage type cuboid structure. The stable structure of cubane or its oligomers make them easily identifiable and are considered to have prospective applications in energy materials¹⁷¹. They have been subjected length dependent electron transfer rate studies both experimentally¹⁷² and theoretically using the two state Marcus-Hush model.¹¹⁴ But the response of cubane or its oligomers to electric field has not been

explored yet. This motivated us to study the conductance as a function of length of a two-terminal device built out of cubane oligomers. A first-principles density functional method with Becke’s three parameter hybrid functional(B3LYP)¹¹⁸ within the Density Functional Theory(DFT) is used to construct the single particle Green’s function; the bias effect is explicitly included in our approach within a *many-body* (single determinant) framework. Ignoring the dephasing phenomenon, the calculated current-voltage ($I_{sd} - V_{sd}$) characteristic in the device shows an Ohmic behavior in a low-bias regime. An increase in the length of the wire results in an exponential decay in the magnitude of conductance, which is in excellent agreement with the exponential decay feature of the electron transfer rate predicted experimentally¹⁷² and also from the length dependent trend of the electron transfer coupling matrix (V_{AB})¹¹⁴. We then proceed to study the effect of “phase-breaking” scattering on charge transport across the same system as a function of external bias and length of the oligomer. The contribution of electronic current from the “phase-breaking” collisions is modeled using the Büttiker’s multi-probe approach. This approach requires the presence of a virtual electron reservoir. The electrons which travel from source to drain via this pseudo-reservoir lose their phase information as soon as they enter this imaginary third probe and thus are the ones which contributes to the “phase-breaking” current. Our calculations show that the “out of phase” tunneling of electrons starts contributing to the net current only after an “off-set” voltage. The magnitude of the “off-set” voltage is found to be inversely proportional to the length of the wires, meaning the longest wire has the minimum “off-set” voltage. The “off-set” bias depends on the position of the first trans-

mission peak closest to the Fermi level. This is due to the fact that dephasing reduces the constructive interference within elastic transport in the resonant tunneling regime and thus reduces the electronic current. Electron-phonon(e-ph) interaction is one of the major reasons of dephasing within the device. Estimation of electron-phonon coupling energies reveal that with increase in external bias, a greater number of vibrational modes interact strongly with conducting electrons, thus leading to a stronger dephasing effect.

6.2 Computational Details

It can be noted here that including the bias effect in formulations beyond the ground state mean-field DFT¹⁷⁴ is a very difficult task. In covalently bonded junctions, which is our case here, the modification of the molecule-lead coupling with change in external bias is an important quantity that should be captured in the formulation. In this context the ground state based DFT is a reasonably good approach and is being successfully used.^{55,57,121,175} $H(\epsilon)$, if solved using first order perturbation theory will give only linear shifts to the zeroth order energy eigenvalues. However, a fully self-consistent evaluation of $H(\epsilon)$ reveals a non-linear increase in the energy eigenvalues with the application of \vec{E} . Thus this approach not only includes the first order effect of the field on the dipole moment of the molecule, but also on its polarizability and higher order terms.

The interaction of electrons and phonons is modeled using a phenomenological Hamiltonian in which only *diagonal* interaction terms of the matrix is used in the orbital index^{164,176}. In this model, assuming the e-ph interaction to be weak, linear e-ph coupling terms are only retained. The dimensionless coupling constant, $g_{i,n}$ is found to be^{164,176}:

$$g_{i,n} = \frac{1}{\sqrt{2}\hbar\omega_n} \left(\frac{\partial \varepsilon_i}{\partial Q_n} \right) \quad (6.1)$$

Making a canonical transformation, the coupling energy can be calculated as^{164,176}:

$$I_{i,n} = g_{i,n}^2 \hbar \omega_n \quad (6.2)$$

The coupling energy along with the coupling constant gives a quantitative answer as to how a particular electronic energy level interacts with a particular phonon mode. The coupling energies of the various electronic levels and phonon modes of the molecule are calculated both before and after the inclusion of an external bias.

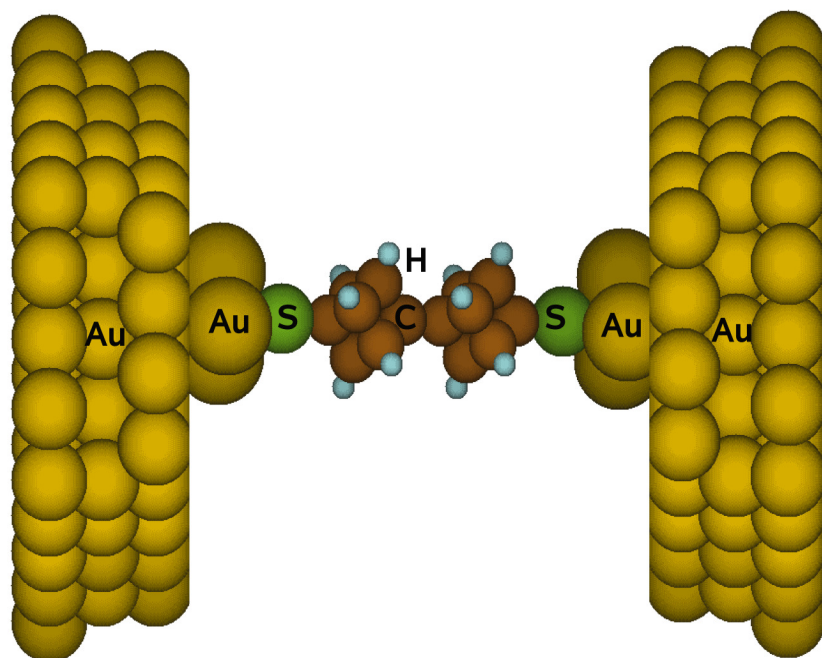


Figure 6.1: Schematic of a two-terminal device built out of a Cubane oligomer with $N=2$ i.e with two cubane cages¹⁶⁹. Reprinted figure with permission from Partha P. Pal and Ranjit Pati, J. Phys. Chem. C 2011, ©(2011)The American Chemical Society. Copyright permission in Appendix F.

6.3 Results and Discussions

6.3.1 Geometry

As mentioned in the introduction section, the three molecular wires are created with 1,2, and 3 cubane molecules respectively. The isolated wires, terminated with a thiol (-SH) group, are optimized by Gaussian(G03)⁴⁸ that uses localized atomic gaussian basis sets. The functional B3LYP is used within DFT for the optimization and subsequent electronic structure calculations. The advantage of using a *posteriori* B3LYP approach is that the Becke's three parameter(B3) functional¹¹⁸ includes the exact Hartree-Fock exchange partially and the Lee-Yang-Parr(LYP) functional⁵⁰, which takes care of both local and non-local correlation terms. Convergence criterion for energy, maximum, and root-mean-square electron density are chosen to be 10^{-6} , 10^{-6} , and 10^{-8} a.u. respectively. The optimized structure of a single cubane with -SH group attached to it turns out to be very close to that of pure cubane.^{171,177} Both experimental results and theoretical calculations with pure cubane yields C-C bond length to be 1.57 Å^{171,177}. The C-C bond length obtained from our calculation is also 1.57 Å on an average, which is same as the previously obtained experimental¹⁷⁷ and theoretical values¹⁷¹. Same is seen for the C-H bond length. Previously measured and calculated values are 1.1 Å¹⁷⁷ and 1.09 Å¹⁷¹ respectively. Our calculations

yield a value of 1.09 Å for the same. When the length of the molecular wire is increased with addition of more cubanes, the C-C and C-H bond-lengths of the individual units remain the same. The C-C bond length between the Carbons of neighbouring cage-units is 1.47 Å. In order to design a prototype device out of these molecular wires, they are sandwiched between two Au electrodes with the help of the anchoring thiolate (-S-) group. The Sulphur atom of the -S- group is placed in the three-fold hollow site of the Au(111) plane¹¹⁹ as shown in Fig. 6.1. Attaching a molecule to the electrode generates a rearrangement of the charges at the molecule-electrode junctions. But this reshuffling does not affect the whole electrode due to the phenomenon of metallic charge screening within it. Ideally, the accuracy of the calculations would increase when more number of electrode atoms are included in the *active region* of the device. But inclusion of more atoms will lead to substantial increase in the computing time. So, here, for practical reason, we have assumed 3 Au atoms on each electrode to be perturbed by the molecular wire. The distance between S and Au atoms is optimized to get to the minimum energy configuration(Fig. 6.2). The optimized S-Au bond length comes out to be 2.80 Å. As in the previous study, our aim here is to see the effect of length of a molecular spacer on the I-V characteristics of the device and so the S-Au distances are kept fixed for all the three devices.

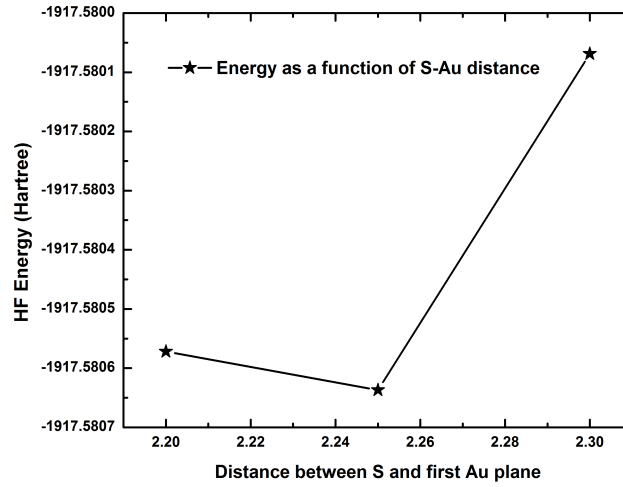


Figure 6.2: Hartree-Fock energy as a function of the distance between the S atom and the plane of the first layer of Au atoms.

6.3.2 Potential Profile

In order to simulate the non-equilibrium charge-transport process in the device configuration, the bias is applied as discussed in Chapter 3, Section II. The electrostatic potential is then calculated self-consistently¹⁰³ at each atomic position. The difference between the electrostatic potential at a finite bias and zero bias for each atomic position, called as the Relative Electrostatic Potential (REP) here, is plotted in Fig. 6.3. It is seen that the individual cage units act as potential barriers in the REP profile. Thus, more number of cage units

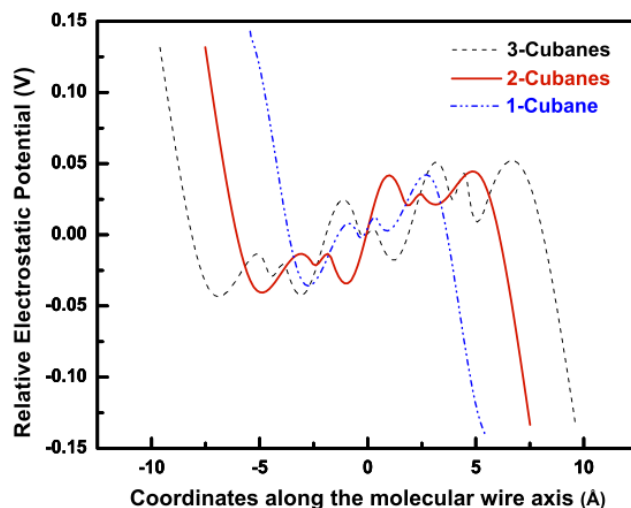


Figure 6.3: Relative Electrostatics Potential (REP) profile of the *active region* in the three different molecular wires at an external voltage of $V_{sd} = 0.27$ V¹⁶⁹. Reprinted figure with permission from Partha P. Pal and Ranjit Pati, J. Phys. Chem. C 2011, ©(2011)The American Chemical Society. Copyright permission in Appendix F.

means more number of potential barriers, and it becomes more difficult for the electrons to tunnel across the molecular wire which is also reconfirmed in the I-V characteristics. Among the different wires studied, the wire with 3 cubanes has the maximum number of potential barriers and later on shows minimum current for a particular bias. It is also observed, for a particular wire, the barrier height changes as the applied electric field is increased, which clearly emphasizes the importance of an explicit inclusion of the external bias. The chemical potential at the two metal-molecule junctions are the REPs at the junctions, which are later used in the current calculations as the integration limits.

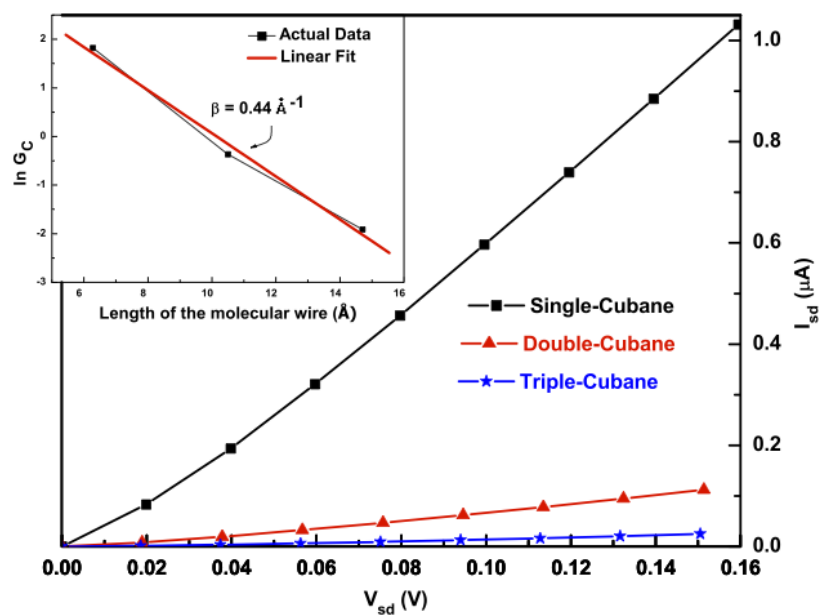


Figure 6.4: Current (I_{sd}) as a function of source-drain bias (V_{sd}). Inset shows the plot of $\ln(G_c)$ vs. length of the molecular wire (L). A straight line is fitted into the data points to calculate β ¹⁶⁹. Reprinted figure with permission from Partha P. Pal and Ranjit Pati, J. Phys. Chem. C 2011, ©(2011)The Americal Chemical Society. Copyright permission in Appendix F.

6.3.3 Current(I_{sd})-Voltage(V_{sd}) characteristics

6.3.3.1 Coherent Tunneling

The low-bias current-voltage characteristics of this system is similar to that of the previously studied BCP molecular wire¹⁷³ in an earlier chapter. In this low-bias Ohmic regime [0-0.16V] the $I_{sd} - V_{sd}$ characteristics is linear (Fig. 6.4). The current in the longest wire is least among the three wires. There is almost one order drop in the current when one compares the values for the one-cage wire and the two cage wire in this entire regime. But when one compares the current between the two-cage and the three-cage wire there is not much change (a factor of ~ 0.5). This can easily be understood from the barrier heights. The difference between the barrier heights of the one-cage wire and the two-cage is significantly more than that of the two-cage and the three-cage wire. Since the $I_{sd} - V_{sd}$ plot is linear in the low-bias regime, it is easy to calculate the magnitude of conductance for the three different wires namely, $\frac{dI_{sd}}{dV_{sd}}$. The decrease in the value of conductance with increase in length of the wire follows an exponential relation:

$$G_c[L] = G_0 e^{-\beta L} \quad (6.3)$$

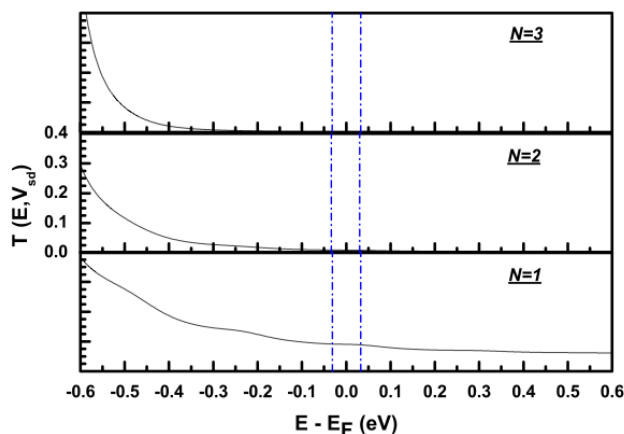


Figure 6.5: Variation of transmission function $[T(E, V_{sd})]$ with injection energy (E) in the 3 molecular wires for a fixed external voltage of $V_{sd} = 0.06$ V. $N = 1, 2, 3$ denotes the number of cubane cages in the oligomer. The dotted line denotes the chemical potential window. The scale for y-axis is same for all the panels¹⁶⁹. Reprinted figure with permission from Partha P. Pal and Ranjit Pati, J. Phys. Chem. C 2011, ©(2011)The American Chemical Society. Copyright permission in Appendix F.

where β is the decay constant associated with the decrease in the conductance value with the increase in the length of the molecular wire (L). This exponential decay feature of the conductance is in excellent agreement with the length dependent decay feature in the electron transfer rate predicted from the electron transfer coupling matrix values, which re-affirm the accuracy of our theoretical approach. It should be noted that the conductance value is proportional to the electron transfer rate, and hence V_{AB} . In the latter case the V_{AB} was calculated using the two-state Marcus-Hush model^{114–117}. For a deeper analy-

sis into the reason behind the decrease in current with increase in the length of the wire we plotted the transmission function as a function of injection energy for three different wires (Fig. 6.5). The transmission functions for all the wires are devoid of any spikes within the integration window. Similar features were also observed in the bicyclo[1.1.1]pentane (BCP) molecular wires¹⁷³. The nearly flat transmission function explains the linear increase of current with voltage. Also, comparing the values of transmission function within the integration window it is seen that the most significant change in the value of the function occurs from one to two-cage wire. The difference between the values of the function for the 2-cage and 3-cage is very less. This also reflects the reason behind a drastic decrease in the value of the current from one to two cage structure. To determine the β -value, we plotted the variation in $\ln G_c$ with the length of the wire (L) as shown in the inset of Fig. 6.4. The distance between the terminal S-atoms is considered to be the length of the wire. The data points are fitted to a straight line to calculate the β as 0.44 \AA^{-1} . Earlier, pulse radiolysis measurements performed on cubane yielded a β value of 0.90 \AA^{-1} ¹⁷². Within the two-state Marcus-Hush model the β was calculated as 1.42 \AA^{-1} ¹¹⁴. The discrepancies in the values of the various β s obtained can be linked to the different chemical groups used to terminate the cubane molecules in prior reports. Biphenyl and naphthyl were used as end groups in the experiment. Moreover, the pulse radiolysis measurements¹⁷² were done in a solution phase in which the solvent can always increase the overall rate of electron transfer. In the theoretical calculations using the Marcus-Hush model, the cubane molecules were terminated by $-\text{CH}_2$ chemical groups¹¹⁴ whereas in this work the cubane molecules are attached

to the Au-electrodes by the -S- group. The presence of the metallic atoms and the covalent bond between the S-Au renormalizes the many-body states of the molecular wire. Thus the molecular moiety becomes more conducive to current flow and possess a relatively lower β value.

6.3.3.2 Phase-breaking tunneling

Interaction of electrons with vibronic modes of the oligomer might create or destroy phonons either of which would force the electron to undergo phase and energy relaxation. In our formulation, an electron making transition from a lower energy state to higher energy state or vice versa is accompanied by a reverse transition following the conservation of energy. But the electron ends up in losing its phase information due to these type of transitions. The contribution of this ‘phase-breaking’ phenomenon to the total current in the device can be accounted for by using Büttiker’s multi-probe approach, which has already been described in Chapter 3, Section 3.2.2. In this approach, an imaginary ‘vibronic’ probe is floated into the main current-carrying channel. It is assumed that a part of the electron flux travels from the source to drain via the pseudo-probe resulting in the loss of their phase information. The effect of the third probe enters the scheme in the form an extra ‘vibrational’ broadening term in the Green’s function of the device (eqn. 3.21). The effective transmission function is concocted utilizing the boundary condition that no net current flows in/out of

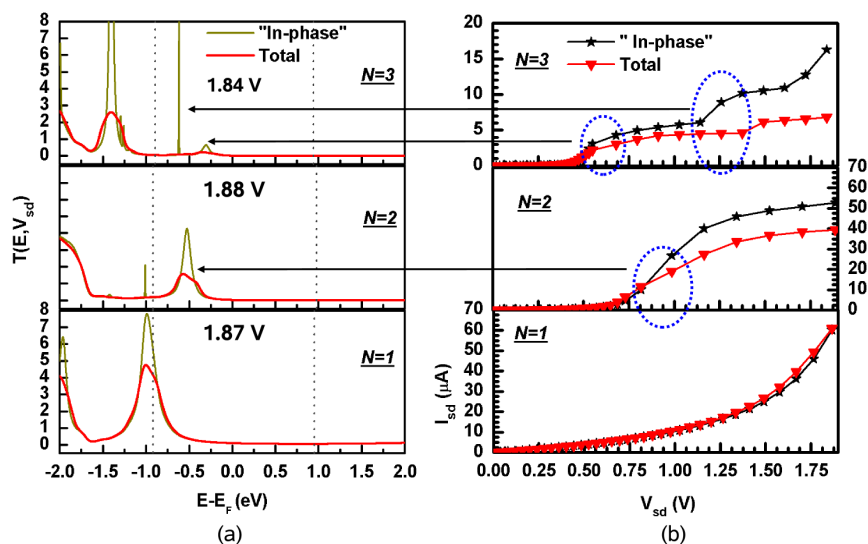


Figure 6.6: (a) Transmission function $[T(E, V_{sd})]$ vs. injection energy (E) in the three molecular devices. The plots are for a fixed external voltage of $V_{sd} = 1.87, 1.88, 1.84$ Volts for $N = 1, 2$, and 3 respectively. The chemical potential window is shown by the dotted line. The Fermi level is scaled to zero in the x-axis. (b) Current (I_{sd}) as a function of source-drain bias (V_{sd}) in the three molecular wires. ‘In-phase’ denotes the current in the absence of vibronic probe. ‘Total’ denotes the current in the presence of the vibronic probe. Note that the scale of y-axis of the 3 cubane wire is different. $N = 1, 2, 3$ denotes the number of cubane cages in the oligomer¹⁶⁹. Reprinted figure with permission from Partha P. Pal and Ranjit Pati, J. Phys. Chem. C 2011, ©(2011)The American Chemical Society. Copyright permission in Appendix F.

the imaginary probe (eqn. 3.23). Using this approach we included the “out of phase” current to the $I_{sd} - V_{sd}$ characteristics for the three molecular wires which is plotted in Fig. 6.6(b). A range for the initial guess value of D_{e-ph} is estimated from the e-ph coupling energies calculated in the next section of the paper. The range comes out to be from 0.0001 eV^2 to 0.25 eV^2 . Since the e-ph interactions are considered to be weak, a relatively small value of 0.005 eV^2 is chosen for D_{e-ph} in the current calculations. However, it is important to

note that the value of D_{e-ph} mentioned above is just a weighting factor used to compute the Σ_{e-ph} (please see Chapter 3 Section 3.2.2). A change in the initial guess value of D_{e-ph} does modify the electronic current quantitatively but does not have any qualitative effect on the $I_{sd} - V_{sd}$ characteristics. In the low bias regime, the phenomenon of dephasing does not have a significant effect on the current in all the three wires. However, a closer look reveals that dephasing raises the current slightly in this regime, as observed in elsewhere¹²¹. This is owing to the reduction in the destructive interference due to phase randomization, which increases the conduction of the system¹²¹. After a certain “off-set” bias, which is different in the three oligomers, dephasing reduces the total current across the junction. The “off-set” voltages for the two-cage and the three-cage wires are ~ 1.0 V and 0.5 V respectively. The “off-set” voltage for the single cage wire is expected to arrive at a higher voltage than that considered here. A plot of transmission function as a function of injection energy reveals that the “off-set” bias in the three wires is determined by the position of the peak closest to the Fermi level. This is due to the fact that the addition of dephasing reduces the height of the transmission peak which in turn reduces the current through the junction. The first peak in the transmission function of the N=3 oligomer is around 0.25 eV from the Fermi energy as seen in Fig. 6.6(a). This peak falls within the chemical potential window at an external bias of ~ 0.5 V. The transmission function at this peak is substantially reduced when dephasing is included. Thus, the current for $V_{sd} > 0.5$ V is reduced when phase-breaking tunneling is included. Similarly, since the first transmission peak in the N=2 oligomer is at an energy of 0.5 eV [Fig. 6.6(a)] away from the Fermi

level, the current at a bias of $V_{sd} > 1.0\text{V}$ decreases substantially when the non-coherent elastic transport is accounted for. The molecular wire with a single cubane unit($N=1$) has the first peak in the transmission function at $\sim 1.0\text{ eV}$ from the Fermi level [Fig. 6.6(a)]. So, the “off-set” bias is expected to be around 2.0 V which is beyond the scale of the plots provided. Peaks in the transmission function occur when there is resonant tunneling of electrons i.e the discrete energy levels of the molecule matches with the injection energy in the lead. Within the coherent elastic transport model the conductivity of the junction at this point suddenly increases due to the constructive interference as seen by the dotted circles in Fig. 6.6(b). But, the inclusion of phase randomization partially destroys the constructive interference in this regime and thus adds an additional resistance thereby reducing the current through the junction. It is to be noted here that the transmission function values at resonance obtained in our calculations are ~ 5 . A possible reason could be due to the single particle nature of eqn. 3.17 (before dephasing). Since our calculation is at the mean field level, which does not include the many-body dynamical correlations between the channel states, a higher transmission function values at resonance is expected. This is the reason why mean field approach usually overestimates the current at least by an order of magnitude. These important issues have been pointed out by many authors recently^{178,179}. In addition, we have considered a strongly coupled metal-molecule junction, where the significant metal induced screening resulting in a strong broadening could be responsible for such high transmission. It should be noted that our emphasis is on the relative difference in current between the oligomers of different length. E-ph interactions is one of the main

Table 6.1
Frequency of vibrational modes in three different oligomers, N=1,2,3.¹⁶⁹

N=1 (cm ⁻¹)	N=2 (cm ⁻¹)	N=3 (cm ⁻¹)
126	43	22
132	47	28
202	55	37
238	142	65
243	148	67
.	.	.
.	.	.
.	.	.
.	.	.
3125	3117	3115
3127	3125	3125
3136	3127	3125

sources of dephasing and these interactions increase with the increase in external bias. So, in the next section we look at the e-ph interactions in the three oligomers as a function of external bias.

6.3.4 Electron Phonon Coupling

The vibrational spectra of the *active region* of the device is calculated using the Gaussian (G03) electronic structure code. The vibronic frequencies are determined by inserting the atoms in a harmonic potential. The normal mode corresponding to each frequency are then calculated by a canonical transformation. This method is applied only on the atoms of molecular moiety because they are much lighter than the electrode atoms. The above

formulation, although with some assumptions, works reasonably well under equilibrium conditions i.e at zero bias, is not the best choice when an external bias is applied across the electrodes. In this case, ideally the structure should be allowed to relax under the effect of the electric field and the vibronic frequencies must be recalculated in the presence of an electronic current. Whereas this is a formidable task, a simpler formulation allows us to include the electric field dependent electronic eigen states while calculating the e-ph coupling energies at a finite bias.

The phonon frequencies for the three different wires are listed in Table 6.1. Some of the frequencies in the first column (one cage unit) are very close to those of pure cubane i.e. without the thiol group attached to it. However, it is seen that as the length of the wire is increased, lower frequency vibrational modes are available, for e.g the lowest frequency for the 6.28, 10.5, and 14.7Å wires are 126, 43, 22 cm^{-1} respectively. The decrease in the lowest frequency with increase in the length of the wire (also an increase in mass of the wire) is similar to an observed shift in vibrational spectra with different isotopes of Hydrogen¹⁸⁰. Thus the low frequency mode of the longest wire can be excited at a low bias. This is consistent with the substantial contribution from phase-relaxation scattering to the total current at the lowest external bias in the N=3 wire. In an earlier theoretical paper on a chain of Au atoms, non-zero occupation of vibrational modes was found at a lower external bias for a longer chain than for a shorter chain.¹⁵⁸ On the similar lines, the longest wire in our case has some of its vibrational modes active at a relatively low bias and is consistent with the fact that the dephasing current starts to contribute to the total current

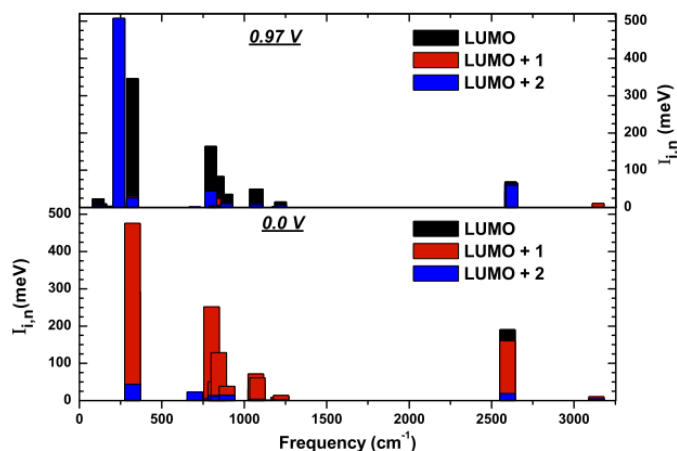


Figure 6.7: Electron-phonon coupling energies ($I_{i,n}$) for various vibrational modes in the molecular wire with a single cage-unit. i and n denote electronic energy eigen states and normal modes of vibration respectively. The lower panel and the upper panel correspond to $V_{sd} = 0$ V and $V_{sd} = 0.97$ V respectively¹⁶⁹. Reprinted figure with permission from Partha P. Pal and Ranjit Pati, J. Phys. Chem. C 2011, ©(2011)The Americal Chemical Society. Copyright permission in Appendix F.

at a bias lower than the other two wires [Fig 6.6(b)] considered here.

The dimensionless e-ph coupling constant and the corresponding energies are calculated by using eqns. 6.1 and 6.2 respectively. This part of the analysis requires two questions to be answered. They are: (a) which are the vibrational modes that affect the electron transport, and (b) how does this e-ph interaction evolve with increase in the bias? One expects the low energy vibrational modes to be easily excited by the application of external bias which would be the answer to question (a). More specifically, at a very low bias, the modes in

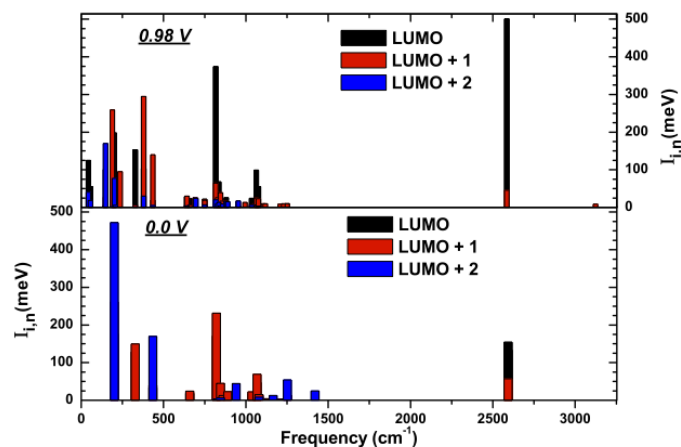


Figure 6.8: Electron-phonon coupling energies ($I_{i,n}$) for various vibrational modes in the molecular wire with 2 cage-units. i and n denote electronic energy eigen states and normal modes of vibration respectively. The lower panel and the upper panel correspond to $V_{sd}=0$ V and $V_{sd}=0.98$ V respectively¹⁶⁹. Reprinted figure with permission from Partha P. Pal and Ranjit Pati, J. Phys. Chem. C 2011, ©(2011)The Americal Chemical Society. Copyright permission in Appendix F.

which most of the atoms in the molecular moiety vibrates in a direction parallel¹²² to flow of charge(for e.g the mode in Fig 6.9) interact strongly with the conduction electrons. As the bias is increased, higher energy electrons will be injected into the molecule and they will tend to excite higher frequency vibrational modes. Some of these modes, whose normal coordinates are predominantly perpendicular (for e.g the one shown in Fig 6.10) to the flow of current, will now start to interact with the flowing charge. To answer question (b) we look into the interaction energies of phonons with the orbitals which contributes to

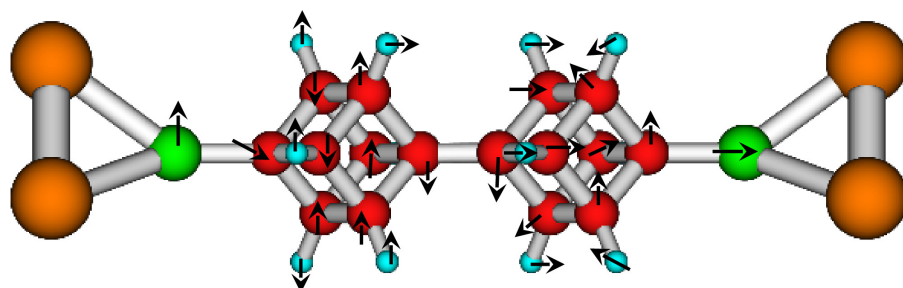


Figure 6.9: One of the many vibrational modes of the $N = 2$ oligomer which interact strongly with frontier orbitals at zero bias¹⁶⁹. Reprinted figure with permission from Partha P. Pal and Ranjit Pati, J. Phys. Chem. C 2011, ©(2011)The American Chemical Society. Copyright permission in Appendix F.

charge transport. The molecular levels within the chemical potential at the two junctions would possess the maximum probability to contribute to the current. The next highest probability would be the energy level close to the chemical potential but outside the window. In our case, for all the three wires, the renormalized molecular LUMO+1, LUMO+2 lie within the chemical potential window [Fig 6.6(a)]. The next closest level is the LUMO. All these levels are obtained from the diagonalization of the $H_{mol}(\epsilon)$ and then filling up the energy levels following the Pauli's exclusion principle. The coupling energies of different phonon modes with the LUMO + n ($n = 0, 1, 2$) are calculated. The possibility of

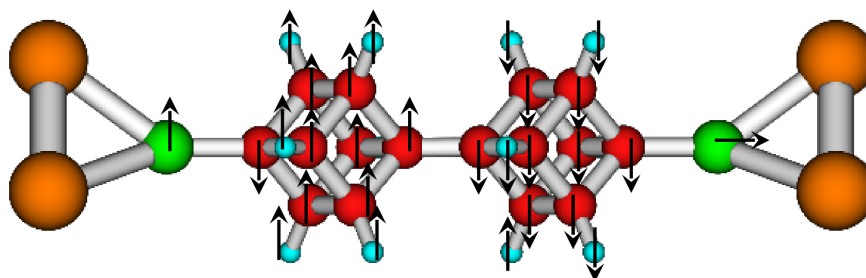


Figure 6.10: One of the newer modes of the $N = 2$ oligomer which starts to interact strongly with frontier molecular orbitals at $V_{sd} = 0.98$ V¹⁶⁹. Reprinted figure with permission from Partha P. Pal and Ranjit Pati, J. Phys. Chem. C 2011, ©(2011)The American Chemical Society. Copyright permission in Appendix F.

other levels contributing to the electronic current is not ruled out, but these three channels can be assumed to participate the most. The e-ph coupling energies for the three wires are calculated at zero bias and at a bias ~ 1.0 V. For brevity, we have plotted the e-ph interaction energies for $N=1$ and $N=2$ oligomers in Fig. 6.7 and 6.8 respectively. For the wire with a cubane monomer (Fig. 6.7), the difference between the number of vibronic modes interacting with the frontier orbitals at zero bias and at 0.97 V is very small. If we define Δ as the increase in the number of phonon modes which couple strongly (5 meV or more) with the frontier orbitals when the external bias is increased to ~ 1.0 V, then for the $N=1$

oligomer, $\Delta_{N=1} \approx 3$. But for the two cage units, there is a remarkable increase in the number of vibrational modes strongly interacting with electrons at 0.98 V as observed from the e-ph coupling energy plot in Fig 6.8. At zero bias, there are 18 modes which are strongly coupled to one of the frontier orbitals(Fig 6.8), whereas at a bias of 0.98 V there are ~ 43 modes strongly interacting with the same orbitals. Thus in this case $\Delta_{N=2} \approx 25 > \Delta_{N=1}$. A similar calculation on N=3 oligomer shows that $\Delta_{N=3} > \Delta_{N=2}$. The scenario remains the same for any $V_{sd} > 1.0$ V. This is consistent with the picture in Fig. 6.6(b). In the N=1 wire, the relative increase in current with inclusion of dephasing is $\sim 6.6\%$ at 1.5 V whereas the relative decrease in current due to dephasing at the same external bias is $\sim 33.4\%$ and 72% for N=2 and N=3 oligomers respectively. The relative change in the current is calculated using the formula: $\frac{Total-Coherent}{Total} \times 100$. Thus dephasing effects are maximum for the longest wire which is consistent with the earlier relation $\Delta_{N=3} > \Delta_{N=2} > \Delta_{N=1}$. Note that these normal modes were also present in zero bias but did not have substantial interaction energy with the electronic levels. A similar increase in the coupling between some important vibrational modes and certain electronic levels with increase in external bias was also observed earlier.¹⁰¹

6.4 Summary

Using first principles methodology, we studied current-voltage characteristics of three molecular wires constructed out of cubane oligomers ($N = 1, 2, 3$). In the low bias Ohmic regime, the conductance of the wires show an exponential decay with an increase in length, which is in agreement with experimental findings. With the inclusion of dephasing the low-bias current-voltage characteristics still remains linear. However, after a certain “off-set” bias dephasing starts to decrease the electronic current across the molecular junctions. The “off-set” bias is found to decrease with the increase in length of the molecular wire. The magnitude of the “off-set” bias depends upon the position of the peak nearest to the Fermi level in the bias dependent transmission function. This is due to the fact that phase randomization reduces the constructive interference at the resonant tunneling peaks and hence reduces the magnitude of the current. E-ph interaction, which is one of the main causes of dephasing, increases with external bias irrespective of the length of the wire. At a low bias, the vibrational modes in which the atoms vibrate predominantly in a direction parallel to the current flow strongly interacts with the conduction electrons. But as the bias is increased, the modes in which most of the atoms vibrate perpendicular to the direction of current flow starts to couple more strongly with the traversing electrons, thus increasing the overall e-ph interaction. This increase in e-ph coupling strength with bias is directly proportional to the increase in the length of the oligomer. Thus, this is consistent with

the existence of the smallest “off-set” bias in the longest oligomer($N=3$) under study. This study gives an estimate of the length scale and a bias scale upto which dephasing effect can be neglected on cubane oligomer based molecular devices.

Chapter 7

Conclusion and Future work

7.1 Conclusions

In this section, we summarize the findings of the projects compiled in this dissertation. In the first part, using a single particle Green's function approach, we study the various factors that affect the bias dependent electron transport in molecular nano-junctions, namely the potential profile in the wire, charge screening length at the electrode, and the atomic level geometric information at the metal-molecule interface. The potential profile along the molecular spacer undergoes substantial modifications when the external bias is varied, thus reinforcing the need of explicit inclusion of the electric field in the Hamiltonian of the active region of the device. An accurate estimate of self-energy is required for the agree-

ment of the theoretical and the experimentally measured electronic current. Determination of self-energy requires the knowledge of the metal-molecule contact geometry under experimental conditions. Our calculated current and conductance values of a Au-BDT-Au junction is found to be at least one order higher than the experimental values. A parametric calculation of the self-energy leads us to conclude that it has vital role to play in determining the conductance characteristics of the molecular junctions under study. Thereafter we modify our formalism to make it parameter-free. This does not solve the problem. We conclude that a strongly coupled metal-molecule junctions leads us to overestimate the current and conductance values. So we change our strategy and concentrate on comparative studies of electron transport on molecular spacers of different lengths. We tested our formalism on a strongly coupled metal-molecular wire-metal system with the wire being constructed out of bicyclo[1.1.1]pentane (BCP) oligomers. In the low bias Ohmic regime, it is seen that the conductance of the wire reduces exponentially with increase in its length. This is in very good agreement with the previously obtained exponential decay feature of the electron transfer rate in the same oligomer using the electron transfer coupling matrix values. Thereafter we did a similar study on cubane oligomers. In the low bias regime, we obtained a similar exponential decay of the conductance with increase in length of the oligomers. This is also in excellent agreement with the previously measured exponential decay in conductance with increase in length with the help of pulse radiolysis measurements. Subsequently, we looked into the dephasing effects on charge transport across Au-cubane-Au junctions as a function of external bias and length of the oligomer. Our calculations show that the

‘phase-breaking’ scattering events do not have a severe effect on the total current in the low bias Ohmic regime. However, after a certain cut-off bias (which varies with the length of the oligomer), the phase-relaxing scattering starts to have a substantial contribution to the total electronic current. Moreover, the magnitude of the cut-off bias was found to decrease with increase in length of the molecular wire. Deeper analysis shows that the cut-off bias depends on the position of the peak in the transmission function which is closest to the Fermi energy. The peak position of the transmission function changes with the length of the wire. With inclusion of phase randomization, the height of the peak in the transmission function reduces, thus decreasing the magnitude of current. Electron-phonon interaction being the main cause of ‘phase-loss’ in the current-carrying electrons directed us to look into the normal modes of vibration in the molecular wires and their interaction with frontier molecular orbitals. The e-ph interactions were studied using the Holstein Hamiltonian which considers only the linear terms of the e-ph coupling. Our results show that the average e-ph coupling increases with external bias due to increase in the number of vibronic modes which interact with traversing electrons. Through this project, we were able to figure out the length scale and the bias-scale up to which the ‘phase-breaking’ effects can be neglected while modeling charge transport across cubane oligomers.

7.2 Future Directions

So far, our theoretical studies have been on strongly coupled junctions. Under experimental conditions, the metal-molecule junction does not form a strong bond. In fact in all the experiments done so far various values of conductance have been observed for a certain metal-molecule junction. The different conductance values have been attributed to different junction geometries. Also, experimentalists have faced the difficulty of having control over fabricating the junctions which leads to various junction geometries. From all this observations we can comment that the metal-molecule junction is not a strongly coupled junction. Theoretically modeling weakly coupled junctions is very challenging task since the correlation energy becomes important when solving the Schrödinger for the active region of the device. Also, the dynamical effects play an important role in the transport characteristics of a weakly coupled junction. So, in future, one needs find a robust scheme which takes into account both the static and the dynamic correlation factors.

References

- [1] G. E. Moore, Electronics **38**, 8 (1965).
- [2] M. Schulz, Nature **399**, 729 (1999).
- [3] D. A. Muller, T. Sorsch, S. Moccio, F. H. Baumann, K. Evans-Lutterodt, G. Timp, Nature **399**, 758 (1999).
- [4] A. Aviram, and M. A. Ratner, Chem. Phys. Lett. **29**, 277 (1974).
- [5] M. A. Reed, C. Zhou, C. J. Muller, T. P. Burgin, and J. M. Tour, Science **278**, 252 (1997).
- [6] X. D. Cui, A. Primak, X. Zarate, J. Tomfohr, O. F. Sankey, A. L. Moore, T. A. Moore, D. Gust, G. Harris, and S. M. Lindsay, Science **294**, 571 (2001).
- [7] W. Liang, M. P. Shores, M. Bockrath, J. R. Long, and H. Park, Nature **417**, 725 (2002).
- [8] B. Xu, and N. J. Tao, Science **301**, 1221 (2003).
- [9] X. Xiao, B. Xu, and N. J. Tao, Nano Lett. **4**, 267 (2004).

- [10] X. Li, J. He, B. Xu, S. M. Lindsay, and N. J. Tao, J. Am. Chem. Soc. **128**, 2135 (2006).
- [11] M. Tsutsui, Y. Teramae, S. Kurokawa, and A. Sakai, Appl. Phys. Lett. **89**, 163111 (2006).
- [12] F. Chen, X. Li, J. Hihath, Z. Huang, and N. J. Tao, J. Am. Chem. Soc. **128**, 15874 (2006).
- [13] M. Di Ventra and S. T. Pantelides, Appl. Phys. Lett. **76**, 3448 (2000).
- [14] A. M. Bratkovsky, P. E. Kornilovitch, Phys. Rev. B **67**, 115307 (2003).
- [15] A. W. Ghosh, T. Rakshit, and S. Datta, Nano Lett. **4**, 565 (2004).
- [16] L. H. Yu, Z. K. Keane, J.W. Ciszek, L. Cheng, M. P. Stewart, J. M. Tour, and D. Natelson, Phys. Rev. Lett. **93**, 266802 (2004).
- [17] J. O. Lee, G. Lientschnig, F. Wiertz, M. Struijk, R. A. J. Janssen, R. Egberink, D. N. Reinhoudt, P. Hadley, C. Dekker, Nano Lett. **3**, 113 (2004).
- [18] B. Xu, X. Xiao, X. Yang, L. Zang, and N. J. Tao, J. Am. Chem. Soc. **127**, 2386 (2005).
- [19] Z. K. Keane, J. W. Ciszek, J. M. Tour, D. Natelson, Nano Lett. **6**, 1518 (2006).
- [20] T. M. Perrine and B. D. Dunietz, Phys. Rev. B **75**, 195319 (2007).
- [21] T. M. Perrine, R. G. Smith, C. Marsh, and B. D. Dunietz, J. Chem. Phys **128**, 154706 (2008).

- [22] H. He, R. Pandey, and S. P Karna, *Nanotechnology* **19**, 505203 (2008).
- [23] H. Song, Y. Kim, Y. H. Jang, H. Jeong, M. A. Reed, and T. Lee, *Nature* **462**, 1039 (2009).
- [24] F. Moresco, G. Meyer, K-H. Rieder, H. Tang, A. Gourdon and C. Joachim, *Phys. Rev. Lett.* **86**, 672 (2001).
- [25] M. S. Graige, G. Feher, and M. Y. Okamura, *Proc. Natl. Acad. Sci.* **95**, 11679 (1998).
- [26] W. B. Davis, M. A. Ratner, and M. R. Wasielewski, *J. Am. Chem. Soc.* **123**, 7877 (2001).
- [27] F. Valencia, A. H. Romero, M. Kiwi, R. Ramírez, and A. Toro-Labbe, *Phys. Rev. B* **71**, 033410 (2005).
- [28] L. Venkataraman, J. E. Klare, J. E. Nuckolls, M. S. Hybertson, and M. L. Steigerwald, *Nature* **442**, 904 (2006).
- [29] R. Pati and S. P. Karna, *Phys. Rev. B* **69**, 155419 (2007).
- [30] S. Mandal and R. Pati, *Phys. Rev. B* **83**, 195420 (2011).
- [31] J. Repp, P. Liljeroth, and G. Meyer, *Nature Physics* **6**, 975 (2010).
- [32] J. J. Sakurai, *Advanced Quantum Mechanics*, (Addison-Wesley, Massachusetts, 1967).
- [33] L. I. Schiff, *Quantum Mechanics* (McGraw-Hill Book Company, 1968)

- [34] R. Pati, *Theory of Electronic Structures and Nuclear Quadrupole Interactions in Molecular Solids and Semiconductor Surfaces*. Doctoral Thesis, State University of New York at Albany. 23-40, 1998.
- [35] P. Panigrahi, *Controlling Electronic and Magnetic Properties of Ultra Narrow Multilayered Nanowires.*, Doctoral Thesis, Michigan Technological University. 13-39, 2009.
- [36] M. Weissbluth, *Atoms and Molecules*, (Academic Press, New York, 1978).
- [37] M. Born and J. R. Oppenheimer, Ann. Physik **84**, 457 (1927).
- [38] A. Rubio, *Efficient implementation of time-dependent density functional theory for the dynamical description of biomolecules and nanostructure*, BCAM, Bilbao 18th September 2009.
- [39] J. Muscat, A. Wander, and N. M. Harrison, Chem. Phys. Lett. **342**, 397 (2001).
- [40] H. Jiang, R. Orlando, M. A. Blanco, and R. Pandey, J. Phys.:Condens. Matter **16**, 3081 (2004).
- [41] H. He, R. Orlando, M. A. Blanco, R. Pandey, E. Amzallag, I. Baraille, and M. Rérat, Phys. Rev. B **74**, 195123 (2006).
- [42] N. W. Ashcroft, N. David Mermin, *Solid State Physics* (Holt, Rinehart and Winston, New York, USA, 1976).
- [43] C. Kittel, *Introduction to Solid State Physics* (Wiley, New York, USA, 1971).

- [44] C. Kergueris, J. P. Bourgoin, S. Palacin, D. Esteve, C. Urbina, M. Magoga, and C. Joachim, Phys. Rev. B **59**, 12505 (1999).
- [45] A. R. Williams, P. J. Feibelman, and N. D. Lang, Phys. Rev. B **26**, 5433 (1982).
- [46] G. P. Brivio, and M. I. Trioni, Rev. Mod. Phys. **71**, 231 (1999).
- [47] K. S. Thygesen and A. Rubio, Phys. Rev. B **77**, 115333 (2008).
- [48] GAUSSIAN 03, Gaussian Inc., Pittsburgh, PA, 2003.
- [49] P. Hohenberg, W. Kohn, Phys. Rev. **136**, B864 (1964).
- [50] R. G. Parr, and W. Yang, *Density-Functional Theory of Atoms and Molecules*(Oxford Science, Oxford, 1994).
- [51] W. Kohn, L. J. Sham, Phys. Rev. **140**, A1133 (1965).
- [52] S. Datta, W. Tian, S. Hong, R. Reifenberger, J. I. Henderson, and C. P. Kubiak, Phys. Rev. Lett. **79**, 2530 (1997).
- [53] J. Taylor, H. Guo, and J. Wang, Phys. Rev. B **63**, 245407 (2001).
- [54] K. S. Thygesen, and A. Rubio, J. Chem. Phys. **126**, 091101 (2007).
- [55] G. C. Solomon, C. Harrmann, T. Hansen, V. Mujica, and M. A. Ratner, Nature Chem. **2**, 223 (2010).
- [56] S. Datta, *Electron Transport in Mesoscopic Systems* (Cambridge University Press, Cambridge, England, 1997).

- [57] R. Pati, M. McClain, and A. Bandyopadhyay, Phys. Rev. Lett. **100**, 246801 (2008).
- [58] Vienna *ab initio* Simulation Package(VASP), Technische Universität Wien, 1999; G. Kresse, J. Furthmüller, Phys. Rev. B **54**, 11169 (1996).
- [59] Y. Meir, N. S. Wingreen, Phys. Rev. Lett. **68**, 2512 (1992).
- [60] R. Pati, L. Senapati, P. M. Ajayan, and S. K. Nayak, Phys. Rev. B **68**, 100407(R) (2003).
- [61] Y. Xia, and G. M. Whitesides, Adv. Mater **7**, 471 (1995).
- [62] A. Ulman, Chem Rev. **96**, 1533 (1996).
- [63] D. Krüger, H. Fuchs, R. Rousseau, D. Marx, and M. Parrinello, Phys. Rev. Lett. **89**, 186402 (2002).
- [64] Z. Huang, F. Chen, P. A. Bennett, and N. J. Tao, J. Am. Chem. Soc. **129**, 13225 (2007).
- [65] W. Tian, S. Datta, S. Hong, R. Reifengerger, J. I. Henderson, and C. P. Kubiak, J. Chem. Phys. **109**, 2874 (1998).
- [66] P. S. Damle, A. W. Ghosh, and S. Datta, Phys. Rev. B(Rapid Comm.) **64**, 201403 (2001).
- [67] E. G. Emberly, and G. Kirczenow, Phys. Rev. B **58**, 10911 (1998).
- [68] J. M. Seminario, A. G. Zacarias, and J. M. Tour, J. Phys. Chem. A **103**, 7883 (1999).

- [69] L. E. Hall, J. R. Reimers, N. S. Hush, and K. Silverbrook, J. Chem. Phys. **112**, 1510 (2000).
- [70] D. M. Newns, Phys. Rev. B **178**, 1123 (1969).
- [71] M. Di Ventura, S. T. Pantelides, and N. D. Lang, Phys. Rev. Lett. **84**, 979 (2000).
- [72] W. T. Geng, J. Nara, and T. Ohno, App. Phys. Lett. **85**, 5992 (2004).
- [73] J. Tomfohr, and O. F. Sankey, J. Chem. Phys. **120**, 1542 (2004).
- [74] C. K. Wang, Y. Fu, and Y. Luo, Phys. Chem. Chem. Phys. **3**, 5017 (2001).
- [75] C. K. Wang, and Y. Luo, J. Chem. Phys. **119**, 4923 (2003).
- [76] P. A. Derosa, and J. M. Seminario, J. Phys. Chem. B **105**, 471 (2001).
- [77] P. Delaney, and J. C. Greer, Phys. Rev. Lett. **93**, 036805 (2004).
- [78] C. Toher, A. Filippetti, S. Sanvito, and Kieron Burke, Phys. Rev. Lett. **95**, 146402 (2005).
- [79] C. Toher, and S. Sanvito, Phys. Rev. Lett. **99**, 056801 (2007).
- [80] S. Ke, H. U. Baranger, and W. Yang, J. Chem. Phys. **126**, 201102 (2007).
- [81] C. Toher, and S. Sanvito, Phys. Rev. B **77**, 155402 (2008).
- [82] N. Sai, M. Zwolak, G. Vignale, and M. Di Ventura, Phys. Rev. Lett. **94**, 186810 (2005).
- [83] J. B. Neaton, M. S. Hybersten, and S. G. Louie, Phys. Rev. Lett. **97**, 216405 (2005).

- [84] M. H. Tsai, T. H. Lu, and Y. H. Tang, J. Appl. Phys. **104**, 043703 (2008).
- [85] K. Varga, and S. T. Pantelides, Phys. Rev. Lett. **98**, 076804 (2007).
- [86] D. A. Andrews, R. P. Van Duyne, and M. A. Ratner, Nano Lett. **8**, 1120 (2008)
- [87] S. Yeganeh, M. A. Ratner, M. Galperin, and A. Nitzan, Nano Lett. **9**, 1770 (2009).
- [88] A. Nitzan, and M. A. Ratner, Science **300**, 1384 (2003).
- [89] N. J. Tao, Nature Nanotechnology **1**, 173 (2006).
- [90] S. M. Lindsay, and M. A. Ratner, Adv. Mater. **19**, 23 (2007).
- [91] J. Ferrer, and V. M. Garcia-Suarez, J. Mater. Chem. **19**, 1696 (2009).
- [92] Y. Dubi and M. Di Ventra, Rev. Mod. Phys. **83**, 131 (2011).
- [93] P. P. Pal and R. Pati, *unpublished manuscript*.
- [94] P. L. Barbieri, P. A. Fantin, and F. E. Jorge, Molecular Physics **104**, 2945 (2006).
- [95] G. Kresse, and J. Furthmüller, Phys. Rev. B **54**, 11169 (1996). The value is 0.035 states/eV \times spin
- [96] K. Stokbro, J. Taylor, M. Brandbyge, J. L. Mozos, and P. Ordejon, Comput. Mater. Sci. **27**, 151 (2003).
- [97] Y. Xue, and M. A. Ratner, Phys. Rev. B **68**, 115406 (2003).
- [98] J. Cizek, and J. Paldus, Physica Scripta **21**, 251 (1980).

- [99] C. J. Cramer, *Essentials of Computational Chemistry* (Chichester:John Wiley and Sons, 2002).
- [100] C. Møller, M. S. Plesset, Phys. Rev. **46**, 618 (1934).
- [101] N. Sergueev, D. Roubtsov, and H. Guo, Phys. Rev. Lett. **95**, 146803 (2005).
- [102] J. Jiang, M. Kula, W. Lu, and Y. Luo, Nano. Lett. **5**, 1551 (2005).
- [103] B.G. Johnson, P. M. W. Gill, J. A. Pople, Chem. Phys. Lett. **206**, 239 (1993).
- [104] C. L. Closs, and J. R. Miller, Science **240**, 440 (1988).
- [105] A. Bandyopadhyay, R. Pati, S. Sahu, F. Peper, and D. Fujita, Nature Physics **6**, 369 (2010).
- [106] J. Park, A. N. Pasupathy, J. I. Goldsmith, C. Chang, Y. Yaish, J. R. Petta, M. Rinkoski, J. P. Sethna, H. D. Abruna, P. L. McEuen, and D. C. Ralph, Nature **417**, 722 (2002).
- [107] E. Lörtscher, H. B. Weber, and H. Riel, Phys. Rev. Lett. **98**, 176807 (2007).
- [108] C. Joachim, J. K. Gimzewski, and A. Aviram, Nature **408**, 541 (2000).
- [109] J. R. Heath, and M. A. Ratner, Phys. Today **56(5)**, 43 (2003).
- [110] P. F. H. Schwab, M. D. Levin, and J. Michl, Chem Rev. **99**, 1863 (1999).
- [111] K. B. Wiberg, D. S. Connor, and G. M. Lampman, Tetrahedron Lett. **10**, 531 (1964).

- [112] C. Liang, and M. D. Newton, J. Phys. Chem. **97**, 3199 (1993).
- [113] R. Pati, and S. P. Karna, J. Chem. Phys. **115**, 1703 (2001).
- [114] R. Pati, and S. P. Karna, Chem. Phys. Lett. **351**, 302 (2002).
- [115] N. S. Hush, Electrochim. Acta **13**, 1005 (1968).
- [116] R. A. Marcus, N. Sutin, Biochim. Biophys. Acta **811**, 265 (1985).
- [117] M. D. Newton, Adv. Chem. Phys. **106**, 303 (1999).
- [118] A. D. Becke, J. Chem. Phys. **98**, 5648 (1993).
- [119] J. Zhou, F. Hagelberg Phys. Rev. Lett. **97**, 045505 (2006).
- [120] Z. Bihary and M. A. Ratner, Phys. Rev. B **72**, 115439 (2005).
- [121] J. Maassen, F. Zahid and H. Guo, Phys. Rev. B **80**, 125423 (2009).
- [122] M. Di Ventra, *Electron Transport in Nanoscale Systems* (Cambridge University Press, Cambridge, England, 2008).
- [123] T. P. Pareek, S. K. Joshi, and A. M. Jayannavar, Phys. Rev. B **57**, 8809 (1998).
- [124] Z. Huang, F. Chen, R. D'Agosta, P. A. Bennett, M. Di Ventra, and N. J. Tao, Nature Nanotech. **2**, 698 (2007).
- [125] H. M. Pastawski, L.E.F. Foa Torres, E. Medina, Chem. Phys. **281**, 257 (2002).
- [126] M. Büttiker, Phys. Rev. B **33**, 3020(1986); IBM J. Res. Dev. **32**, 63 (1988).

- [127] M. A. Reed and T. Lee, *Molecular Nanoelectronics* (American Scientific Publishers, California, USA, 2003).
- [128] S. Datta, *Quantum Transport: Atom to Transistor* (Cambridge University Press, Cambridge, 2005).
- [129] J. L. D'Amato and H. M. Pastawski, Phys. Rev. B **41**, 7411 (1990).
- [130] J. Shi, Z. Ma, and X. C. Xie, Phys. Rev. B **63**, 201311(R) (2001).
- [131] R. Golizadeh-Mojarad and S. Datta, Phys. Rev. B **75**, 081301(R)(2007).
- [132] G. D. Mahan, *Many-Particle Physics* (Plenum Press, New York, USA 1990).
- [133] H. Haug and A.-P. Jauho, *Quantum Kinetics in Transport and Optics of Semiconductors* (Springer, Berlin, 1996).
- [134] R. C. Jaklevic, and J. Lambe, Phys. Rev. Lett. **17**, 1139 (1966).
- [135] P. K. Hansma, Phys. Rep. **30**, 145 (1977).
- [136] K. W. Hipps and U. Mazur, J. Phys. Chem. **97**, 7803 (1993).
- [137] T. Seideman, J. Phys.: Condens. Matter **15**, R521 (2003).
- [138] N. Lorente, R. Rurali, and H. Tang, J. Phys.: Condens. Matter **17**, S1049 (2005).
- [139] B. C. Stipe, M. A. Rezaei, and W. Ho, Science **280**, 1732 (1998).
- [140] J. G. Kushmerick, J. Lazorcik, C. H. Patterson, R. Shashidhar, D. S. Seferos, and G. C. Bazan, Nano. Lett. **4**, 639 (2004).

- [141] W. Wang, T. Lee, I. Kretzschmar, and M. A. Reed, *Nano Lett.* **4**, 643 (2004).
- [142] D. P. Long, J. L. Lazorcik, B. A. Mantooth, M. H. Moore, M. A. Ratner, A. Troisi, Y. Yao, J. W. Ciszek, J. M. Tour, R. Shashidhar, *Nat. Mater.* **5**, 901 (2006).
- [143] J. Hihath, C. R. Arroyo, G. Rubio-Gollinger, N. J. Tao, and N. Agraït, *Nano Lett.* **8**, 1673 (2008).
- [144] M. Taniguchi, M. Tsutsui, K. Yokota, and T. Kawai, *Nanotechnology* **20**, 434008 (2009).
- [145] J. Hihath, C. Bruot, and N. J. Tao, *Acs-Nano* **4**, 3823 (2010).
- [146] R. H. M. Smit, Y. Noat, C. Untiedt, N. D. Lang, M. C. van Hemert, and J. M. van Ruitenbeek, *Nature (London)* **419**, 906 (2002).
- [147] N. Agraït, C. Untiedt, G. Rubio-Bollinger, and S. Vieira, *Phys. Rev. Lett.* **88**, 216803 (2002).
- [148] N. Agraït, C. Untiedt, G. Rubio-Bollinger, and S. Vieira, *Chem. Phys.* **281**, 231 (2002).
- [149] M. J. Montgomery and T. N. Todorov, *J. Phys. Condens. Matter* **15**, 8781 (2003).
- [150] Y.-C. Chen, M. Zwolak, and M. Di Ventra, *Nano Lett.* **4**, 1709 (2004).
- [151] A. Troisi and M. A. Ratner, *Phys. Rev. B* **72**, 033408 (2005).
- [152] J. Bonča and S. A. Trugman, *Phys. Rev. Lett.* **75**, 2566 (1995).

- [153] E. G. Emberly and G. Kirczenow, Phys. Rev. B **61**, 5740 (2000).
- [154] H. Ness, S. A. Shevlin, and A. J. Fisher, Phys. Rev. B **63**, 125422 (2001).
- [155] M. J. Montgomery, J Hoekstra, T N Todorov, and A P Sutton, J. Phys. Condens. Matter **15**, 731 (2003).
- [156] R. Lake and S. Datta, Phys. Rev. B **46**, 4757(1992).
- [157] A. Pecchia, A. Di Carlo, A. Gagliardi, S. Sanna, T. Frauenheim, and R. Gutierrez, Nano Lett. **4**, 2109 (2004).
- [158] T. Frederiksen, M. Brandbyge, N. Lorente, and A.-P. Jauho, Phys. Rev. Lett. **93**, 256601 (2004).
- [159] M. Galperin, M. A. Ratner, and A. Nitzan, J. Chem. Phys. **121**, 11965 (2004).
- [160] M. Galperin, M. A. Ratner, and A. Nitzan, Nano Lett. **4**, 1605 (2004).
- [161] G. C. Solomon, A. Gagliardi, A. Pecchia, T. Frauenheim, A. Di Carlo, J. R. Reimers, and N. S. Hush, J. Chem. Phys. **124**, 094704 (2006).
- [162] T. Frederiksen, M. Paulsson, M. Brandbyge, and A.-P. Jauho, Phys. Rev. B **75**, 205413 (2007).
- [163] C. Caroli, R. Combescot, P. Nozieres, and D. Saint-James, J. Phys. C **5**, 21 (1972).
- [164] K. Yokota, M. Taniguchi, and T. Kawai, Chem. Phys. Lett. **487**, 268 (2010).
- [165] R. Härtle, C. Benesch, and M. Thoss, Phys. Rev. Lett. **102**, 146801 (2009).

- [166] C. Benesch, M. Čížek, J. Klimeš, I. Kondov, M. Thoss, and W. Domcke, J. Phys. Chem. C **112**, 9880 (2008).
- [167] A. Troisi and M. A. Ratner, Small **2**, 172 (2006) and references therein.
- [168] M. Galperin, M. A. Ratner, and A. Nitzan, J. Phys: Condens. Matter **19**, 103201 (2007) and references therein.
- [169] P. P. Pal and R. Pati, J. Phys. Chem. C *accepted*, (2011).
- [170] P. E. Eaton, and T. W. Cole, J. Am. Chem. Soc. **86**, 962 (1964).
- [171] K. Miaskiewicz and D. A. Smith, Chem. Phys. Lett. **270**, 376 (1997).
- [172] B. Paulson, K. Pramod, P. Eaton, G. Closs, J. R. Miller, J. Phys. Chem. **97**, 13042 (1993).
- [173] P. P. Pal , and R. Pati, Phys. Rev. B **82**, 045424 (2010).
- [174] F. Evers, K. Burke, Nano and Molecular Electronics Handbook, Edited by S. E. Lyshevski, (CRC Press 2007) and reference therein.
- [175] Y. F. Wang, J. Kröger, R. Berndt, H. Vázquez, M. Brandbyge, and M. Paulsson, Phys. Rev. Lett. **104**, 176802 (2010).
- [176] N. O. Lipari, C. B. Duke, and L. Pietronero, J. Chem. Phys. **65**, 1165 (1976).
- [177] L. Hedberg, K. Hedberg, P. E. Eaton, N. Nodari, A. G. Robiette, J. Am. Chem. Soc. **113**, 1514 (1991).

- [178] G. Vignale, M. Di Ventra, Phys. Rev. B **79**, 014201 (2009).
- [179] D. Roy, G. Vignale, and M. Di Ventra, Phys. Rev. B **83**, 075428 (2011).
- [180] D. Djukic, K. S. Thygesen, C. Untiedt, R. H. M. Smit, K. W. Jacobsen, and J. M. Ruitenbeek, Phys. Rev. B. **71**, 161402(R)(2005).

Appendix A

Hartree Approximation

For the Hartree approximation^{32,33}, one needs to start from a trial wavefunction of the form:

$$\psi(r_1, r_2, \dots, r_N) = \phi_1(r_1)\phi_2(r_2)\dots\phi_N(r_N) \quad (\text{A.1})$$

Our aim is to minimise the expectation value of the Hamiltonian,

$$\hat{H}_e = -\frac{\hbar^2}{2m_e} \sum_i \nabla_i^2 - \sum_i \sum_A \frac{Z_A e^2}{|\vec{r}_i - \vec{R}_A|} + \sum_{i>j} \sum \frac{e^2}{|\vec{r}_i - \vec{r}_j|} \quad (\text{A.2})$$

The expectation value($\langle \psi | H | \psi \rangle$) w.r.t to the trial wavefunction is:

$$\begin{aligned} & \int \dots \int \phi_1^*(r_1) \phi_2^*(r_2) \dots \phi_N^*(r_N) H \phi_1(r_1) \phi_2(r_2) \dots \phi_N(r_N) d^3 r_1 \dots d^3 r_N \\ &= \sum_i \int \phi_i^*(r_i) \left(-\frac{\hbar^2}{2m_e} \nabla_i^2 - \sum_A \frac{Z_A e^2}{|\vec{r}_i - \vec{R}_A|} \right) \phi_i(r_i) d^3 r_i \\ &+ \sum_{i>j} \sum \int \int \phi_i^*(r_i) \phi_j^*(r_j) \frac{e^2}{|\vec{r}_i - \vec{r}_j|} \phi_i(r_i) \phi_j(r_j) d^3 r_i d^3 r_j \end{aligned} \quad (\text{A.3})$$

since the ϕ -s are normalized. To find the minimum of $\langle H \rangle$ each ϕ_i has to be varied separately. In order to do that we need to pull out the terms which contains ϕ_i . They are:

$$\begin{aligned} & \int \phi_i^*(r_i) \left(-\frac{\hbar^2}{2m_e} \nabla_i^2 - \sum_A \frac{Z_A e^2}{|\vec{r}_i - \vec{R}_A|} \right) \phi_i(r_i) d^3 r_i \\ &+ \sum_{i \neq j} \int \int \phi_i^*(r_i) \phi_j^*(r_j) \frac{e^2}{|\vec{r}_i - \vec{r}_j|} \phi_i(r_i) \phi_j(r_j) d^3 r_i d^3 r_j \end{aligned} \quad (\text{A.4})$$

which is essentially equal to:

$$\int \phi_i^*(r_i) H_i \phi_i(r_i) d^3 r_i \quad (\text{A.5})$$

, the expectation of H_i w.r.t the function $\phi_i(r_i)$ where H_i is:

$$H_i \equiv -\frac{\hbar^2}{2m_e} \nabla_i^2 - \sum_A \frac{Z_A e^2}{|\vec{r}_i - \vec{R}_A|} + \sum_{i \neq j} \int |\phi_j^* \phi_j| \frac{e^2}{|\vec{r}_i - \vec{r}_j|} d^3 r_j \quad (\text{A.6})$$

According to the variational principle, the expectation value in eqn. A.5 is minimum when $\phi_i(r_i)$ is an eigenfunction of H_i which leads us to the condition:

$$\left[-\frac{\hbar^2}{2m_e} \nabla_i^2 - \sum_A \frac{Z_A e^2}{|\vec{r}_i - \vec{R}_A|} + \sum_{i \neq j} \int |\phi_j^* \phi_j| \frac{e^2}{|\vec{r}_i - \vec{r}_j|} d^3 r_j \right] \phi_i(r_i) = \epsilon_i \phi_i(r_i) \quad (\text{A.7})$$

Appendix B

Hartree-Fock Theory

In Hartree-Fock theory^{32,33}, the guess for the many electron wavefunction is the Slater determinant of the single-particle wave functions, which is:

$$\psi = \frac{1}{\sqrt{N!}} \begin{vmatrix} \phi_1(r_1) & \phi_2(r_1) & \cdots & \cdots & \phi_N(r_1) \\ \phi_1(r_2) & \phi_2(r_2) & \cdots & \cdots & \phi_N(r_2) \\ \cdots & \cdots & \cdots & \cdots & \cdots \\ \cdots & \cdots & \cdots & \cdots & \cdots \\ \phi_1(r_N) & \phi_2(r_N) & \cdots & \cdots & \phi_N(r_N) \end{vmatrix} = \det[\phi_1(r_1), \phi_2(r_2), \dots, \phi_N(r_N)] \quad (\text{B.1})$$

We need to minimize the Hamiltonian, $A.2$ w.r.t the above wave function. The expectation value of H w.r.t this wave function is:

$$\begin{aligned}
& \int \dots \int \det[\phi_1(r_1), \phi_2(r_2), \dots, \phi_N(r_N)]^* H \det[\phi_1(r_1), \phi_2(r_2), \dots, \phi_N(r_N)] d^3 r_1 \dots d^3 r_N \\
&= \sum_i \int \phi_i^*(r_i) \left(-\frac{\hbar^2}{2m_e} \nabla_i^2 - \sum_A \frac{Z_A e^2}{|\vec{r}_i - \vec{R}_A|} \right) \phi_i(r_i) d^3 r_i \\
&+ \sum_{i>j} \sum \int \int \phi_i^*(r_i) \phi_j^*(r_j) \frac{e^2}{|\vec{r}_i - \vec{r}_j|} \phi_j(r_j) \phi_i(r_i) d^3 r_i d^3 r_j \\
&- \sum_{i>j} \sum \int \int \phi_i^*(r_i) \phi_j^*(r_j) \frac{e^2}{|\vec{r}_i - \vec{r}_j|} \phi_i(r_j) \phi_j(r_i) d^3 r_i d^3 r_j
\end{aligned} \tag{B.2}$$

again since the ϕ -s are normalized. To find the minimum of $\langle H \rangle$ each ϕ_i has to be varied separately, which gives us the following equation.

$$\begin{aligned}
& \left(-\frac{\hbar^2}{2m_e} \nabla_i^2 - \sum_A \frac{Z_A e^2}{|\vec{r}_i - \vec{R}_A|} \right) \phi_i(r_i) + \sum_j \int \phi_j^*(r_j) \frac{e^2}{|\vec{r}_i - \vec{r}_j|} \phi_j(r_j) d^3 r_j \phi_i(r_i) \\
&- \sum_j \int \phi_j^*(r_j) \phi_i(r_j) \frac{e^2}{|\vec{r}_i - \vec{r}_j|} \phi_i(r_i) d^3 r_j = \epsilon_i \phi_i(r_i)
\end{aligned} \tag{B.3}$$

Appendix C

Estimation of Electron-phonon coupling using the Holstein Model.

The Hamiltonian, using the second quantized notations, can thus be defined as^{164,176}:

$$H = \sum_i \varepsilon_i \{0\} a_i^\dagger a_i + \sum_n \left(b_n^\dagger b_n + \frac{1}{2} \right) \hbar \omega_n + \sum_{i,n} g_{i,n} a_i^\dagger a_i \left(b_n^\dagger + b_n \right) \hbar \omega_n \quad (\text{C.1})$$

where the first term is the unperturbed single electron energy levels ($\varepsilon_i \{0\}$) and the second term corresponds to the normal vibrational modes of the molecule. The last term represents the linear e-ph coupling with a dimensionless constant of $g_{i,n}$. Physically, $g_{i,n}$ can be interpreted as the shift in the energy eigenvalues, labeled as ε_i , when the position of the atomic

nuclei is changed following the coordinates of the normal mode, n . In the absence of any e-ph interaction the electronic and the vibrational energy levels would evolve independently and the Hamiltonian in this case would be:

$$H = H_e + H_{ph} = \sum_i \epsilon_i a_i^\dagger a_i + \sum_n \left(b_n^\dagger b_n + \frac{1}{2} \right) \hbar \omega_n \quad (C.2)$$

As mentioned earlier, e-ph interaction will produce a shift in the single electron energy levels, ϵ_i which can now be expanded in terms of the dimensionless normal coordinates (Q_n 's) by using the Taylor series^{164,176}:

$$\begin{aligned} \epsilon_i\{Q_1 Q_2 \dots Q_n \dots\} = \epsilon_i\{0\} &+ \sum_n \left(\frac{\partial \epsilon_i}{\partial Q_n} \right)_0 Q_n \\ &+ \sum_{n,m} \left(\frac{\partial^2 \epsilon_i}{\partial Q_n \partial Q_m} \right) \frac{Q_n Q_m}{2} + \dots \end{aligned} \quad (C.3)$$

where $\epsilon_i\{0\}$ is the energy eigen-value of the electronic state in the absence of interaction with any phonon mode. The dimensionless normal coordinates are related to the creation/annihilation operators by^{32,33}:

$$Q_n = \frac{1}{\sqrt{2}}(b_n + b_n^\dagger); \dot{Q}_n = \frac{1}{\sqrt{2}}(b_n - b_n^\dagger); (b_n, b_m^\dagger) = \delta_{nm} \quad (C.4)$$

Inserting the shifted electronic energy eigenvalue given by eqn. C.3 into eqn. C.2 and neglecting second order terms we have^{164,176}:

$$H = \sum_i a_i^\dagger a_i \left[\varepsilon_i \{0\} + \sum_n \left(\frac{\partial \varepsilon_i}{\partial Q_n} \right) \frac{1}{\sqrt{2}} (b_n + b_n^\dagger) \right] + \sum_n \hbar \omega_n \left(b_n^\dagger b_n + \frac{1}{2} \right) \quad (C.5)$$

Comparing the coefficients of the three terms in eqns. C.1 and C.5 the dimensionless coupling constant, $g_{i,n}$ is found to be^{164,176}:

$$g_{i,n} = \frac{1}{\sqrt{2} \hbar \omega_n} \left(\frac{\partial \varepsilon_i}{\partial Q_n} \right) \quad (C.6)$$

Making a canonical transformation, the coupling energy can be calculated as:

$$I_{i,n} = g_{i,n}^2 \hbar \omega_n \quad (C.7)$$

The coupling energy along with the coupling constant gives a quantitative answer as to how a particular electronic energy level interacts with a particular phonon mode. The coupling energies of the various electronic levels and phonon modes of the molecule are calculated both before and after the inclusion of an external bias.

Appendix D

Copyrights

The copyright permission for Fig. 1.1 is distributed under GNU Free Documentation License (GDFL)

GNU Free Documentation License

The GNU Free Documentation License (GNU FDL or simply GFDL) is a copyleft license for free documentation, designed by the Free Software Foundation (FSF) for the GNU Project. It is similar to the GNU General Public License, giving readers the rights to copy, redistribute and modify a work and requires all copies and derivatives to be available under the same license. Copies may also be sold commercially, but, if produced in larger quantities (greater than 100), the original document or source code must be made available to the work's recipient. The GFDL was designed for manuals, textbooks, other reference and instructional materials, and documentation which often accompanies GNU software.

However, it can be used for any text-based work, regardless of subject matter. For example, the free online encyclopedia Wikipedia uses the GFDL for all of its text.

Wikipedia:Public domain

For all practical purposes on Wikipedia, the public domain comprises copyright-free works: anyone can use them in any way and for any purpose. Proper attribution to the author or source of a work, even if it is in the public domain, is still required to avoid plagiarism. The public domain is generally defined (e.g. by the U.S. Copyright Office) as the sum of works that are not copyrighted, i.e. * that were not eligible for copyright in the first place, or * whose copyright has expired. However, there is no such thing as the public domain on the Internet. International treaties, like the Berne Convention, are not self-executing and do not supersede local law. There is no globally valid "International Copyright Law" that would take precedence over local laws. Instead, signatory countries of the Berne Convention have adapted their laws to comply with the minimum standards set forth by the treaty, often with stronger provisions than required. Whether or not something is copyright-free in some country depends on the laws of individual countries. Wikipedia, and the Wikimedia Foundation, its legal body, are based in Florida, United States. Although legislation is sometimes unclear about which laws are to apply on the Internet, the primary law relevant for Wikipedia is that of the United States. For re-users of Wikipedia content, it is the laws of their respective countries. In the U.S., any work published before January 1, 1923 anywhere in the world[1] is in the public domain. Other countries are not bound to that

1923 date, though. Complications arise when special cases are considered, such as trying to determine whether a work published later might be in the public domain in the U.S., or when dealing with unpublished works. When a work has not been published in the U.S. but in some other country, that other country's copyright laws also must be taken into account. Re-users of Wikipedia content also might find the explanations here useful.

Appendix E

Copyrights

The Copyright permission from The American Physical Society for the article by Partha P. Pal and Ranjit Pati, Phys. Rev. B **82**, 045424 (2010). The permission applies to Figure 5.1.

Subject: Re: Copyright required

Sent By: [apscepubl](#) On: April 22, 2011 3:26 PM

To: Partha Pratim Pal

Dear Partha Pal,

Thank you for your email. As the author, you have the right to use the article or a portion of the article in a thesis or dissertation without request from APS, provided the bibliographic citation and the APS copyright credit line are given on the appropriate pages.

Best wishes,

Eileen LaManca
Publications Marketing Coordinator
American Physical Society
<http://librarians.aps.org/>

Physics - Spotlighting exceptional research: <http://physics.aps.org/>

>>> Partha Pal <pppal@mtu.edu> 4/20/2011 3:08 PM >>>

Hi,

I want to reproduce the journal article (Phys. Rev. B vol-82, page-045424, year-2010) in my Doctoral Thesis.
I am the first author of this article.
Can I have a permission to do so ?

Regards,

Partha Pratim Pal
Department of Physics
Michigan Technological University
Houghton, Michigan-49931

Figure E.1: Copyright permission from American Physical Society (APS) for using all or a portion of the text from the article Phys. Rev. B **82**, 045424 (2010), by Partha P. Pal and Ranjit Pati.

Appendix F

Copyrights

The Copyright permission from The Americal Chemical Society for the article by Partha P. Pal and Ranjit Pati, J. Phys. Chem. C 2011. The permission applies to Figures 6.1, 6.9, and 6.10.



American Chemical Society

Publications Division
Copyright Office
VIA FAX: 906-487-2933 DATE: May 27, 2011

1155 Sixteenth Street, NW
Washington, DC 20036
Phone: (1) 202-872-4368 or -4367
Fax: (1) 202-776-8112 E-mail: copyright@acs.org

MEMORANDUM

TO: Partha Pratim Pal, 2002 Woodmar Drive, Apt. #D, Houghton MI 49931

FROM: C. Arleen Courtney, Copyright Associate

This is regarding your request for permission to include your paper(s) or portions of text from your paper(s) in your thesis/dissertation. Permission is now automatically granted; please pay special attention to the **implications** paragraph below. The Copyright Subcommittee of the Joint Board/Council Committees on Publications approved the following:

Copyright permission for published and submitted material from theses and dissertations

ACS extends blanket permission to students to include in their theses and dissertations their own articles, or portions thereof, that have been published in ACS journals or submitted to ACS journals for publication, provided that the ACS copyright credit line is noted on the appropriate page(s).

Publishing implications of electronic publication of theses and dissertation material

Students and their mentors should be aware that posting of theses and dissertation material on the Web prior to submission of material from that thesis or dissertation to an ACS journal may affect publication in that journal. Whether Web posting is considered prior publication may be evaluated on a case-by-case basis by the journal's editor. If an ACS journal editor considers Web posting to be "prior publication", the paper will not be accepted for publication in that journal. If you intend to submit your unpublished paper to ACS for publication, check with the appropriate editor prior to posting your manuscript electronically.

Reuse/Replication of the Entire Work in Theses or Collections: Authors may reuse all or part of the Submitted, Accepted or Published Work in a thesis or dissertation that the author writes and is required to submit to satisfy the criteria of degree-granting institutions. Such reuse is permitted subject to the ACS' "Ethical Guidelines to Publication of Chemical Research" (<http://pubs.acs.org/page/policy/ethics/index.html>), the author should secure written confirmation (via letter or email) from the respective ACS journal editor(s) to avoid potential conflicts with journal prior publication/embargo policies. Appropriate citation of the Published Work must be made. If the thesis or dissertation to be published is in electronic format, a direct link to the Published Work must also be included using the ACS Articles on Request author-directed link - see <http://pubs.acs.org/page/policy/articlesonrequest/index.html>

* Prior publication policies of ACS journals are posted on the ACS website at <http://pubs.acs.org/page/policy/prior/index.html>

If your paper has not yet been published by ACS, please print the following credit line on the first page of your article: "Reproduced (or 'Reproduced in part') with permission from [JOURNAL NAME], in press (or 'submitted for publication'). Unpublished work copyright [CURRENT YEAR] American Chemical Society." Include appropriate information.

If your paper has already been published by ACS and you want to include the text or portions of the text in your thesis/dissertation, please print the ACS copyright credit line on the first page of your article: "Reproduced (or 'Reproduced in part') with permission from [FULL REFERENCE CITATION.] Copyright [YEAR] American Chemical Society." Include appropriate information.

Submission to a Dissertation Distributor: If you plan to submit your thesis to LHM or to another dissertation distributor, you should not include the unpublished ACS paper in your thesis if the thesis will be disseminated electronically, until ACS has published your paper. After publication of the paper by ACS, you may release the entire thesis (not the individual ACS article by itself) for electronic dissemination through the distributor; ACS's copyright credit line should be printed on the first page of the ACS paper.

Figure F.1: Copyright permission from American Chemical Society (ACS) for using all or a portion of the text from the article in J. Phys. Chem. C 2011, by Partha P. Pal and Ranjit Pati.